Durham E-Theses

Localised conduction electrons in carbon nanotubes and related structures

Watson, Michael J.

How to cite:

Watson, Michael J. (2005) *Localised conduction electrons in carbon nanotubes and related structures*, Durham theses, Durham University. Available at Durham E-Theses Online: http://etheses.dur.ac.uk/2775/

Use policy

Localised Conduction Electrons in Carbon Nanotubes and Related Structures

Michael J. Watson

A Thesis presented for the degree of
Doctor of Philosophy

Topological Solitons Research Group
Department of Mathematical Sciences
University of Durham
England

August 2005

Dedicated to

Mum and Dad

Localised Conduction Electrons in Carbon Nanotubes and Related Structures

Michael J. Watson

Abstract

Single localized polaron (quasiparticle) states are considered in structures relating to carbon nanotubes. The hamiltonian is derived in the tight-binding approximation first on a hexagonal lattice and later on a general carbon nanotube with specifiable chirality, and shares close links with the Davydov model of excitations of a one-dimensional molecular chain. First-order interactions of the lattice degrees of freedom with the electron on-site and exchange terms are included. The system equations are shown, under certain approximations, to share a close relationship with the nonlinear Schrödinger equation - an equation that is known to possess localised solutions. The ground state of system is investigated numerically and is found to depend crucially upon the strengths of the electron-phonon interactions.

Declaration

The work in this thesis is based on research carried out at the Topological Solitons Research Group, the Department of Mathematical Sciences, Durham University, England. No part of this thesis has been submitted elsewhere for any other degree or qualification and is all my own work unless referenced to the contrary in the text.

Acknowledgements

In helping me on the road to writing this thesis I would like to thank a number of people. Firstly, Mum and Dad, to whom this work is dedicated. You have always had unwavering confidence in me and always given me every opportunity to succeed, for which I am forever grateful. Thanks also to Gran and Grandad, Lis and James for your support, and Julia for making me really happy in my last year.

Secondly, I wish to thank Wojtek for showing extreme confidence in me and being immensely understanding during a couple of extremely tough times. Your encouragement has been invaluable over the three years. I would also like to thank other collaborators Bernard, Larissa and Sasha both for helping with my studies and being very friendly. Also Lukasz, for lots of interesting chats and making me laugh- mainly on one particular evening!

Cheers to the lads in the department: Owen, James, Jose, Wadey, Shorty and Rich. You have all made me laugh loads and I have had some great times with you all, particularly on our days out. Thanks to Leo for his fresh outlook on life and helping me see the positive in any situation.

Thanks to Sharry, the man with whom I had my greatest collaboration in trying to bring home the University Departmental 5-a-side trophy to the Maths dept. I have to say that this would have been the crowning achievement of my three years at Durham. Also all the lads in the team and at Friday footie.

Quick word of thanks for Anton and Gav for being great housemates in my final year and to Michael the caretaker and Pam and the other cleaners for some good chats and laughs in the morning when no-one else is around!

Also thanks to Lisa, Steve, Simon, Ian V, Matt K and finally Cathy.

Contents

List of Figures

Chapter 1

Introduction

There exists within crystals a fascinating interplay between the electrons and the lattice of ions. The electronic and atomic states are intricately connected in a very complex manner. A change in the electronic state alters the configuration of the ions and vice-versa. Since the quantum of the vibrational field is the phonon, these effects are known as electron-phonon interactions. The strength of this interaction turns out to be of crucial significance in determining the ground states of the conduction electrons in the crystal. In order to find the eigenstates of such a complicated system in a crystal with a huge number of sites one must turn to a whole host of approximations. The aim of the work presented here was to investigate the effect of the electron-phonon interaction upon the electronic and lattice ground states under a host of well founded simplifications in novel structures known as carbon nanotubes.

In solid-state physics one usually segregates the electrons in the crystal into two catergories. Firstly, the core electrons are assumed to be tightly bound to the individual nuclei. Secondly, the valence electrons are less bound, and due to the bringing together of the atoms into the periodic lattice and therefore the overlap of the electronic wavefunctions, these electrons are free to move around the crystal [1], [2]. It is the conduction electrons which are of principle importance in determining the electrical properties of the crystal. When a conduction electron moves through the crystal it may be accompanied by a local lattice distortion, occuring due to the electron-phonon interaction [3]. This entity, consisting of the electron and its related lattice deformation, can be considered as a composite quasiparticle with its
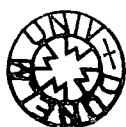
own characteristics such as energy, effective mass, momentum etc. [4].

An extremely interesting and novel effect may occur in crystals where the electron-phonon interaction is particularly strong. Under such circumstances a localisation or self-trapping effect may occur. The lattice distortion that existed due to the presence of the conduction electron itself is then responsible for the spatial capturing of the electron. The minimum energy configuration is then one in which the electron moves in some spatially localized region, accompanied by a permanent lattice distortion. This quasiparticle (localized electron + lattice distrotion) is known as the polaron. The technology used to describe this localized quasiparticle has been extremely important in other areas of science, particularly in describing the dispersionless transport of energy within organic materials [5].

When physicists began their quest for a description of the energy levels of conduction electrons in crystals, captivating phenomena such as the polaron were undiscovered. The electron energy levels were solved in the field of a static array of atoms. One of the foundations of solid-state theory is Bloch's theorem. This is related to the description of single electrons in a perfectly periodic potential due to the static atoms. The theorem states that the electronic eigenstates can be chosen to be of the form of a plane wave multiplied by a function with the periodicity of the crystal [1], [6]. The Schrödinger equation can then be solved in certain regimes such as in the tight-binding approximation or for a weak periodic potential. Such arguments form the basis of modern solid-state theory and lead to the concept of an energy band.

Energy bands are a result of the Pauli-exclusion principle, which states that only one fermion may occupy a given quantum state. When a large number of degenerate systems, such as isolated atoms, are brought together to form a crystal there must be some removal of the degeneracy in order to create consistent occupiable electron states. In a crystal this is achieved by the broadening of the energy levels into bands. Calculations involving Bloch states show that there exists a hierarchy of quasi-continuous levels, each containing $2N$ electron states (where N is the number of atoms in the crystal) [6], [7], [8]. Each individual electron state is labelled by three parameters: a wavevector $\mathbf{k}$, a band index m and a spin index σ (The effects

of the spin of the electron are neglected in this text). The allowed wave-vectors in macroscopic crystals are usually determined by the Born-von Karman condition, which takes the form of a three-dimensional periodic boundary condition. It is assumed that the bulk properties of the solid will not depend upon the boundary conditions, and furthermore this method gives the correct number of electron states. The band index m simply denotes which of the hierachy of energy bands the electron state is situated within.

One of the crowning achievements of the early band calculations was the successful justification of the classification of substances into the three catergories: insulator, metal and semiconductor. In an insulator the energy bands are either entirely filled or completely empty. No electrical conduction can occur since in an applied field the electrons are unable to change their wavevector - the Pauli exclusion principle forbids them from doing so since there are no empty states in the band. In order to achieve conduction an electron must gain enough energy to move into a higher band, where there are many free k-states. In an insulator the energy required to do this is much greater than the thermal energy at room temperature. In a metal there exists at least one partially filled band, and so by the previous argument conduction is always possible. The semiconductor describes the intermediate regime where the energy gap is of the order of the thermal energy at room temperature, which is typically around an electron-volt. In fact, it is semiconducting substances to which the work in this document applies.

In a more complete model of crystal dynamics one must consider the vibrations of the atoms around their equilibrium positions [6]. Since the interatomic potential is complicated, the usual treatment is to expand it in a Taylor series dependent upon the individual site displacements. Since the gradient of the potential vanishes in equilibrium the first order term vanishes. In the harmonic approximation, only the second order terms are included. In such a model one assumes that the deviations of the atoms from their equilibrium positions in the perfect crystal are small. The normal modes of vibration are then found by transforming to collective coordinates in wavevector (q) space, and any vibrational pattern can then be described in terms of a superposition of these normal modes. In a quantum mechanical context one

talks about the excitation of a vibrational mode of frequency ν in terms of the creation of a phonon with the same frequency. This analogy gives the particle description of the crystal vibrational field. In order to describe phonon interactions one must consider the anharmonic terms in the potential. Such terms are important in describing accurately, for example, the crystal specific heat, or neutron scattering effects [10]. However these interactions can often be ignored, in the limit of small displacement as is the case with the work presented here. For ideas relating to anharmonic potentials in these models see for example [60].

These arguments allow the understanding of the individual electronic levels and possible vibrational patterns of the crystal. However it is evident that there must exist an intricate interplay between these seperate phenomena within the crystal lattice. As previously discussed, the conduction electron moving through the crystal creates a lattice distortion because of its charge field. Likewise a slightly deformed crystal produces a perturbation on the electronic Bloch states, thus modifying in some way the electron energy levels. In the scenario where the number of conduction electrons is very small, electron-electron interactions may be neglected. To the crystal hamiltonian one must then add only a potential term describing the interaction of the electrons with the ions. Written in **k**-space, this naturally leads to the concept of the Frölich hamiltonian (see chapter 2) [6,9]. Such an equation can be treated perturbatively and predicts the existence of the polaron.

In a seemingly unconnected area of research, Alexander Davydov and co-workers were investigating the possible mechanisms that could describe the dispersionless transport of energy in alpha-helical proteins [14], [12], [13]. Thermal effects were far too small to account for the magnitude of the energy transfer. This was a problem that was deemed important enough to earn the title of the 'crisis in bioenergetics' [15]. Davydov argued that vibrational energy could distort the structure of the alpha-helix, and through a phonon-coupling effect the oscillation energy could be trapped. Through this mechanism the vibrational energy would become localized and hence would not undergo dispersion. It was shown that in the stationary limit Davydov's equations led to a discrete nonlinear Schrödinger equation describing the excitation field. Such an equation is well known to contain localized solutions, or

solitons, which can be interpreted as describing a trapping of the excitation energy. The relevance to the study of the polaron problem lies in the hamiltonian utilized by Davydov, which is almost identical to the Frölich hamiltonian when written down in the k-space representation.

The eigenstates of this hamiltonian can be found approximately by way of the adiabatic approximation [1]. Its validity originates from the huge difference in mass between the light and mobile electrons and the relatively immobile heavy ions. The adiabatic approximation states that since the electrons react almost instantaneously to any deformation of the crystal, the electrons will effectively be in their ground state for a particular lattice configuration. More rigorously, the wavefunction separates into a product of that for the stationary ions and that for the mobile electrons in the field of the ions. This is often stated as the Born-Oppenheimer approximation. In the adiabatic approximation the task of finding the eigenstates becomes considerably simpler. Under the condition of large enough electron-phonon coupling it has been shown that a further dramatic simplification can be introduced. The eigenstates of the hamiltonian may be found by perturbative methods, and in the zeroth-order adiabatic approximation (valid for high enough electron-phonon coupling) the system equations are identical to the case where the lattice degrees of freedom are treated classically [17], [19], [18]. This is known as the semi-classical approximation. Under this scheme it is straightforward to derive the equations of motion. These take the form of a system of nonlinear equations, with a single equation describing the evolution of the electron field and one equation for each lattice dimension. The strength of the nonlinearity is determined by the electron-phonon coupling parameter and it is therefore this parameter that determines the degree of localization of the quasiparticle state [15]. Note that the problem of energy localization in helical chains is far from solved, with plenty of on-going studies (see for example [16]).

The localized, or quasiparticle solutions are extremely interesting because of the interplay between the localization of the excitation energy and the lattice deformation. Davydov's hamiltonian was set up originally to describe interactions in the alpha-helix, which can be considered in terms of three interacting one-dimensional

molecular chains. The hamiltonian contained one electron-phonon coupling parameter describing the coupling of the on-site excitation energy to the local chain deformation. Inter-chain electron-phonon interactions were ignored. As the value of the coupling parameter tened towards zero the ground state was found to tend towards a state that is completely delocalized. This means that the probability density for the excitation is spread over the entire lattice and the average site displacement is equal to zero. For non-zero values of the electron-phonon coupling the ground state is localized or soliton-like, and hence describes the polaron. Accompanying the localized excitation is a lattice distortion, in which sites are displaced towards the centre of the soliton. As the electron-phonon coupling increases, the state becomes more and more localized and the crystal distortion is more violent [20]. Any semi-permanent lattice distortion that accompanies a trapped state will effect the other electronic levels in the crystal. Furthermore, these effects are even more important in small structures such as carbon nanotubes, which have only one spatially extended dimension.

One further simplification that is frequently made in the field and indeed throughout this work is the tight-binding description [1, 6, 7]. This simplification is invaluable in calculating the electronic energy levels of substances in which the overlap of electronic wavefunctions centred upon neighbouring atoms is small. In these materials the individual atomic description of electron energy levels requires modification, however it is still useful. The wavefunctions are then expansions of a relatively small number of the individual atomic wavefunctions. This simplification allows the calculation of the full electronic band structure of materials in which the approximation is reasonable. The aim of the work presented here was to examine self-trapped polaron states in planar graphite and ultimately carbon nanotubes, which meant that the equations would describe hexagonal arrangements of carbon atoms. The ground state of an individual carbon atom is $1s^2 2s^2 2p^2$. In two-dimensional graphite it is energetically favourable for one of the $2s$ electrons to move into a $2p$ state. Two of the three p electrons then undergo a process called hybridization with the remaining $2s$ electron [22]. This involves the mixing of the s and p wavefunctions in such a way to create, through covalent bonding, the honeycomb arrangement that is seen

in graphite.

The overlap of the electronic wavefunctions between the atoms is small enough in graphite that the tight-binding approximation provides a reasonably accurate description. The implementation of such a method means that complicated long-range interactions may be ignored. In fact, only nearest neighbour interactions are considered. The energy band structures of various carbon nanotubes have been calculated in the tight-binding approximation [22]. Recently more accurate calculations have been performed using ab-initio (or first principles) methods. They have predicted electron energy dispersions that are qualitatively the same as those produced in the tight-binding approximation. However there are some small modifications [23], [24]. As is evident within this work, for the more challenging problem of electron-phonon interactions the tight-binding model gives valuable insight into the possible localized quasiparticle states.

Such considerations have already been made with regards to the two-dimensional square lattice [25], [29]. The work involved a generalisation of Davydov's model to the two-dimensional case, where the aim was to describe the behaviour of single conduction electrons in interaction with the lattice phonons. Models used a single electron-phonon coupling parameter describing the effect of the on-site electron energy upon the local crystal deformation. The two dimensional case was found to yield results that shared similarities with the one-dimensional chain. The electron ground state became localized above a certain critical magnitude of electron-phonon coupling and the degree of localization was once again found to increase with the coupling parameter. Some other ideas were also investigated, such as the effect of anisotropy upon the the groundstate. The importance of studying such effects in two-dimensional materials has increased in recent years because of our ability to create low dimensional systems [31], [32], and one very special class of low-dimensional system is the carbon nanotube.

Carbon nanotubes exhibit some extremely interesting and individual characteristics [21]. Their intrinsic properties depend upon their size and chirality [22], [33], [34], and also upon the level of doping with impurity atoms [36]. The usual way that people think about these structures is to picture a single sheet of planar graphite, i.e.

a hexagonal or honeycomb lattice. Next imagine rolling this sheet into a cylinder, so that equivalent lattice sites coincide consistently where the two sides of the plane join. The diameter of a carbon nanotube is of nanometre size, however the lengths of such tubes can be over a thousand times greater.

Carbon nanotubes originated from a field of research that stretches back over one hundred years. The first man-made carbon fibre was created by Thomas Edison in his efforts to invent the first electric light-bulb. Ever since then researchers have sought to create smaller fibres. Carbon fibres have since been found to be invaluable in forming strong and lightweight materials, most notably for use in the aerospace industry [22] [35]. The emphasis in experimental research was to produce greater yields of fibres with fewer defects, so that materials with the maximum possible strength could be consistently produced. As time passed people began to wonder if there was some minimum sized fibre that could be produced. After the discovery of the 'buckyball' C_{60}, researchers started to consider tubes of carbon atoms arranged as in graphite, with the ends capped by C_{60} like structures [33]. The real breakthrough arrived in 1991, when Iijima experimentally discovered carbon nanotubes using transmission electron microscopy [37]. The types of tubes produced in that research were actually multi-walled, meaning that the structures observed were made of multiple concentric nanotubes. Recent improvements in experimental procedures have allowed more efficient production of single-walled carbon nanotubes [38], [39], [40]. The impact of commercially available carbon nanotubes on a large scale would be enormous due to their remarkable properties.

Perhaps the most amazing attribute of carbon nanotubes is that they may be semiconducting or metallic, depending upon their geometrical structure. Returning to the thought experiment of carbon nanotube construction, imagine rolling the two-dimensional sheets of graphite at some angle (this angle is referred to as the chiral angle). It turns out that the choice of this angle, together with the tube radius, determines the nature of the electronic band structure. A simple explanation for this effect comes from the so-called zone folding technique [22], [44]. Consider once again the two-dimensional graphite sheet. Graphite exhibits metallic behaviour, however it is actually a zero-gap semiconductor (fig 1.1). This means that there is no overlap

between the valence band and the conduction band, however, they do coincide at a special point on the Brillouin zone boundary in the electron wavevector space. This is known as the K-point of the Brillouin zone. When the sheet of graphite is rolled into a carbon nanotube, the electron wavefunction obeys the relevant boundary conditions around the tube circumference. These periodic boundary conditions restrict the allowed conduction electron wavevectors to a subset of those involved in the structure of planar graphite. If this subset includes the K-point then the nanotube behaves like a metal. If the K-point is not included the nanotube will exhibit semiconducting behaviour. The studies involved with this research neglected electron-electron interactions. This approximation is valid if there exists a small number of conduction electrons that are on average spatially well separated from each other. For this reason our attention is restricted to semiconducting tubes at low temperature, so that very few electrons have gained enough thermal energy to be excited across the energy gap.
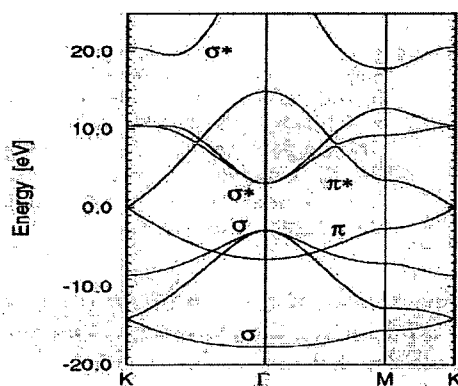
Figure 1.1: *Electronic band structure of graphite [22]. In this case the Fermi level is 0eV.*

Another attribute of a carbon nanotube involves its extremely high mechanical strength along the tube axis (i.e. parallel to the extended dimension). Simulations in molecular dynamics predict that tubes could undergo an increase in length of serveral percent before permanent deformation occurs [50]. Nanotubes also show great flexibility in the direction perpendicular to the nanotube axis and are resiliant to twisting distortions. Single-walled tubes can be bent around sharp corners or

coiled into circles without breaking [46]. The potential uses from the very small to the massive scales are endless. On the tiny scale, nanotubes could contribute to modern nanoscopics [48] or nanolithography [47]. On the very large scale it has been suggested that a rope made of carbon nanotubes could form a tether for an elevator into space [49]. Whether or not this is science fact or fiction is irrelevant, carbon nanotubes will surely revolutionise twenty-first century electronics and mechanics.

As emphasised already in this chapter, self-trapped polaron or quasi-particle states are accompanied by a characteristic lattice deformation. Such a distortion effect could doubtless affect both the mechanical and electrical properties of the tube, and so a full understanding of the possible self-trapped states will form an integral part of carbon nanotube research. Preliminary studies into self-trapped states in the hexagonal lattice have already been published [51]. The system hamiltonian was an adaptation of that considered in earlier studies of self-trapped states upon the square lattice. The authors considered a model of a two-dimensional graphite plane with one of the dimensions much smaller than the other. Periodic boundary conditions were imposed upon the lattice and electron fields along the shortened dimension. The aim of this was to provide a first glimpse into the properties of self-trapped states in carbon nanotubes. Variation of the single electron-phonon coupling parameter showed that the system contained a rich variety of both localized and delocalized ground states. The degree of localization depended as before upon the electron-phonon coupling parameter. The work undertaken in order to produce this document used these studies as a starting point for investigation.

The method employed to analyse self-trapping in this work is valuable in determining the type of ground state of the system for a given set of parameters that describe the physical properties of the solid in question. However the study of self-trapping is not restricted to such models. Self-trapping was first suggested by Landau [52], and subsequent advances were made by Rashba [53] and Toyozawa [54]. In general, one is led to consider two regimes. In the weak coupling limit the ground state corresponds to a polaron band describing a free conduction electron in the crystal under a slight perturbation. In the strong coupling limit the ground state corresponds to the self-trapped state which has an energy below the bottom of the

conduction band, approximately independent of $\mathbf{k}$. For details of the techniques used in studying self-trappin in different coupling regimes see for example [55], or for interesting work relating to honeycomb structures see [56]. Due to the massive expansion in computing potential over the last decade, numerically intensive ab initio or first principle calculations, which involve no underlying assumptions, have also advanced the understanding of self-trapping [57], [58]. We note here only that other such methods exist to study self-trapping effects in carbon nanotubes and encourage the reader to refer to the literature cited above. We now describe the structure of the thesis.

In chapter 2 the groundwork necessary for an understanding of the material in the thesis is discussed. A model is presented that is formally similar to Davydov's model for excitons in molecular chains. However in this context we aim to describe the self-trapping of conduction electrons in one-dimension. The derivation of the hamiltonian is discussed with reference to the various approximations that must be imposed. In chapter 3 the formalism is adapted to the hexagonal lattice. In an advancement of the model considered in [51], two electron-phonon coupling parameters are used to specify the dependence of the electron on-site and hopping energies upon the lattice deformation. The meanings of these terms will become clearer after progression through the sections. Chapter 4 presents some interesting numerical results of the system equations derived in chapter 3, showing the dependence of the electronic and lattice ground state upon the electron-phonon coupling parameters. The generalisation of the model to a carbon nanotube is presented in chapter 5. The complications relating to the three-dimensional lattice displacements are discussed, and the equations of motion for the system are analysed under various approximations. The numerical solutions to the equations are presented in chapter 6, which show some extremely interesting features of the kinds of trapped and untrapped quasiparticle states in carbon nanotubes. Finally in chapter 7 all conclusions are drawn and scope for future work considered.

Chapter 2

Preliminaries - Trapped electron states in one-dimensional chains

In this chapter we introduce the concepts that featured in conducting research work into localised electron states in hexagonal lattices and carbon nanotubes. Much of the work can be found in the references by Brizhik and Eremko [17], and the original ideas by Davydov [5]. There exists a wealth of research into these systems. For some alternative work on the 1d chain, see for example [11], [79] or [61]. We consider a tight-binding prescription for the coupling of conduction electrons to phonons in the 1d atomic chain. The chapter focusses upon the tools that may be used to find the adiabatic eigenstates of such a system, both polaronic and delocalized in nature. This section is intended to ensure a smooth transition to the description of such effects in more complicated lattices relating to carbon nanotubes.

2.1 Tight-binding Hamiltonian

2.1.1 Tight-binding electron states

In a crystal lattice, the bringing together of a large number of degenerate systems (i.e. the individual atoms) results in the broadening of the energy levels into a band. As previously discussed, the tight-binding approximation is an extremely useful tool in attempting to describe materials in which the overlap of the individual

atomic wavefunctions is small. In this section we will consider the model of a one-dimensional chain of N atoms, each pair being separated by a distance d in the pure crystal. For the time-being we assume that each atom is fixed to lie at its equilibrium position, i.e. we have a static crystal model. The electronic wavefunctions therefore obey the Bloch condition, and are labelled by a wavenumber k and a band index m. The transformation of the Bloch states into a spatial representation allows their representation in a complete basis of states $|n\rangle$ defined at the lattice sites labelled by the integer n. We can write the hamiltonian operator in this representation in second quantised form by performing the following expansions:

$$
\begin{aligned}
\hat{H} &= \sum_{n,n'} |n'\rangle\langle n'|\hat{H}|n\rangle\langle n| \\
&= \sum_{n,n'} H_{n'n}|n'\rangle\langle 0_e|0_e\rangle\langle n| \\
&= \sum_{n,n'} H_{n'n}a_{n'}^{\dagger}a_n,
\end{aligned}
\tag{2.1}
$$

where $a_n^{\dagger}(a_n)$ is the creation (annihilation) operator for the electron at site n in the one-dimensional crystal and $|0_e\rangle$ is the electron vacuum state. The creation and annihilation operators obey the usual fermionic anticommutation relations [6]:

$$
\{a_n, a_{n'}\} = \{a_n^{\dagger}, a_{n'}^{\dagger}\} = 0; \qquad \{a_n, a_{n'}^{\dagger}\} = \delta_{nn'}.
\tag{2.2}
$$

In the complete analysis one must consider the electron spin, and therefore include the spin index σ, however in our models we neglect the effects of spin and thus omit the spin index. One must simply remember that the occupation number of each of the respective electron states can be $0, 1$ or 2.

Next we make the extremely simplifying assumption that the matrix elements $\langle n'|\hat{H}|n\rangle$ are negligable for non-nearest neighbour interactions, i.e. $H_{n'n} \approx 0$ ($|n' - n| > 1$). This is valid if the overlaps of the electronic wavefunctions on non-neighbouring sites are small, and this leads to the tight-binding electron hamiltonian:

$$
\hat{H}_e = \sum_n \left[E_0 a_n^{\dagger}a_n - J(a_n^{\dagger}a_{n+1} + a_n^{\dagger}a_{n-1}) \right],
\tag{2.3}
$$

where E_0 is the on-site electron energy and $-J$ gives the strength of the exchange interaction. The tight-binding electron hamiltonian may be diagonalized by switching

to the representation in wavenumber (k) space by use of the Fourier transform:

$$a_n = \frac{1}{\sqrt{N}} \sum_k e^{iknd} \tilde{a}_k, \tag{2.4}$$

and the expression:

$$\sum_n e^{i(k-k')nd} = N\delta_{k-k'}, \tag{2.5}$$

which leads to:

$$\hat{H}_e = \sum_k E(k) \tilde{a}_k^\dagger \tilde{a}_k;$$
$$E(k) = E_0 - 2J\cos(kd). \tag{2.6}$$

The wavenumber k obeys the Born-von Karman boundary condition, and so may take on the N values $\frac{2\pi n_i}{N}$, where $1 < n_i < N$. $E(k)$ is the tight-binding electron energy dispersion relation. This procedure describes the usual Bloch prescription for the calculation of electronic levels in the static crystal. Of course, in order to describe real physical crystals, one must consider the effects of vibrations and therefore phonons.

2.1.2 Phonons in the 1d atomic chain

We now consider the crystal vibrations. Each atom is allowed to move about its equilibrium position, with u_n being the classical atomic displacement of the atom at site n. In the tight-binding model we can again make the simplifying assumption that non-nearest neighbour interactions are neglected. Considering first the classical case, the potential between neighbouring atoms can be expanded as a Taylor series in the displacements u_n. In the limit of small displacement one can consider terms up to second order. Higher order terms are neglected. Since the gradient of the potential vanishes when the lattice sites are at their equilibrium positions, the first order terms vanish and we are left with:

$$V = V_0 + \frac{1}{2} \sum_n K(u_n - u_{n-1})^2, \tag{2.7}$$

where K is the coefficient of elasticity. This is simply the usual expression describing the potential of the classical harmonic oscillator. The anharmonic terms that in the

quantum regime are necessary to describe phonon interactions are neglected in this model (see [60] for information). Switching to a quantum description, ignoring the additive constant V_0 and rearranging slightly:

$$V = \sum_n K[\hat{u}_n^\dagger \hat{u}_n - \frac{1}{2}\hat{u}_n^\dagger \hat{u}_{n-1} - \frac{1}{2}\hat{u}_{n-1}^\dagger \hat{u}_n]. \tag{2.8}$$

Just as in the case of the electron hamiltonian, the lattice potential is diagonalized by transforming into wavenumber (q) space:

$$\hat{u}_n = \frac{1}{\sqrt{N}} \sum_q e^{iqnd} \tilde{u}_q, \tag{2.9}$$

The complete phonon hamiltonian also includes the kinetic terms, and in its diagonal form is given by:

$$\hat{H}_{ph} = \frac{1}{2} \sum_q \left[\frac{\tilde{p}_q^\dagger \tilde{p}_q}{M} + \omega^2(q) \tilde{u}_q^\dagger \tilde{u}_q \right];$$

$$\omega(q) = \sqrt{\frac{k}{M}} \sin\left(\frac{qd}{2}\right). \tag{2.10}$$

The wavenumbers q again satisfy the Born-von Karman boundary condition, and the u_q are the normal coordinates. The lattice state labelled by q describes the collective excitation of all sites in the crystal, corresponding to the normal mode of vibration of wavenumber q. Any general vibrational pattern may be represented as a superposition of the normal modes. In the quantum mechanical case it is usual to refer to the particle like description of the vibrational field by linking the excitation of the mode of wavenumber q with the creation of a phonon of the same frequency. In following the usual procedure in quantising the harmonic oscillator, we introduce the bosonic annihilation and creation operators of phonons of wavenumber q [6]:

$$\tilde{u}_q = \sqrt{\frac{\hbar}{2M\omega(q)}}(\tilde{b}_q + \tilde{b}_{-q}^\dagger),$$

$$\tilde{p}_q = i\sqrt{\frac{M\hbar\omega(q)}{2}}(\tilde{b}_q^\dagger - \tilde{b}_{-q}). \tag{2.11}$$

This procedure transforms the hamiltonian into the usual form describing the quantum harmonic oscillator:

$$\hat{H}_{ph} = \sum_q \hbar\omega(q)\left(\tilde{b}_q^\dagger \tilde{b}_q + \frac{1}{2}\right), \tag{2.12}$$

which is simply a sum of N hamiltonians describing independent harmonic oscillators. So far we have diagonalized the tight-binding electron and phonon models individually. As emphasized in the introduction, the electronic and lattice states are intricately connected. It is therefore important to consider the electron-phonon interaction.

2.1.3 Tight-binding electron-phonon interactions

We now discuss the coupling of the lattice displacements to the electron on-site and exchange interaction energies given in (2.3). The constants E_0 and J now become functions of the lattice separations in such a way that we arrive at a total hamiltonian of the form:

$$\hat{H} = \hat{H}_e + \hat{H}_{ph} + \hat{H}_{int}, \tag{2.13}$$

where $\hat{H}_e$ and $\hat{H}_{ph}$ are the respective tight-binding electron and phonon hamiltonians considered in the previous two sub-sections. The new part to the hamiltonian describes the electron-phonon interaction:

$$\hat{H}_{int} = \sum_n \left[\chi a_n^\dagger a_n (\hat{u}_{n+1} - \hat{u}_{n-1}) + \right.$$
$$\left. + G[a_n^\dagger a_{n+1}(\hat{u}_{n+1} - \hat{u}_n) + a_n^\dagger a_{n-1}(\hat{u}_n - \hat{u}_{n-1})] \right]. \tag{2.14}$$

In this form of the electron-phonon interaction we have only considered corrections to the electron energy up to first order in the lattice displacements. Just as in the case of the phonon hamiltonian we are working in the limit of small displacement. The constants χ and G couple the respective on-site and exchange electron energies to to the lattice. Note that translational invariance is in built due to the fact that $\hat{H}_{int}$ is a function only of the interatomic separations.

2.1.4 Frölich Hamiltonian

The transformations (2.4,2.9) that were used to diagonalize the electron and phonon hamiltonians are now applied to the interaction hamiltonian. This process results

in the following form for the interaction hamiltonian:

$$\hat{H}_{int} = \frac{1}{\sqrt{N}} \sum_{k,q} F(k,q) \tilde{a}_{k+q}^{\dagger} \tilde{a}_k \tilde{u}_q \tag{2.15}$$

$$= \frac{1}{\sqrt{N}} \sum_{k,q} \Phi(k,q) \tilde{a}_{k+q}^{\dagger} \tilde{a}_k (\tilde{b}_q + \tilde{b}_{-q}^{\dagger}), \tag{2.16}$$

where

$$F(k,q) = 2i[\chi \sin(q) + G \sin(k) \cos(q)] - 2G \sin(k)[1 + \sin(q)],$$

$$\Phi(k,q) = \sqrt{\frac{\hbar}{2M\omega(q)}} F(k,q). \tag{2.17}$$

The total hamiltonian in its transformed incarnation is:

$$\hat{H} = \sum_k E(k) \tilde{a}_k^{\dagger} \tilde{a}_k + \sum_q \hbar\omega(q) \tilde{b}_q^{\dagger} \tilde{b}_q$$

$$+ \frac{1}{\sqrt{N}} \Phi(k,q) \sum_{k,q} \tilde{a}_{k+q}^{\dagger} \tilde{a}_k (\tilde{b}_q + \tilde{b}_{-q}^{\dagger}). \tag{2.18}$$

This is of the same form as the Frolich hamiltonian, often used in studying electron-phonon interactions in condensed matter physics [62], [6]. The function $\Phi(k,q)$ contains all details of the interaction. We now consider one particular method in order to look for the eigenstates of this hamiltonian.

2.2   The adiabatic approximation

When an electron is in the conduction band it may be energetically favourable for it to move in a spatially localized region. Accompanying the localized electron is a cloud of phonons, that produce a local deformation in the lattice. This deformation screens the electron field and thus reduces its electrostatic energy. In order to look for such quasiparticle solutions to the Frölich hamiltonian (2.16), we use the trial wavefunction [17]:

$$|\Psi\rangle = |\Phi\rangle |\psi_e\rangle. \tag{2.19}$$

Which is a product of the electron wavefunction and a coherent phonon state $|\Phi\rangle = U|0_{ph}\rangle$. $|0_{ph}\rangle$ is the phonon vacuum state and U is a coherent operator of molecular

displacements [63], [64] given by the expression:

$$U = \exp\left[\sum_q (\beta(q)b_q^\dagger - \beta^*(q)b_q)\right],$$
(2.20)

where there is one coefficient $\beta(q)$ corresponding to each phonon operator $\tilde{b}_q^\dagger$. The electron state is:

$$|\psi_e\rangle = \sum_k \phi_\lambda^*(k)\tilde{a}_k^\dagger|0\rangle = C_\lambda^\dagger|0_e\rangle.$$
(2.21)

Note that the normalisation of the state $|\psi_e\rangle$ leads to the following condition upon the coefficients:

$$\sum_k |\phi_\lambda(k)|^2 = 1$$
(2.22)

In seeking solutions in the form of the wavefunction (2.19), we are invoking the adiabatic approximation, where it is assumed that because the mobile electrons react to external fields much more rapidly than the lattice of heavy ions, one is essentially solving for the levels of an electron in a static arrangement of ions. One can think of this choice of the ansatz in terms of an operator of quasi-particle creation. The quasi-particle wavefunction $|\psi_e\rangle$ has been expanded in the basis of quasi-particle states labelled by the quantum number λ (see section 2.21). The orthonormality of these states is expressed by the relation $\sum_k \phi_\lambda(k)\phi_{\lambda'}(k) = \delta_{\lambda\lambda'}$. Accompanying the quasiparticle creation is the coherent phonon state specified by the unitary operator U. The values of the coefficients $\beta(q)$ within the unitary transformation U are to be determined later from the requirement that the total wavefunction $|\Psi\rangle$ is an eigenstate of the hamiltonian.

It is informative to consider some properties of the coherent state specified by U. First we define the state $|\beta(q)\rangle$ as the following operator acting upon the quasi-particle vacuum:

$$|\beta(q)\rangle = \exp(\beta(q)\tilde{b}_q^\dagger - \beta^*(q)\tilde{b}_q)|0_{ph}\rangle.$$
(2.23)

Now note that the coherent state $|\beta(q)\rangle$ of the phonon mode specified by q, which is in the form of an exponential, can be written in expanded form as:

$$|\beta(q)\rangle = \exp\left(-\frac{1}{2}|\beta(q)|^2\right)\sum_n \frac{(\beta(q)\tilde{b}_q^\dagger)^n}{n!}|0_{ph}\rangle,$$
(2.24)

where in this case n runs from 0 to ∞ (see [63] for details). It is then straightforward to show the following [65]:

$$
\begin{aligned}
\tilde{b}_q|\beta(q)\rangle &= \beta(q)|\beta(q)\rangle; \\
\langle\beta(q)|\tilde{b}_q^\dagger &= \langle\beta(q)|\beta^*(q); \\
\langle\beta(q)|\tilde{b}_q^\dagger\tilde{b}_q|\beta(q)\rangle &= \langle\beta(q)|\hat{n}_q|\beta(q)\rangle = |\beta(q)|^2,
\end{aligned}
\tag{2.25}
$$

i.e. $|\beta(q)\rangle$ is a right eigenstate of the phonon annihilation operator and therefore a left eigenstate of the phonon creation operator. It is our aim to find the values of the coefficients that produce a consistent phonon cloud for the quasiparticle.

It is very useful to make a slight digression to consider the representation of the unitary operator in terms of base states defined at the lattice sites labelled by n. Using (2.11), it is straightforward to calculate that:

$$
\begin{aligned}
\sum_q (\beta(q)b_q^\dagger - \beta^*(q)b_q) &= -\frac{i}{\hbar}\sum_n (\alpha_n\hat{p}_n - \pi_n\hat{u}_n); \\
\beta(q) &= \left(\frac{M\omega(q)}{2\hbar}\right)^{\frac{1}{2}}\alpha_q + i\left(\frac{1}{2M\hbar\omega(q)}\right)^{\frac{1}{2}}\pi_q,
\end{aligned}
\tag{2.26}
$$

where β_n and π_n are the respective Fourier transforms of the coefficients $\beta(q)$ and $\pi(q)$. Using the property (2.25) of the coherent state $|\beta(q)\rangle$ along with (2.19) and (2.26) we obtain:

$$
\begin{aligned}
\langle\Phi|\hat{u}_n|\Phi\rangle &= \alpha_n; \\
\langle\Phi|\hat{p}_n|\Phi\rangle &= \pi_n.
\end{aligned}
\tag{2.27}
$$

This completes the connection between the representation of the unitary operator in q-space and in real space. The product wavefunction (2.19), written in real space takes the form of Davydov's ansatz [65], [15]:

$$
\begin{aligned}
|\Psi\rangle &= |\Phi\rangle|\psi_e\rangle; \\
|\psi_e\rangle &= \sum_n \phi_n(t)\hat{a}_n^\dagger|0_e\rangle; \\
|\Phi\rangle &= S|0_{ph}\rangle; \\
S &= \exp\left(-\frac{i}{\hbar}\sum_n [\beta_n(t)\hat{p}_n - \pi_n(t)\hat{u}_n]\right),
\end{aligned}
\tag{2.28}
$$

where $\hat{p}_n$ is the momentum operator conjugate to $\hat{u}_n$. Davydov introduced this form of the wavefunction when attempting to describe the localization of vibrational energy in the alpha-helix. Davydov actually considered an exciton operator $\hat{B}_n^\dagger$ that creates a quantum of vibrational excitation at the molecule in the chain labelled by n. (Actually the model was slightly more complicated than this, since the alpha-helix contains two separate chains that twist around each other, therefore it is necessary to include cross-chain interactions). The Davydov hamiltonian is formally extremely similar to the case that we consider here. Davydov's analysis proceeded by attempting to minimize the average value of the energy $\langle \Psi | \hat{H} | \Psi \rangle$ by calculating the Schrödinger equation for the amplitudes $\phi_n(t)$ and hamilton's equation for the average displacement $\alpha_n(t)$. This method involves a classical treatment of the lattice displacements, and hence is sometimes called the semi-classical approximation. Our methodology will proceed in a quantum mechanical context in q-space. As we shall see, this will lead to a connection between Davydov's semi-classical method and a certain approximation, namely that of complete adiabaticity, made in q-space.

We proceed with our original argument by using the unitary operator of coherent atomic displacement (2.20) to transform the hamiltonian into the following form:

$$
\begin{aligned}
\tilde{H} = U^\dagger \hat{H} U \\
= \sum_k E(k) \tilde{a}_k^\dagger \tilde{a}_k + \\
+ \frac{1}{\sqrt{N}} \sum_{k,q} \Phi(k,q) \tilde{a}_{k+q}^\dagger \tilde{a}_k \left[\tilde{b}_q + \tilde{b}_{-q}^\dagger + \frac{1}{N}(\beta(q) + \beta^*(-q)) \right] + \\
+ \sum_q \hbar\omega(q) \left[\tilde{b}_q^\dagger \tilde{b}_q + \frac{1}{N}(\beta^*(q)\tilde{b}_q^\dagger + \beta^*(q)\tilde{b}_q) \right] + W,
\end{aligned} \qquad (2.29)
$$

where the energy of the lattice deformation is:

$$
W = \frac{1}{N} \sum_q \hbar\omega(q) |\beta(q)|^2. \qquad (2.30)
$$

The extra terms in the Hamiltonian $\tilde{H}$ appear due to the commutation of the unitary operator U through the hamiltonian. After this transformation the hamiltonian is in a more natural format from which to study localized solutions. The aim is to look for the eigenstates $|\Psi_e\rangle$ in the form of some fermionic creation operator acting

upon the quasiparticle vacuum $C_\lambda^\dagger|0\rangle$. By following this method one can partially diagonalize the hamiltonian through the introduction of the opreators C_λ via the unitary transformation [66], [67]:

$$\tilde{a}_k = \sum_\lambda \phi_\lambda(k)C_\lambda, \tag{2.31}$$

which is consistent with (2.21). Application of the unitary transformation (2.31) to the hamiltonian $\tilde{H}$ results in the diagonalization of the terms containing only electron operators, provided we demand that the coefficients $\phi_\lambda(k)$ satisfy the following equation [17]:

$$E(k)\phi_\lambda(k) + \frac{1}{N}\sum_q \Phi(k,q)(\beta(q)+\beta^*(-q))\phi_\lambda(k-q) = E_\lambda\phi_\lambda(k). \tag{2.32}$$

This is the method of partial diagonalisation first introduced by Eremko, Gaididei and Vakhnenko [66]. If this equation is satisfied, then the energy E_λ is the eigenenergy of the state labelled by λ. These states include all possible consistent bound and continuous states, with the lattice state yet to be determined by the coefficients of the unitary operator U. The hamiltonian can then be written as a sum of two seperate parts $\tilde{H} = \tilde{H}_0 + \tilde{H}_1$. The part $\tilde{H}_0$ contains all the parts that are diagonal with respect to the fermionic operators C_λ:

$$\tilde{H}_0 = \sum_\lambda \left[E_\lambda + \frac{1}{\sqrt{N}}\sum_q f_{\lambda,\lambda}(k,q)(b_q + b_{-q}^\dagger)\right]C_\lambda^\dagger C_\lambda +$$
$$+ \sum_q \hbar\omega(q)\left[b_q^\dagger b_q + \frac{1}{\sqrt{N}}(\beta(q)b_q^\dagger + \beta_q^* b_q)\right] + W, \tag{2.33}$$

where:

$$f_{\lambda,\lambda'} = \sum_k \Phi(k,q)\phi_\lambda^*(k)\phi_{\lambda'}(k-q). \tag{2.34}$$

Thus the part of the hamiltonian $\tilde{H}_0$ takes the form of a Frölich hamiltonian with some extra phonon terms that are to be used to determine the consistent lattice configurations. The second part of the hamiltonian $\tilde{H}_1$ is non-diagonal with respect to the fermionic operators, and hence refers to phonon induced non-adiabatic transitions between the quasiparticle eigenstates specified by the quantum number λ:

$$\tilde{H}_1 = \frac{1}{\sqrt{N}}\sum_{q,\lambda\neq\lambda'} f_{\lambda\lambda'}(q)C_\lambda^\dagger C_{\lambda'}(b_q + b_{-q}^\dagger). \tag{2.35}$$

It has been shown that under certain conditions, namely large enough electron-phonon coupling [18], the non-adiabatic corrections are small. The state vector of the system may then be represented in a perturbative regime as $|\psi_0\rangle + |\psi_1\rangle + \ldots$. In this work, we look for the eigenstates of the zeroth-order adiabatic hamiltonian $\tilde{H}_0$. For details of non-adiabatic corrections to the eigenstates see [19].

2.2.1 Electronic eigenstates in the adiabatic approximation

Consider the case of a semiconductor containing a small number of donor atoms. (Equivalently, acceptor atoms producing a model describing holes). One may then consider the effects of single quasiparticles. The state describing the quasiparticle in the band λ is:

$$|\psi_e\rangle = C_\lambda^\dagger |0\rangle_e |0\rangle_{ph}. \tag{2.36}$$

For any individual value of the band index λ, we can act with the creation operator $C_\lambda^\dagger$ no more than twice. This is due to the Pauli exclusion principle and the consideration of electron spin. In this work we consider only single quasi-particle effects. Some multi-particle states have been considered in [17]. In order to look for eigenstates the state (2.36) is operated on by $\tilde{H}_0$. This gives:

$$\tilde{H}_0 C_\lambda^\dagger |0\rangle = \left[W + E_\lambda + \frac{1}{\sqrt{N}} \sum_q [\hbar\omega(q)\beta(q) + f_{\lambda\lambda}^*(q)]b_q^\dagger + h.c.] \right] C_\lambda^\dagger |0\rangle, \tag{2.37}$$

where $|0\rangle = |0\rangle_e |0\rangle_{ph}$. Therefore the state (2.36) is an eigenstate of the hamiltonian $\hat{H}_0$ with energy $W + E_\lambda$, provided that the coefficients $\beta(q)$ of the unitary transformation U are chosen to satisfy the relation:

$$\hbar\omega(q)\beta(q) + f_{\lambda\lambda}^*(q) = 0. \tag{2.38}$$

We now have two equations (2.32) and (2.38) that determine the self-consistent quasi-particle states in the zeroth order adiabatic approximation. In order to transform these equations into a representation in real space we perform the Fourier transformation:

$$\phi_\lambda(k) = \frac{1}{\sqrt{N}} \sum_n \phi_\lambda(n)e^{-ikn},$$

$$\phi_\lambda(n) = \frac{1}{\sqrt{N}} \sum_n \phi_\lambda(k)e^{ikn}. \tag{2.39}$$

The fields $\phi_\lambda(n)$ are to be thought of as the probability amplitude to find the quasi-particle in the band λ at the site n. The transformation of equations (2.32) and (2.38) results in a pair of equations that express the relationships between the electron probability amplitude and the lattice displacements defined at each crystal site. The equations describe the self-consistent states of the electron and associated lattice deformation in the zeroth-order adiabatic approximation in the energy band λ. Note that there is a similar way to arrive at the equations, to which our attention now turns.

2.3 The semi-classical approximation

We now wish to illustrate the correspondence between the zeroth-order adiabatic approximation, and the semi-classical treatment of the tight-binding hamiltonian [17]. In the latter approximation one follows Davydov's original idea in minimizing the average value of the hamiltonian $\langle \Psi | \hat{H} | \Psi \rangle$. The semi-classical labelling of the method arises due to the classical treatment of the averge displacements u_n through the calculation of Hamilton's equations. Using the Davydov ansatz for the form of $|\Psi\rangle$ (2.26) in the site representation, and the properties of the coherent state (2.25), we arrive at the semi-classical hamiltonian:

$$
\begin{aligned}
H &= \langle \Psi | \hat{H} | \Psi \rangle \\
&= \sum_n \Bigg[(E_0 + W)|\phi_n|^2 - J[\phi_n^* \phi_{n+1} + \phi_n^* \phi_{n-1}] + \chi|\phi_n|^2 (u_{n+1} - u_{n-1}) \\
&\quad + G[\phi_n^* \phi_{n+1}(u_{n+1} - u_n) + \phi_n^* \phi_{n-1}(u_n - u_{n-1})] \Bigg],
\end{aligned}
\tag{2.40}
$$

where we have used the labelling u_n for the average value of the displacement of the site n, replacing the earlier labelling α_n. We also use ϕ_n to refer to the quantity $\phi_\lambda(n)$. The lattice potential energy is:

$$
W = \frac{1}{2} \sum_{n=1}^{N} \Bigg[M \left(\frac{\partial u_n}{\partial t} \right)^2 + K(u_{n+1} - u_n)^2 \Bigg].
\tag{2.41}
$$

In deriving the equations of motion, the basic assumption is that $|\psi_e\rangle$ is a solution to the time-dependent Schrödinger equation:

$$
i\hbar \frac{\partial}{\partial t} |\psi_e\rangle = \hat{H}|\psi_e\rangle
\tag{2.42}
$$

Where $\hat{H}$ in this case is the hamiltonian (2.13) written in the site representation. Acting from the left with $\langle\psi_e|$ on both sides of equation (2.42) and using the commutation relations (2.2), one is led to the following equation for the coefficients $\phi_n(t)$:

$$i\hbar\frac{\partial\phi_n}{\partial t} = (E_0 + W)\phi_n - J(\phi_{n+1} + \phi_{n-1}) + \chi\phi_n(u_{n+1} - u_{n-1})$$
$$+G[\phi_{n+1}(u_{n+1} - u_n) + \phi_{n-1}(u_n - u_{n-1})]; \qquad (2.43)$$

Utilizing the formulas for the expection values of Heisenberg operators:

$$i\hbar\frac{\partial}{\partial t}\langle\Phi(t)|\hat{u}_n|\Phi(t)\rangle = \langle\Phi(t)|[\hat{u}_n,\hat{H}]|\Phi(t)\rangle;$$
$$i\hbar\frac{\partial}{\partial t}\langle\Phi(t)|\hat{p}_n|\Phi(t)\rangle = \langle\Phi(t)|[\hat{p}_n,\hat{H}]|\Phi(t)\rangle \qquad (2.44)$$

We arrive at the equations of motion governing the displacement field:

$$M\frac{\partial^2 u_n}{\partial t^2} = K(u_{n+1} + u_{n-1} - 2u_n) + \chi(|\phi_{n+1}|^2 - |\phi_{n-1}^2|)$$
$$+G[\phi_n^*\phi_{n+1} - \phi_n^*\phi_{n-1} + c.c.]. \qquad (2.45)$$

Looking at equation (2.32) describing the condition on the field $\phi(k)$, one can see that this leads to the semi-classical hamiltonian and the Schrödinger equation for ϕ_n by multiplying both sides of (2.32) by $\phi^*(k)$ and summing over k. This equation then takes on a very similar form to the interaction term (2.15) written in k-space. The differences lie in the fact that the equation is now written in terms of the averaged normal coordinates $\beta(q)$ and the amplitudes ϕ_n. Since the coefficients ϕ_n and ϕ_k and the electron operators $\hat{a}_{k,\xi}$ and $c_{k,\xi}$ transform in the same way, the inverse transformation leads to the semi-classical hamiltonian (2.40). This can be checked by explicit calculation in the one-dimensional case. This illustrates the correspondence between the semi-classical regime and the zeroth-order adiabatic approximation. In order to consider the modelling of self-trapped conduction electron states in the zeroth-order adiabatic approximation in one dimension it is therefore sufficient to approach the problem in the semi-classical approximation.

The equations of motion (2.44,2.45) may be solved numerically, but one must also take into consideration the normalisation condition:

$$\sum_n |\phi_n|^2 = 1, \qquad (2.46)$$

which comes from the quasiparticle normalisation $\langle \psi_e | \psi_e \rangle = 1$. The stationary configurations can be found by either modelling the stationary equations or by introducing absorbative terms into the dynamic equations. Alternatively, one can find approximate analytical solutions to the stationary equations in 1d.

2.4 Path to the nonlinear Schrödinger equation

Back in our representation in k-space, one can use the constraints imposed upon the coefficients $\beta(q)$ described by equation (2.38), and substitute these into the equation governing the coefficients $\phi_\lambda(k)$ of the unitary transformation (2.32). This gives a single nonlinear equation governing the quasiparticle field amplitudes $\phi_\lambda(k)$ [19], [17]:

$$E(k)\phi_\lambda(k) - \frac{1}{N}\sum_{k,q}\frac{2|\Phi(k,q)|^2}{\hbar\omega(q)}\Gamma(q)\phi_\lambda(k-q) = E_\lambda\phi_\lambda(k), \qquad (2.47)$$

where:

$$\Gamma(q) = \sum_k \phi_\lambda(k)\phi_\lambda^*(k-q). \qquad (2.48)$$

This equation describes the electron configurations in the zeroth-order adiabatic approximation. We now turn to an analysis of this equation in the continuum limit. To begin it is necessary to define the function of the continuum variable x, which is the Fourier transform of the function $\phi_\lambda(k)$.

$$\phi_\lambda(x) = \frac{1}{\sqrt{N}}\sum_k \phi_\lambda(k)e^{ikx}, \qquad (2.49)$$

where the inverse transformation is:

$$\phi_\lambda(k) = \frac{1}{\sqrt{N}}\int_{-N/2}^{N/2}\phi_\lambda(x)e^{-ikx}dx. \qquad (2.50)$$

Under certain conditions, namely a long-wave approximation, the equation for the coefficients $\phi_\lambda(k)$ (2.32) reduces to a nonlinear Schrödinger equation [19]. By stating the long wave approximation, we assume that in real space the solution is given by a wave-packet that is sufficiently broad compared to the lattice spacing so that it is localized in k-space. Under these circumstances and setting the lattice spacing

$d = 1$:

$$\begin{aligned}
E(k) &\approx E_0 - 2J + Jk^2; \\
F(k,q) &\approx F(0,q) \approx 4\chi^2 q^2 \left(1 - \frac{q^2}{3}\right); \\
\omega(q) &\approx \frac{K}{M} \frac{q^2}{4} \left(1 + \frac{q^2}{12}\right).
\end{aligned}$$
(2.51)

Multiplying (2.45) by e^{ikx}, summing over k and taking into account (2.47) leads to the following equation:

$$\Lambda\phi_\lambda(x) + J\frac{d^2\phi_\lambda(x)}{dx^2} + \frac{G'}{N}|\phi_\lambda(x)|^2\phi_\lambda(x) = 0,$$
(2.52)

which is the well known nonlinear Schrödinger equation (NLSE) and $\Lambda = E_0 - E_\lambda - 2J$. The nonlinearity parameter is $G' = \frac{16K\chi^2}{M}$. This equation in one-dimension is well known to possess stable localized solutions, or solitons. In fact it is straightforward to show [15] that for $G = 0$ the system of discrete equations reduce down to a single discrete version of the nonlinear Schrödinger equation [68]. It is therefore evident that in the long-wave zeroth-order adiabatic approximation a conduction electron in interaction with the lattice degrees of freedom can occupy a spatially localized state. The eigenvalue Λ is:

$$\begin{aligned}
\Lambda &= -Jg_0^2; \\
g_0 &= \frac{G'}{4NJ},
\end{aligned}$$
(2.53)

and measures the energy of the quasiparticle in relation to the conduction band minimum specified in (2.6). The normalised solution to equation (2.50) is:

$$\phi(x) = \sqrt{\frac{g_0}{2}} \frac{1}{\cosh(g_0 x)}.$$
(2.54)

Figure 2.1 shows the quasiparticle probability density $|\phi(x)|^2$ for two different values of the parameter g_0. A higher value of the parameter g_0 corresponds to higher values of electron-phonon coupling and therefore a more strongly localized solution. The eigenvalue Λ depends quadratically upon the value of g_0, and hence a more localized solution has a more significant separation in energy from the conduction band minimum. For small values of the electron-phonon coupling one must consider the effects of more significant non-adiabaticity, and hence the zeroth-order adiabatic

approximation is invalid. Secondly, for extremely well localized solutions with soliton width comparable to the lattice spacing, the long wave approximation is invalid, however this approximation is not needed for the case $G = 0$, where the long-wave approximation is not required.
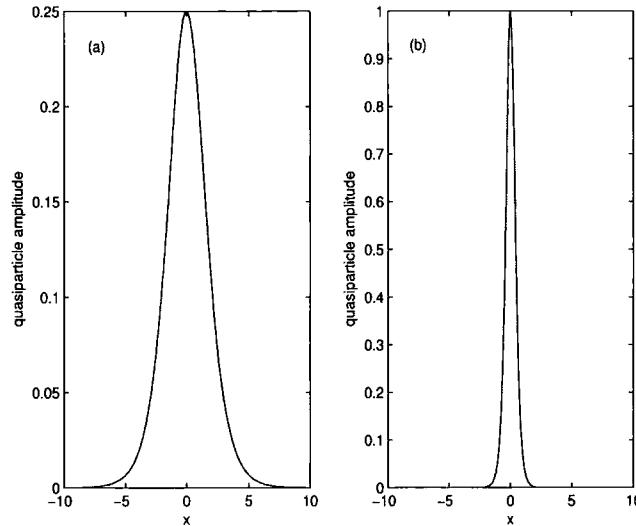
Figure 2.1: *Normalised solutions of the nonlinear Schrödinger equation (2.50) showing the quasiparticle probability density $|\phi(x)|^2$ in the continuum limit. The lattice spacing was set to $d = 1$, other parameters were $J = 1, K = 1$ and $M = 1$. The figures show curves for two different values of g_0: (a) $g_0 = 0.5$, $\Lambda = -0.25$; (b) $g_0 = 2.0$, $\Lambda = -4.0$.*

2.5 Summary

To conclude this chapter we summarise the material discussed. We have described the formulation of a theory of a small number of conduction electrons in a crystal, i.e. where electron-electron correlations are neglected. The model was derived in the tight-binding approximation in which only nearest-neighbour interactions are included. Upon allowing small displacements of the atoms about their equilibrium positions, one was led to consider first-order corrections to the electron energy due to the electron-phonon interaction. This led to a hamiltonian which, when writ-

ten in second quantised form, depends upon the electron creation and annihilation operators at each site, and the operators of atomic displacement.

A transformation of the hamiltonian into wavenumber space showed that the hamiltonian can be represented in the Frölich form, with a certain function $\Phi(k, q)$ describing the details of the electron-phonon interaction. We then looked for quasiparticle solutions in the adiabatic approximation, following the method in [66], where the wavefunction separates into two parts governing the electronic and atomic degrees of freedom. The state vector is represented by a unitary operator of coherent atomic displacement acting upon the quasiparticle vacuum. This process encourages one to consider the eigenstates of a transformed hamiltonian, which is in a more natural representation with which to consider localized states. Self-consistent eigenstates were found in the zeroth-order adiabatic approximation under the condition that the electron and lattice degrees of freedom were related in a certain specified way. The zeroth-order adiabatic approximation is valid in the limit of sufficiently strong electron-phonon coupling [18], and so such in this limit the models may be physically useful.

An alternative route to the self-consistent stationary equations involves the semiclassical treatment first considered by Davydov [5]. This involves a quantum mechanical treatment of the electron field, while the average atomic displacements are described classically. The analysis involves minimizing the average value of the hamiltonian ($\langle\Psi|\hat{H}|\Psi\rangle$), the evolution of which is described by the Schrödinger equation for the electron field and Hamilton's equation for the classically described site displacements. In the stationary limit these equations are identical to the self-consistent adiabatic equations describing the electron probability amplitude and the atomic displacements.

In the continuum limit the system of equations lead to a nonlinear Schrödinger equation describing the electron field. This equation is well known to posses stable localized solutions, which describe the situation where it is energetically favourable for the conduction electron to become spatially localized within the crystal, accompanied by a local deformation of the lattice.

In this chapter we have discussed a selection of tools that prove useful in looking

for localized quasiparticles in atomic chains. The subject of the remainder of the thesis is to show how these ideas were applied to lattices relating to carbon nanotubes. We begin in the next chapter with a discussion of localized quasiparticle states in the two-dimensional hexagonal lattice.

Chapter 3

Quasiparticle trapping in an hexagonal lattice

In this chapter we formulate a model describing the interactions of a single conduction electron with lattice site displacements in a hexagonal lattice. First-order interactions of both the electron on-site energy and the exchange interaction energy with the lattice displacements are considered. The hamiltonian, written down in the tight-binding approximation and physical site representation, is shown to correspond to a Frölich hamiltonian after a transformation into k-space. The stationary equations are then found in the zeroth-order adiabatic approximation, and these are found to correspond to the semi-classical Hamiltonian and dynamic equations of motion in the site representation. Much of the work is similar to that introduced in our collaboration paper [77], which describes the case of zig-zag or armchair tubes. The method discussed here considers a different tiling of the hexagonal lattice, which leads to a more straightforward diagonalization of the electron and phonon hamiltonians and is readily generalizable to nanotubes of arbitrary chirality in the zone-folding approximation (see chapters 5 and 6).

3.1 Introduction

The main aim of this chapter is to apply the tools presented in chapter 2 to the case of a 2d lattice - namely the hexagonal lattice. As discussed previously, the

behaviour of conduction electrons in these lattices may give an initial insight into the properties of carbon nanotubes, due to the close relationship between the two lattices. The model presented in this section is more complicated for two principle reasons: (a) the lattice involved is studied in two-dimensions; (b) the hexagonal lattice has a two-atom basis. The latter of these two is the single most complicating factor. The extra atom in the basis results in a more complex diagonalization of the electron and phonon parts of the tight-binding hamiltonian. Because of this the function $\Phi(k, q)$, that contains the details of the electron-phonon interaction in the Frölich hamiltonian, is complicated. We begin with a discussion of the geometry that is the origin of these technicalities.

3.2 Hexagonal lattice geometry

The hexagonal lattice is an oblique lattice with a basis of two atoms (figure 3.1). This structure is found in graphite, which consists of 2d hexagonal planes of carbon atoms stacked on top of one another. The inter-plane separation (3.35A) is large compared with the nearest neighbour distance in the hexagonal lattice (1.42A). Since interactions between separate planes are weak, studying a single 2d plane gives significant clues as to the behaviour of conduction electrons in bulk graphite. The electronic configuration of an isolated carbon atom in its ground state is $1s^2 \, 2s^2 \, 2p^2$ [22]. In two-dimensional graphite, one of the $2s$ and the two $2p$ orbitals undergo a hybridisation in order to create three in-plane σ-bonds separated by angles of 120°. There also exists one out-of-plane π-bond per carbon atom. It is this bonding structure that leads to the hexagonal geometry depicted in figure 3.1.

3.2.1 Coordinates

The primitive lattice vectors a_1 and a_2 are shown in figure 3.1. Note that this particular choice for the primitive vectors was taken to avoid confusion with the main reference for the geometry of carbon nanotubes [22]. The nearest neighbour
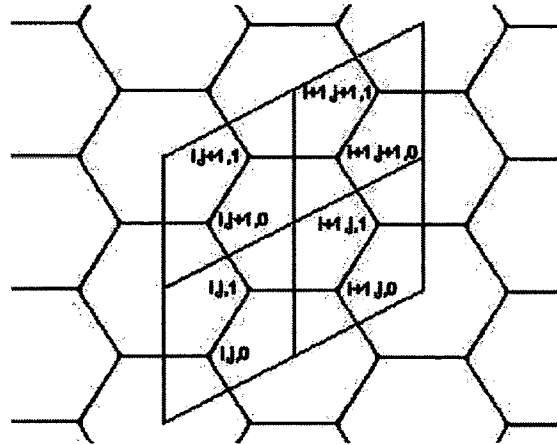
Figure 3.1: *Geometry of the 2d hexagonal lattice, which is oblique and has a basis of two atoms. Each atom is labelled by the integers (i, j, ρ)*

separation is $d = |\mathbf{a}_1|/\sqrt{3}$. In terms of cartesian coordinates:

$$\mathbf{a}_1 = a\left(\frac{\sqrt{3}}{2}, \frac{1}{2}\right); \qquad \mathbf{a}_2 = a\left(\frac{\sqrt{3}}{2}, -\frac{1}{2}\right) \tag{3.1}$$

We choose a tiling of the hexagonal lattice such that each primitive cell is labelled by two integers (i, j), where the position vector of each cell is $R_{i,j} = i\mathbf{a}_1 + j(\mathbf{a}_1 - \mathbf{a}_2)$. The two atoms in the basis are denoted as $\rho = 0, 1$ respectively, thus each atom is labelled by the three integers (i, j, ρ). Taking the origin of coordinates to lie on the atom labelled by $\rho = 0$, the atomic site vectors are:

$$\begin{aligned} R_{i,j,\rho} &= r_1\mathbf{a}_1 + R_2\mathbf{a}_2 \\ R_1 &= i + j + \frac{2\rho}{3}; \qquad R_2 = -j - \frac{\rho}{3} \end{aligned} \tag{3.2}$$

In order to ease reference to the nearest neighbours of each site, it is convenient to define the following indices functions [76]:

$$\begin{aligned} r(i, j, 0) &= (i, j, 1); & r(i, j, 1) &= (i, j, 0); \\ l(i, j, 0) &= (i - 1, j, 1); & l(i, j, 1) &= (i + 1, j, 0); \\ d(i, j, 0) &= (i, j - 1, 1); & d(i, j, 1) &= (i, j + 1, 0), \end{aligned} \tag{3.3}$$

where r, l, d refer to the three nearest neighbours of each site (figure 3.2). Notice that the atoms labelled by $\rho = 0$ are related to the $\rho = 1$ atoms by a rotation of the
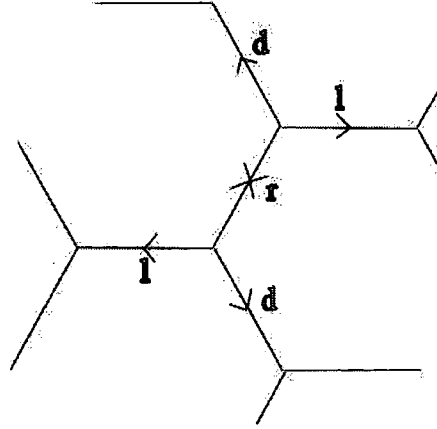
Figure 3.2: *Labelling of the nearest neighbours*

lattice by 180°, and vice-versa, so that $rr(i,j,\rho) = dd(i,j,\rho) = ll(i,j,\rho) = (i,j,\rho)$. We now define the lattice vectors adjoining nearest neighbours:

$$D\delta^0_{i,j,\rho} = R_{\delta(i,j,\rho)} - R_{i,j,\rho}, \tag{3.4}$$

where the object δ can represent any of the three indices operators r, l, d. In order to construct the hamiltonian it is necessary to consider small displacements of the lattice sites about their equilibrium positions.

3.2.2 Site displacements

Corresponding to each nearest-neighbour pair in the lattice, we construct a displacement vector which measures the deviation of the lattice vectors under individual site displacements from their equilibrium positions in the pure crystal:

$$d\delta_{i,j,\rho} = (u_{\delta(i,j,\rho)} - u_{i,j,\rho})\mathbf{e_x} + (v_{\delta(i,j,\rho)} - v_{i,j,\rho})\mathbf{e_y}. \tag{3.5}$$

The quantities u and v are the individual site displacements in the cartesian coordinate system:

$$u_{i,j,\rho} = |u_{i,j,\rho}|\mathbf{e_x};$$
$$v_{i,j,\rho} = |v_{i,j,\rho}|\mathbf{e_y}. \tag{3.6}$$

We now calculate the magnitude of the nearest neighbour separations:

$$|D\delta^0_{i,j,\rho} + d\delta_{i,j,\rho}| \approx d + \frac{D\delta^0_{i,j,\rho} \cdot d\delta_{i,j,\rho}}{d} = d + W\delta_{i,j,\rho}. \tag{3.7}$$

The magnitude has been expanded to first-order in the site displacements u and v. Thus the quantity $W\delta$ gives the first order correction due to site displacements of the tight-binding bond specified by δ. This is important in allowing the construction of the tight-binding hamiltonian in analogy to the 1d chain discussed in the previous chapter. The first order expressions for the $W\delta$'s can be written in the compact form:

$$
\begin{aligned}
Wr_{i,j,\rho} &= \frac{(-1)^\rho}{2}(u_{r(i,j,\rho)} - u_{i,j,\rho}) + \frac{\sqrt{3}(-1)^\rho}{2}(v_{r(i,j,\rho)} - v_{i,j,\rho}); \\
Wl_{i,j,\rho} &= (-1)^\rho(u_{i,j,\rho} - u_{l(i,j,\rho)}); \\
Wd_{i,j,\rho} &= \frac{(-1)^\rho}{2}(u_{d(i,j,\rho)} - u_{i,j,\rho}) + \frac{\sqrt{3}(-1)^\rho}{2}(v_{i,j,\rho} - v_{d(i,j,\rho)}).
\end{aligned}
\tag{3.8}
$$

We are now in a position to turn to the formulation of the tight-binding hamiltonian on the hexagonal lattice.

3.3 Hamiltonian

3.3.1 Tight-binding hamiltonian

The tight-binding hamiltonian is written down again as a sum of three parts, the first part describing the conduction electron, the second the lattice potential and the third the electron-phonon interaction.

$$
\hat{H} = \hat{H}_e + \hat{H}_{ph} + \hat{H}_{int}.
\tag{3.9}
$$

The tight-binding electron hamiltonian is:

$$
\hat{H}_e = \sum_{i,j,\rho}\left[E_0 a^\dagger_{i,j,\rho}a_{i,j,\rho} - J\sum_\delta a^\dagger_{i,j,\rho}a_{\delta(i,j,\rho)} \right],
\tag{3.10}
$$

where $a^\dagger_{i,j,\rho}$ and $a_{i,j,\rho}$ are the electron creation and annihilation operators at the site (i, j, ρ), E_0 is the on-site energy and J gives the strength of the exchange interaction. In this case the on-site energy E_0 is equal to the $2p$ orbital energy. This is however different to the energy of the $2p$ orbital in an isolated atom because of the presence of the crystal potential. The obvious choice for the classical phonon hamiltonian involves a sum of terms quadratic in the displacement magnitudes $W\delta$:

$$
\hat{H}_{ph} = \frac{1}{2}\sum_{i,j,\rho}\left(\frac{p^2_{i,j,\rho}}{M} + \frac{q^2_{i,j,\rho}}{M} + KWr^2_{i,j,\rho} + KWl^2_{i,j,\rho} + KWd^2_{i,j,\rho} \right).
\tag{3.11}
$$

where $p_{i,j,\rho}$ and $q_{i,j,\rho}$ are the momenta conjugated to $u_{i,j,\rho}$ and $v_{i,j,\rho}$ respectively and K is the lattice elasticity coefficient. However, looking in the continuum limit, the terms v_x and u_y appear only in the combination $(v_x + u_y)^2$, which implies that the phonon hamiltonian given above contains a zero-mode. This zero mode arises due to the fact that central forces between neighbouring sites in the hexagonal lattice are not enough to provide lattice stability. The zero mode corresponds to a global stretching in one dimension and a compression in the other dimension. In the physical system that we are attempting to describe, bond interactions depend in a complicated manner upon the geometry of the overlapping electronic wavefunctions. Such interactions cannot be written accurately in terms of central terms only. We therefore chose to add well chosen non-central terms in order to exterminate the zero modes and provide a stable lattice. These were chosen in such a way that when we look in the coninuum limit, the first-order terms in the hamiltonian for the fields u and v were the square of their gradients. The added term is:

$$V_\Omega = \frac{1}{2} \sum_{i,j,\rho} \left(K\Omega r_{i,j,\rho}^2 + K\Omega l_{i,j,\rho}^2 + K\Omega d_{i,j,\rho}^2 \right), \tag{3.12}$$

where:

$$\begin{aligned}
\Omega r_{i,j,\rho} &= \frac{\sqrt{3}(-1)^\rho}{2}(u_{r(i,j,\rho)} - u_{i,j,\rho}) - \frac{(-1)^\rho}{2}(v_{r(i,j,\rho)} - v_{i,j,\rho}); \\
\Omega l_{i,j,\rho} &= (-1)^\rho(v_{l(i,j,\rho)} - v_{i,j,\rho}); \\
\Omega d_{i,j,\rho} &= \frac{\sqrt{3}(-1)^\rho}{2}(u_{d(i,j,\rho)} - u_{i,j,\rho}) - \frac{(-1)^\rho}{2}(v_{i,j,\rho} - v_{d(i,j,\rho)}).
\end{aligned} \tag{3.13}$$

Finally we must consider the electron-phonon interaction, where we include first order corrections to the electron on-site and exchange interaction energies dependent upon the lattice displacements:

$$\hat{H}_{int} = \sum_{i,j,\rho} \left[\chi a_{i,j,\rho}^\dagger a_{i,j,\rho} \sum_\delta \hat{W}\delta_{i,j,\rho} + G \sum_\delta a_{i,j,\rho}^\dagger a_{\delta(i,j,\rho)} \hat{W}\delta_{i,j,\rho} \right], \tag{3.14}$$

where χ and G are the electron-phonon coupling constants for the respective modulation of the on-site and exchange energies. Note that previous studies of electron-phonon interactions in a hexagonal lattice [51] concentrated exclusively upon the term proportional to χ and assumed a constant exchange interaction. However

there is an important dependence of the exchange energy upon the lattice displacements that must be considered [59]. The role of the strength of the parameter G in determining the ground state configuration in the adaiabatic approximation is explored intensively in chapter 4, where the results of numerical investigations into the semi-classical equations are discussed.

3.3.2 Diagonalization of the electron and phonon hamiltonians

Before the transformation of the hamiltonian into the Frölich form can take place, it is imperitive that the electron and phonon hamiltonians are diagonalized. The diagonalization procedures are slightly complicated by the two-atom basis. Let us first turn our attention to the electron hamiltonian. The first stage is to transform the creation operator for the electron from the site representation into its representation in **k**-space. Due to the inequivalence of the sites $\rho = 0, 1$, the creation operators at each of the two basis sites must be considered individually. The first stage of the diagonalization is to represent the electron fermionic operators in **k**-space:

$$\hat{a}_{i,j,\rho} = \frac{1}{\sqrt{N_c}} \sum_{\mathbf{k},\xi} e^{i\mathbf{k}.\mathbf{r}_{i,j}} \tilde{a}_{\mathbf{k},\rho}, \tag{3.15}$$

where N_c is the number of primitive cells in the crystal. Contrary to the case of the 1d chain, we have two sets of fermion operators, corresponding to $\rho = 0, 1$. Performance of this Fourier transform on the electron hamiltonian (3.10) results in the expression:

$$\hat{H}_e = \sum_k \left[E_0 (\tilde{a}^\dagger_{\mathbf{k},0} \tilde{a}_{\mathbf{k},0} + \tilde{a}^\dagger_{\mathbf{k},1} \tilde{a}_{\mathbf{k},1}) \right.$$
$$\left. -J \left((1 + e^{-i\mathbf{k}.\mathbf{a_1}} + e^{-i\mathbf{k}.(\mathbf{a_1}-\mathbf{a_2})}) \tilde{a}^\dagger_{\mathbf{k},0} \tilde{a}_{\mathbf{k},1} + h.c. \right) \right], \tag{3.16}$$

where the following relation has been used:

$$\sum_{i,j} e^{i(\mathbf{k}-\mathbf{k}').\mathbf{r}_{i,j}} = N_c \delta_{\mathbf{k}-\mathbf{k}'}. \tag{3.17}$$

This relation applies to all Bravais lattices, a group to which the underlying oblique structure of the hexagonal lattice belongs [1]. The electron hamiltonian is then fully

diagonalized by performing the following unitary transformation:

$$\tilde{a}_{\mathbf{k},0} = \frac{1}{\sqrt{2}}(e^{-\frac{i}{2}\theta}c_{\mathbf{k},0} + e^{-\frac{i}{2}\theta}c_{\mathbf{k},1});$$

$$\tilde{a}_{\mathbf{k},1} = \frac{1}{\sqrt{2}}(e^{\frac{i}{2}\theta}c_{\mathbf{k},0} - e^{\frac{i}{2}\theta}c_{\mathbf{k},1}), \tag{3.18}$$

where the angle θ is the argument of the complex number $1 + e^{-i\mathbf{k}.\mathbf{a_1}} + e^{-i\mathbf{k}.(\mathbf{a_1}-\mathbf{a_2})}$ which appears in equation (3.16):

$$\tan\theta = \frac{\sin(\mathbf{k}.\mathbf{a_1}) + \sin(\mathbf{k}.(\mathbf{a_1} - \mathbf{a_2}))}{1 + \cos(\mathbf{k}.\mathbf{a_1}) + \cos(\mathbf{k}.(\mathbf{a_1} - \mathbf{a_2}))}. \tag{3.19}$$

After the application of the transformations (3.18), the electron hamiltonian is cast into the form:

$$\hat{H}_{el} = \sum_{\mathbf{k},\xi} E_\xi(\mathbf{k})c_{\mathbf{k},\xi}^\dagger c_{\mathbf{k},\xi}, \tag{3.20}$$

where the parameter $\xi = 0, 1$ enumerates the energy bands. The electron energy dispersion is:

$$E_\xi(\mathbf{k}) = \epsilon_0 \pm J\sqrt{1 + 4\cos\left(\frac{\sqrt{3}a}{2}k_x\right)\cos\left(\frac{a}{2}k_y\right) + 4\cos^2\left(\frac{a}{2}k_y\right)}. \tag{3.21}$$

The $\pm$ sign in this expression gives the energies of the two individual electron energy bands $\xi = 0, 1$. We take $\xi = 0$ to correspond to the band which is lower in energy. The next stage is to diagonalize the phonon hamiltonian.

There are two atoms in the crystal basis, each with two vibrational degrees of freedom, hence we expect to describe four vibrational branches in the phonon spectrum. The addition of the terms involving $\Omega\delta$ required to remove the zero modes from the lattice potential results in a de-coupling of the u and v displacement fields. This can be seen explicitly by fully expanding $\hat{H}_{ph}$ using the expressions (3.8) and (3.13) for the fields $W\delta$ and $\Omega\delta$. The phonon hamiltonian therefore decouples into two separate pieces. Furthermore, the separate potentials for u and v are identical in their structure. The expanded phonon hamiltonian is:

$$\hat{H}_{ph} = \frac{1}{2}\sum_{i,j,\rho}\left(\frac{\hat{p}_{i,j,\rho}^\dagger \hat{p}_{i,j,\rho}}{M} + \frac{\hat{q}_{i,j,\rho}^\dagger \hat{q}_{i,j,\rho}}{M} + \sum_\delta K\left[(\hat{u}_{i,j,\rho} - \hat{u}_{\delta(i,j,\rho)})^\dagger(\hat{u}_{i,j,\rho} - \hat{u}_{\delta(i,j,\rho)})\right.\right.$$
$$\left.\left. + (\hat{v}_{i,j,\rho} - \hat{v}_{\delta(i,j,\rho)})^\dagger(\hat{v}_{i,j,\rho} - \hat{v}_{\delta(i,j,\rho)})\right]\right). \tag{3.22}$$

In order to diagonalize we transform into wavevector $(\mathbf{q})$ space:

$$\hat{u}_{i,j,\rho} = \frac{1}{\sqrt{N_c}} \sum_{\mathbf{q}} e^{i\mathbf{k}.\mathbf{r}_{i,j}} \tilde{u}_{\mathbf{q},\rho}; \quad \hat{v}_{i,j,\rho} = \frac{1}{\sqrt{N_c}} \sum_{\mathbf{q}} e^{i\mathbf{k}.\mathbf{r}_{i,j}} \tilde{v}_{\mathbf{q},\rho};$$

$$\hat{p}_{i,j,\rho} = \frac{1}{\sqrt{N_c}} \sum_{\mathbf{q}} e^{-i\mathbf{k}.\mathbf{r}_{i,j}} \tilde{p}_{\mathbf{q},\rho}; \quad \hat{q}_{i,j,\rho} = \frac{1}{\sqrt{N_c}} \sum_{\mathbf{q}} e^{-i\mathbf{k}.\mathbf{r}_{i,j}} \tilde{q}_{\mathbf{q},\rho}. \quad (3.23)$$

The kinetic terms remain diagonal under the Fourier transformation. Because of the similarity between the terms in u and v, we consider here only the terms in u. After Fourier transformation the terms in u become:

$$\hat{H}_{ph(u)} = K \sum_{q} \left[2(\tilde{u}_{\mathbf{q},0}^{\dagger} \tilde{u}_{\mathbf{q},0} + \tilde{u}_{\mathbf{q},1}^{\dagger} \tilde{u}_{\mathbf{q},1}) \right.$$

$$\left. -\tilde{u}_{\mathbf{q},1}^{\dagger} \tilde{u}_{\mathbf{q},0}[1 + e^{-i\mathbf{q}.\mathbf{a_1}} + e^{-i\mathbf{q}.(\mathbf{a_1}-\mathbf{a_2})}] \right]. \quad (3.24)$$

This expression is formally extremely similar to the partially diagonalized electron hamiltonian (3.16). Full diagonalization therefore proceeds in an identical method to that considered for the electron hamiltonian:

$$\tilde{u}_{\mathbf{q},0} = \frac{1}{\sqrt{2}}(e^{-\frac{i}{2}\gamma} Q_{\mathbf{q},0} + e^{-\frac{i}{2}\gamma} Q_{\mathbf{q},1});$$

$$\tilde{u}_{\mathbf{q},0} = \frac{1}{\sqrt{2}}(e^{\frac{i}{2}\gamma} Q_{\mathbf{q},0} - e^{\frac{i}{2}\gamma} Q_{\mathbf{q},1}); \quad (3.25)$$

$$\tan\gamma = \frac{\sin(\mathbf{q}.\mathbf{a_1}) + \sin(\mathbf{q}.(\mathbf{a_1} - \mathbf{a_2}))}{1 + \cos(\mathbf{q}.\mathbf{a_1}) + \cos(\mathbf{q}.(\mathbf{a_1} - \mathbf{a_2}))}. \quad (3.26)$$

The diagonalization procedure transforms the phonon hamiltonian into the following form:

$$\hat{H}_{ph} = \sum_{\mathbf{q},\tau} M\omega_{\tau}^2(\mathbf{q}) Q_{\mathbf{q},\tau}^{\dagger} Q_{\mathbf{q},\tau}, \quad (3.27)$$

where the $Q_{\mathbf{q},\tau}$ are the normal coordinates of the crystal vibrations and $\tau = 0, 1$ enumerates the vibrational branches relating to the diagonalization of the u coordinates. There are another pair of normal coordinates relating to the v diagonalization and these are denoted as $\tau = 2, 3$. These coordinates have identical dispersion relations specified by:

$$M\omega_{\tau}^2(\mathbf{q}) = 2 \pm \sqrt{1 + 4\cos\left(\frac{\sqrt{3}a}{2}q_x\right)\cos\left(\frac{a}{2}q_y\right) + 4\cos^2\left(\frac{a}{2}q_y\right)}, \quad (3.28)$$

and so $\omega_0(\mathbf{q}) = \omega_2(\mathbf{q}), \omega_1(\mathbf{q}) = \omega_3(\mathbf{q})$. The electrons are now specified by the quantum numbers $\xi = 0, 1$ (band index) and wavevector $\mathbf{k}$. The atomic quantum numbers are the branch number $\tau = 0, 1, 2, 3$ and wavevector $\mathbf{q}$. These wavevectors obey the Born-von Karman periodic boundary condition.

Since the phonon hamiltonian is now diagonalized, one can follow the usual procedure of the quantum harmonic oscillator and introduce the bosonic creation and annihilation operators of phonons:

$$Q_{\mathbf{q},\tau} = \sqrt{\frac{\hbar}{2M\omega_\tau(\mathbf{q})}}(\tilde{b}^\dagger_{-\mathbf{q},\tau} + \tilde{b}_{\mathbf{q},\tau}). \tag{3.29}$$

The operator $\tilde{b}^\dagger_{\mathbf{q},\tau}$ creates a phonon of wavevector $\mathbf{q}$ in the vibrational branch τ. Any crystal vibration can be expressed as a combination of these modes. Transformation of the phonon hamiltonian gives (ignoring the zero-point energy):

$$\hat{H}_{ph} = \sum_{\mathbf{q}} \hbar\omega_\tau(\mathbf{q})\tilde{b}^\dagger_{\mathbf{q},\tau}\tilde{b}_{\mathbf{q},\tau}. \tag{3.30}$$

The transformations that have been applied in order to diagonalize the electron and phonon hamiltonians must now be performed upon the interaction hamiltonian $\hat{H}_{int}$ (2.14). This results in the following form:

$$\hat{H}_{int} = \frac{1}{2\sqrt{2N_c}} \sum_{\mathbf{q},\mathbf{k},\xi,\xi',\tau} F(\mathbf{k}, \mathbf{q})c^\dagger_{\mathbf{k},\xi}c_{\mathbf{k}-\mathbf{q},\xi'}Q_{\mathbf{q},\tau}. \tag{3.31}$$

The complicated function $F(\mathbf{k}, \mathbf{q})$ depends upon the values of the coupling constants χ_1 and G_2 and the angles given by (3.19) and (3.26):

$$\begin{aligned}
F_{\xi,\xi',\tau}(\mathbf{k}, \mathbf{q}) &= G_2\Bigg[(-1)^{\xi'+1}\left(e^{i(\theta+\frac{\gamma}{2})}f_\tau(\mathbf{k}) + (-1)^{\tau+1}e^{i(\theta-\frac{\gamma}{2})}f_\tau(\mathbf{k} - \mathbf{q})\right) \\
&\quad + (-1)^{\xi+1}\left(e^{-i(\theta-\frac{\gamma}{2})}f^*_\tau(\mathbf{k} - \mathbf{q}) + (-1)^\tau e^{-i(\theta+\frac{\gamma}{2})}f^*_\tau(\mathbf{k})\right)\Bigg] \\
&\quad + \frac{\chi_1}{2}\left[(-1)^\tau f_\tau(\mathbf{q})e^{i\frac{\gamma}{2}} - (-1)^{(\xi-\xi')}f^*_\tau(\mathbf{q})e^{-i\frac{\gamma}{2}}\right],
\end{aligned} \tag{3.32}$$

where the functions $f_\tau(\mathbf{k})$ are:

$$\begin{aligned}
f_\tau(\mathbf{k}) &= 2e^{-i\mathbf{k}\cdot\mathbf{a_1}} - e^{-i\mathbf{k}\cdot(\mathbf{a_1}-\mathbf{a_2})} - 1 &(\tau = 0, 1); \\
f_\tau(\mathbf{k}) &= \sqrt{3}e^{-i\mathbf{k}\cdot(\mathbf{a_1}-\mathbf{a_2})} - 1 &(\tau = 2, 3). \tag{3.33}
\end{aligned}$$

Then:

$$\hat{H}_{int} = \frac{1}{2\sqrt{2N_c}} \sum_{\mathbf{q},\mathbf{k},\xi,\xi',\tau} \Phi(\mathbf{k},\mathbf{q}) c_{\mathbf{k},\xi}^\dagger c_{\mathbf{k}-\mathbf{q},\xi'} (\tilde{b}_{-\mathbf{q},\tau}^\dagger + \tilde{b}_{\mathbf{q},\tau}), \qquad (3.34)$$

where

$$\Phi_{\xi,\xi',\tau}(\mathbf{k},\mathbf{q}) = \sqrt{\frac{\hbar}{2M\omega_\tau(\mathbf{q})}} F_{\xi,\xi',\tau}(\mathbf{k},\mathbf{q}). \qquad (3.35)$$

The system hamiltonian is now completely expressed in the form of a Frölich Hamiltonian. Comparing this to the Frölich hamiltonian considered in the case of the 1d atomic chain (2.16), the hamiltonian now depends upon the wave-vectors $\mathbf{k}$ and $\mathbf{q}$ as opposed to wavenumbers k and q. Furthermore, the function $\Phi(\mathbf{k},\mathbf{q})$ is considerably more complicated in the hexagonal system. The interaction hamiltonian also describes phonon induced transitions between the electron energy bands labelled by ξ, whereas before we had only a single energy band. As in the case of the 1d chain, the next stage involves searching for the approximate eigenstates of the system by invoking the adiabatic approximation.

3.4   Adiabatic approximation

In order to find the eigenstates we follow the method of [17] and [19] that was introduced in chapter 2, and that has been generalized to armchair and zig-zag nanotubes [76]. Here we use a different tiling and do not separate the wavevectors into circumferential and axial components. By applying the adiabatic approximation we are looking for state-vectors in the form:

$$|\Psi\rangle = U|\psi_e\rangle \qquad (3.36)$$

where U is a unitary operator of coherent atomic displacements induced by the presence of a quasiparticle:

$$U = \exp\left[\sum_{\mathbf{q},\tau}(\beta_\tau(\mathbf{q}) b_{\mathbf{q},\tau}^\dagger - \beta_\tau^*(\mathbf{q}) b_{\mathbf{q},\tau})\right] \qquad (3.37)$$

and $|\psi_e\rangle$ is the wavefunction of the quasi-particle itself, which obeys the normalisation condition $\langle\psi_e|\psi_e\rangle = 1$. There now exists one coefficient $\beta_\tau(\mathbf{q})$ of the unitary

transformation corresponding to each of the the allowed wave-vectors ($\mathbf{q}$) in each vibrational branch labelled by τ. These coefficients are to be determined when attempting to find the self-consistent eigenstates in the zeroth-order adiabatic approximation.

The Schrödinger equation for the total wavefunction $H|\Psi\rangle = E|\Psi\rangle$ leads to the following equation governing the quasiparticle wavefunction:

$$\tilde{H}|\psi_e\rangle = E|\psi_e\rangle \tag{3.38}$$

$$\tilde{H} = U^\dagger H U = W + \tilde{H}_e + H_{int} + H_{ph} + H_d \tag{3.39}$$

where, in analogy to the 1d case:

$$W = \sum_{\mathbf{q},\tau} \hbar\omega_\tau(\mathbf{q})|\beta_\tau(\mathbf{q})|^2 \tag{3.40}$$

gives the energy of the lattice deformation, where the coefficients β in $\mathbf{q}$-space are linked to the actual atomic displacements u and v in real space. H_{int} and H_{ph} are as they appear in the untransformed hamiltonian. The part of the hamiltonian $\tilde{H}$ that is dependent only upon the electron creation/annihilation operators, $\tilde{H}_e$ is:

$$\tilde{H}_e = \sum_{\mathbf{k},\xi} E_\xi(\mathbf{k})c^\dagger_{\mathbf{k},\xi}c_{\mathbf{k},\xi} +$$
$$+ \frac{1}{2\sqrt{2N_c}} \sum_{\mathbf{k},\mathbf{q},\xi,\xi',\tau} F_{\xi,\xi',\tau}(\mathbf{k},\mathbf{q})Q_\tau(\mathbf{q})c^\dagger_{\mathbf{k},\xi'}c_{\mathbf{k}-\mathbf{q},\xi}, \tag{3.41}$$

where:

$$Q_\tau(\mathbf{q}) = \langle\beta_\tau(\mathbf{q})|Q_{\mathbf{q},\tau}|\beta_\tau(\mathbf{q})\rangle \tag{3.42}$$

Referring to the discussion of the coherent state in section 2.2, the state labelled by the coefficient $\beta_\tau(\mathbf{q})$ is a right eigenstate of the phonon annihilation operator. It is also a left eigenstate of the phonon creation operator:

$$b_{\mathbf{q},\tau}|\beta_\tau(\mathbf{q})\rangle = \beta_\tau(\mathbf{q})|\beta_\tau(\mathbf{q})\rangle;$$
$$\langle\beta_\tau(\mathbf{q})|b^\dagger_{\mathbf{q},\tau} = \langle\beta_\tau(\mathbf{q})|\beta^*_\tau(\mathbf{q}), \tag{3.43}$$

Thus, from (3.29):

$$
\begin{aligned}
\langle \beta_\tau(\mathbf{q})|Q_{\mathbf{q},\tau}|\beta_\tau(\mathbf{q})\rangle &= \sqrt{\frac{\hbar}{2M\omega_\tau(\mathbf{q})}} \langle \beta_\tau(\mathbf{q})|(b^\dagger_{-\mathbf{q},\tau} + b_{\mathbf{q},\tau})|\beta_\tau(\mathbf{q})\rangle, \\
&= \sqrt{\frac{\hbar}{2M\omega_\tau(\mathbf{q})}}(\beta^*_\tau(\mathbf{q}) + \beta_\tau(\mathbf{q})).
\end{aligned}
\tag{3.44}
$$

The other extra term that appears in the hamiltonian due to unitary operator U that will later be used to determine the coefficients of the unitary transformation U, and therefore the deformational potential of the quasiparticle is:

$$
H_d = \sum_{\mathbf{q},\tau} \hbar\omega_\tau(\mathbf{q})(\beta^*_\tau(\mathbf{q})b^\dagger_{\mathbf{q},\tau} + \beta_\tau(\mathbf{q})b_{\mathbf{q},\tau}).
\tag{3.45}
$$

The hamiltonian is now in a more natural from with which to investigate localized solutions. We now wish to perform a unitary transformation on the quasiparticle creation and annihilation operators in order to partially diagonalize the hamiltonian, again applying the method developed in [66]. The coefficients of this transformation are determined by the condition that the part of the hamiltonian dependent only upon the quasiparticle creation / annihilation operators $(\tilde{H}_e)$ is diagonal. The transformation is:

$$
c_{\mathbf{k},\xi} = \sum_\lambda \phi_{\lambda,\xi}(\mathbf{k})C_\lambda,
\tag{3.46}
$$

which converts $\tilde{H}_e$ into the diagonal form:

$$
\tilde{H}_e = \sum_\lambda E_\lambda C^\dagger_\lambda C_\lambda,
\tag{3.47}
$$

and where the subscript λ refers to the energy bands of the quasi-particle in the deformed lattice. We therefore have a set of quasiparticle creation and annihilation operators. The requirement of diagonalisation exerted upon the electron part of the hamiltonian results in the following equation describing the transformation coefficients $\phi_{\lambda,\xi}(\mathbf{k})$:

$$
\begin{aligned}
E_\lambda \phi_{\lambda,\xi}(\mathbf{k}) &= E_\xi(\mathbf{k})\phi_{\lambda,\xi}(\mathbf{k}) + \\
&+ \frac{1}{2\sqrt{2N_c}} \sum_{\mathbf{q},\xi',\tau} F_{\xi,\xi',\tau}(\mathbf{k},\mathbf{q})Q_\tau(\mathbf{q})\phi_{\lambda,\xi'}(\mathbf{k}-\mathbf{q}).
\end{aligned}
\tag{3.48}
$$

The following condition on the coefficients follows from the orthonormality of the quasiparticle states $|\lambda\rangle$:

$$\sum_{\mathbf{k},\xi} \phi^*_{\lambda,\xi}(\mathbf{k})\phi_{\lambda',\xi}(\mathbf{k}) = \delta_{\lambda,\lambda'}. \qquad (3.49)$$

Under the unitary transformation (3.46) the interaction hamiltonian transforms into the following form:

$$H_{int} = \frac{1}{2\sqrt{2N_c}} \sum_{\lambda,\lambda',\mathbf{q},\tau} \Phi_{\lambda,\lambda',\tau}(\mathbf{q}) C^\dagger_\lambda C_{\lambda'}(b_{\mathbf{q},\tau} + b^\dagger_{-\mathbf{q},\tau}), \qquad (3.50)$$

where:

$$\Phi_{\lambda,\lambda',\tau}(\mathbf{q}) = \sum_{\mathbf{k},\xi,\xi'} \phi^*_{\lambda,\xi'}(\mathbf{k})\Phi_{\xi,\xi',\tau}(\mathbf{k},\mathbf{q})\phi_{\lambda',\xi}(\mathbf{k}-\mathbf{q}). \qquad (3.51)$$

The equation describing the interaction hamiltonian can be separated into two distinct parts containing terms where $\lambda = \lambda'$ and those where $\lambda \neq \lambda'$ respectively [17]. As in the 1d case, the second case describes phonon induced non-adiabatic transitions between the adiabatic states represented by (3.53). The Hamiltonian is thus represented as:

$$\tilde{H} = \tilde{H}_0 + \tilde{H}_1 \qquad (3.52)$$

where $\tilde{H}_0$ contains everything except for the off-diagonal terms in (3.50), which are represented by $\tilde{H}_1$.

3.4.1 Approximate Eigenstates

At large enough electron-phonon coupling [18] the non-adiabatic terms may be treated perturbatively. As in the 1d case, we assume this approximation to be valid, although this has not been explicitly shown for this lattice. We may represent a system of quasiparticles by the relevant number of creation operators acting upon the vacuum. For the particular case of a one-particle state in the band λ:

$$|\psi_e^{(0)}\rangle = C^\dagger_\lambda|0\rangle_e|0\rangle_{ph}. \qquad (3.53)$$

The occupation number of the state λ, given by the operator $C^\dagger_\lambda C_\lambda$ may take on the values $0, 1$ or 2, since we are describing fermions. Operating on the one-particle

state (3.53) with the adiabatic hamiltonian H_0:

$$H_0|\psi_e^{(0)}\rangle = \left[W + E\lambda + \right.$$
$$\left. + \sum_{\mathbf{q},\tau}\left(\hbar\omega_\tau(\mathbf{q})\beta_\tau(\mathbf{q}) + \frac{1}{2\sqrt{2N_c}}\Phi_{\lambda,\lambda,\tau}^*(\mathbf{q})b_{\mathbf{q},\tau}^\dagger + h.c.\right)\right]|\psi_e^{(0)}\rangle, \quad (3.54)$$

one can see that the one-particle state (3.53) is an eigenstate of the adiabatic hamiltonian with energy $Eg + W$ provided that the coefficients of the unitary operator (3.46) satisfy the equations:

$$\hbar\omega_\tau(\mathbf{q})\beta_\tau(\mathbf{q}) = -\frac{1}{2\sqrt{2N_c}}\Phi_{\lambda,\lambda,\tau}^*(\mathbf{q})$$
$$= -\frac{1}{2\sqrt{2N_c}}\sum_{\mathbf{k},\xi,\xi'}\Phi_{\xi,\xi',\tau}^*(\mathbf{k},\mathbf{q})\phi_{\lambda,\xi'}^*(\mathbf{k})\phi_{\lambda,\xi}(\mathbf{k}-\mathbf{q}). \quad (3.55)$$

Utilising (3.42,3.44), the lattice distortion is therefore determined by the equation:

$$Q_\tau(\mathbf{q}) = -\frac{1}{2\sqrt{2N_c}}\sum_{\mathbf{k},\xi,\xi'}\frac{F_{\xi,\xi',\tau}^*(\mathbf{k},\mathbf{q})}{\omega_\tau^2(\mathbf{q})}\phi_{\lambda,\xi'}^*(\mathbf{k})\phi_{\lambda,\xi}(\mathbf{k}-\mathbf{q}). \quad (3.56)$$

We have therefore seen how the ideas of chapter 2, namely the adiabatic approximation and the technique of partial diagonalization can be generalized to the hexagonal lattice [76]. Again we can use the condition on the normal coordinates (3.56) to reproduce a nonlinear Schrödinger equation in the long-wave limit.

3.5 Nonlinear Schrödinger equation

Entering the expression (3.56) for Q into the equation (3.48) governing the coefficients ϕ, one arrives at a nonlinear equation describing the coefficients $\phi_{g,\lambda}((k)$:

$$0 = (E - E_\xi(\mathbf{k})\phi_\xi(\mathbf{k}) + $$
$$+ \frac{1}{N_c}\sum_{\xi',\xi_1'\xi_1,\mathbf{k}_1,\mathbf{q}_1}G_{\xi,\xi'}^{\xi_1',\xi_1}(\mathbf{k},\mathbf{k}_1,\mathbf{q})\phi_{\xi_1}^*(\mathbf{k})\phi_{\xi_1'}(\mathbf{k}_1+\mathbf{q})\phi_{\xi'}(\mathbf{k}-\mathbf{q}). \quad (3.57)$$

This equation describes the electron probability amplitude in the self-consistent states of electrons and accompanying lattice deformation. In this equation:

$$G_{\xi,\xi'}^{\xi_1',\xi_1}(\mathbf{k},\mathbf{k}_1,\mathbf{q})\phi_{\xi_1}^*(\mathbf{k}) = \frac{1}{8}\sum_\tau\frac{F_{\xi,\xi'}^{(\tau)}(\mathbf{k}-\mathbf{q},\mathbf{q})F_{\xi_1',\xi_1}^{(\tau)*}(\mathbf{k}_1,\mathbf{q})}{\omega_\tau^2(\mathbf{q})}. \quad (3.58)$$

Note that in order to slightly decongest these two equations the quasi-particle band index λ has been omitted. Equation (3.57) describes states that are superpositions of electron states from both energy bands. Even though the equation is extremely complicated, there is an approximate route to the nonlinear Schrödinger equation. Consider the quasiparticle state that is composed entirely of electronic eigenstates close to the minimum of the lowest electron energy band (i.e. $\xi = 0$). Then the nonlinear equation (3.57) simplifies to:

$$
\begin{aligned}
0 &= (E - E_0(\mathbf{k})\phi_0(\mathbf{k}) + \\
&+ \frac{1}{N_c} \sum_{\mathbf{k_1},\mathbf{q}} G(\mathbf{k}, \mathbf{k_1}, \mathbf{q}) \phi_0^*(\mathbf{k_1}) \phi_0(\mathbf{k_1} + \mathbf{q}) \phi_0(\mathbf{k} - \mathbf{q}).
\end{aligned} \tag{3.59}
$$

In order to proceed we introduce the following field of the continuum vector $\mathbf{x}$:

$$
\phi_0(\mathbf{x}) = \frac{1}{N_c} \sum_{\mathbf{k}} e^{i\mathbf{k}\cdot\mathbf{x}} \phi_0(\mathbf{k}). \tag{3.60}
$$

If the solution is a wave packet which is sufficiently broad in the spatial representation, then it will be strongly localized in the representation in $\mathbf{k}$-space. From the electron energy dispersion (3.21) one can see that in the ground state the function $\phi_0(\mathbf{k})$ will be localized around $\mathbf{k} = 0$. In this case we make the following assumptions:

$$
E_0(\mathbf{k}) \approx E_0 - 3J + \frac{J}{4} k_x^2 + \frac{J}{4} k_y^2; \tag{3.61}
$$

$$
G(\mathbf{k}, \mathbf{k_1}, \mathbf{q}) \approx G. \tag{3.62}
$$

The bottom of the energy band labelled by $\xi = 0$ is:

$$
E_0(0) = E_0 - 3J. \tag{3.63}
$$

It is then possible to transform equation (3.57) into a nonlinear Schrödinger equation for $\phi(\mathbf{x})$ by use of the Fourier transformation (3.60):

$$
\Lambda \phi_0(\mathbf{x}) + \frac{J}{4} \frac{d^2 \phi_0(\mathbf{x})}{dx^2} + \frac{J}{4} \frac{d^2 \phi_0(\mathbf{x})}{dy^2} + \frac{G}{N_c} |\phi_0(\mathbf{x})|^2 \phi_0(x) = 0, \tag{3.64}
$$

where $\Lambda = E - E_0(0)$. We have thus shown that under certain conditions the equations describing the self-consistent quasiparticle states in the adiabatic approxmiation reduce to a single nonlinear Schrödinger equation for the two dimensional electron field $\Phi(\mathbf{x})$. For details on solutions to the 2d nonlinear Schrödinger equation

see [69] in the continuum case, [70] in the discrete case and [71] for some interesting results relating to hexagonal lattices. We leave our argument here by noting that certain localized solutions do exist provided that the equation is in less than four dimensions. In one dimension the localized solution is stable for all values of G. In two dimensions the localized solution is stable only for one certain value of G. This localized solution is 'soft', i.e. it can be stretched or compressed without changing the total energy. For $D > 2$ there are no stable solitons, i.e. the ground state is delocalized. Our main method of approaching the question of whether localized solutions exist is through the numerical simulation of the semi-classical hamiltonian and equations of motion, the subject to which our attention now turns.

3.6 Semi-classical Hamiltonian

Using the inverse of the unitary transformation (3.46), the eigenfunction of the adiabatic hamiltonian can be written in the form:

$$|\psi_e\rangle = C_\lambda^\dagger|0\rangle = \sum_{\mathbf{k},\xi} \phi_{p,\xi}(\mathbf{k})c_{\mathbf{k},\xi}^\dagger|0\rangle = \sum_{i,j,\rho} \phi_{i,j,\rho}a_{i,j,\rho}^\dagger|0\rangle, \qquad (3.65)$$

i.e. the fields ϕ transform in a similar manner to the electron creation and annihilation operators. The coefficients $\phi(\mathbf{k})$, transform into those defined upon the physical lattice sites in the following way:

$$\phi_{i,j,\rho} = \frac{1}{2\sqrt{N_c}} \sum_{\mathbf{k},\xi} e^{i\mathbf{k}.\mathbf{r}_{i,j,\rho}} T_{\rho,\xi}(\mathbf{k})\phi_{p,\xi}(\mathbf{k}). \qquad (3.66)$$

Here $\phi_{i,j,\rho}$ is the probability amplitude for the quasiparticle at the site (i, j, ρ) in the hexagonal lattice. Taking the condition (3.48), multiplying by $\phi_\xi(\mathbf{k})$ and summing over $\mathbf{k}$ leads to an interaction term that closely resembles that in the Frölich hamiltonian, but with the fields $\phi_\xi(\mathbf{k})$ replacing the operators $c_{\mathbf{k},\xi}$ and the averaged normal coordinates (3.44) replacing the expression (3.29) involving the phonon operators. Carrying out the inverse transformations therefore leads to a semi-classical hamiltonian of the amplitudes $\phi_{i,j,\rho}$ and the averaged displacements $u_{i,j,\rho}$ and $v_{i,j,\rho}$

defined at the lattice sites. The semi-classical hamiltonian is:

$$
\begin{aligned}
H &= \langle \Phi | \hat{H} | \Phi \rangle \\
&= W + \sum_{i,j,\rho} \Bigg[E_0 |\phi_{i,j,\rho}|^2 - J \sum_\delta \phi_{i,j,\rho}^* \phi_{\delta(i,j,\rho)} \\
&\quad + \chi_1 |\phi_{i,j,\rho}|^2 \sum_\delta W \delta_{i,j,\rho} + G_2 \sum_\delta \phi_{i,j,\rho}^* \phi_{\delta(i,j,\rho)} W \delta_{i,j,\rho} \Bigg].
\end{aligned}
\tag{3.67}
$$

To continue the semi-classical method we calculate the equations of motion, which correspond to the Schrödinger equation for the quasiparticle field and Hamilton's equations for the averaged displacements u and v:

$$
\begin{aligned}
i\hbar \frac{\partial \phi_{i,j,\rho}}{\partial t} &= (W + E_0)\phi_{i,j,\rho} - J \sum_\delta \phi_{\delta(i,j,\rho)} + \\
&\quad + \chi \phi_{i,j,\rho} \sum_\delta W_{\delta(i,j,\rho)} + G \sum_\delta \phi_{\delta(i,j,\rho)} W_{\delta(i,j,\rho)};
\end{aligned}
\tag{3.68}
$$

$$
\begin{aligned}
M \frac{\partial^2 u_{i,j,\rho}}{\partial t^2} &= -k\Big(3u_{i,j,\rho} - \sum_\delta u_{\delta(i,j,\rho)}\Big) + (-1)^\rho \chi[\phi_{r(i,j,\rho)} + \phi_{d(i,j,\rho)} - 2\phi_{l(i,j,\rho)}] \\
&\quad + (-1)^\rho G[\phi_{i,j,\rho}^* \phi_{r(i,j,\rho)} + \phi_{i,j,\rho}^* \phi_{d(i,j,\rho)} - 2\phi_{i,j,\rho}^* \phi_{l(i,j,\rho)} + h.c.];
\end{aligned}
\tag{3.69}
$$

$$
\begin{aligned}
M \frac{\partial^2 v_{i,j,\rho}}{\partial t^2} &= -k\Big(3v_{i,j,\rho} - \sum_\delta v_{\delta(i,j,\rho)}\Big) + \sqrt{3}(-1)^\rho \chi[\phi_{r(i,j,\rho)} - \phi_{d(i,j,\rho)}] \\
&\quad + \sqrt{3}(-1)^\rho G[\phi_{i,j,\rho}^* \phi_{r(i,j,\rho)} - \phi_{i,j,\rho}^* \phi_{d(i,j,\rho)} + h.c.].
\end{aligned}
\tag{3.70}
$$

Accompanying these equations is the normalisation condition:

$$
\sum_{i,j,\rho} |\phi_{i,j,\rho}|^2 = 1,
\tag{3.71}
$$

which comes from the normalisation of the quasiparticle state $\langle \psi_e | \psi_e \rangle$. Note that in the stationary case the Schrödinger equation is connected to the condition (3.48) in k-space by the inverse transformation (3.66). We have therefore illustrated a connection between the semi-classical and adiabatic treatments of the hexagonal lattice.

3.7 Chapter summary

This chapter has focussed upon applying the ideas discussed in chapter 2 to the case of a two-dimensional hexagonal lattice. A consideration of the lattice geometry led

to the formulation of a tight-binding hamiltonian with first order couplings of the electron field to the lattice degrees of freedom. The electron and phonon hamiltonians were diagonalized by transforming into wave-vector space and taking certain linear combinations of the creation and annihilation operators. Applying the same transformations to the interaction hamiltonian led to a Frölich type hamiltonian with a complicated function $\Phi(\mathbf{k}, \mathbf{q})$ specifying the details of the electron-phonon interaction.

Solutions were then sought in the adiabatic approximation where the state vector is in the form of a product of a quasiparticle field and a coherent phonon state. The hamiltonian was then transformed into a form more natural for the consideration of soliton solutions. This hamiltonian was partially diagonalized by a unitary transformation with the coefficients of this transformation being chosen so that the electron part of the hamiltonian is diagonal, as was the method used in [77] and [17]. This led to the consideration of the hamiltonian in the zeroth-order adiabatic approximation. The requirement that the quasiparticle be an eigenstate of this hamiltonian led to a set of constraints on the coefficients of the coherent phonon field. These equations together determined the self-consistent states of localized electron + phonon field in the adiabatic approximation.

It was shown that in the continuum limit and for states exclusively constructed from states in the lower band the equations reduced to a single nonlinear relation describing the quantum amplitudes of the quasiparticle field. After a transformation into real space it was found that these amplitudes obeyed a nonlinear Schrödinger equation - an equation known to possess localized solutions. The zeroth-order adiabatic equations are related to the semi-classical equations, in which the site displacements are treated classically. The equations of motion corresponding to the semi-classical hamiltonian were calculated, and the numerical modelling of these dynamic equations is the subject of the next chapter.

Chapter 4

Numerical Solutions describing conduction electrons in interaction with a hexagonal lattice

In this chapter we analyse the numerical solutions to the system of equations introduced in chapter 3 to describe the electron-phonon system in the 2d hexagonal lattice. The minimum energy configuration of the electron and lattice states are found for a wide range of values of the electron-phonon coupling constants. Both delocalized and localized states are found to exist for certain values of the couplings. The type of solution and degree of localization is explored as a function of the electron-phonon interaction.

4.1   Hamiltonian parameters

There are a significant number of parameters that could be varied within the hamiltonian for the electron-phonon system. These are: K- the lattice elasticity coefficient, J- the exchange interaction energy, χ- the coupling of the electron on-site energy to the lattice displacements and G- the coupling of the exchange interaction to the lattice displacements. By suitably rescaling the parameters in the equations, it was possible to reduce the number of parameters that required variation. Performing

the following rescalings:

$$u = lU; \qquad v = lV; \qquad s = lS; \qquad k = \frac{\kappa}{l^2}J;$$

$$\chi_1 = \frac{X_1}{l^2}J; \qquad G_2 = \frac{G}{l^2}J; \qquad \epsilon_0 = \tilde{\epsilon}_0. \tag{4.1}$$

allows the specification of all parameters in terms of units of J. Therefore in all simulations we set $J = 1$. Next, the unit of length l was chosen to be such that the parameter related to the elasticity coefficient $\kappa = 1$. From certain references, the physical values of some of the parameters have been calculated for carbon nanotubes [22], [73], [74], [24]:

$$d = 1.42A; \qquad J = 2.4 - 3.1eV;$$

$$G \approx 4.8 - 6\frac{eV}{A}; \qquad k = 36.5 \times 10^4 \frac{dyn}{cm}. \tag{4.2}$$

The re-scalings were a subset of those that have been performed on the model describing zig-zag nanotubes [76]. Choosing $\kappa = 1$ therefore leads to a lengthscale $l = (3.24 - 3.7) \times 10^{-11}m$, which is approximately a quarter of the size of the actual nearest neighbour distance in graphite. The exchange energy coupling: $G = \frac{G_2 l}{J}$ then has a value of around $0.6 - 0.74$. It seemed from the literature that the value of χ was somewhat unknown, and so its magnitude was varied through a range of values comparable to G.

Simulation of the equations (3.68-3.70) involved the use of a fourth order Runge-Kutta method. In order to represent carbon nanotubes to a first approximation, periodic boundary conditions were imposed upon the lattice in both the $\hat{x}$ and $\hat{y}$ directions. The lattice was chosen to be significantly larger in one direction than the other, in an attempt to represent zig-zag nanotubes. If the lattice were mapped onto a cylindrical surface, it would correspond to a nanotube with chiral vector $(n, m) = (5, 0)$ and would contain 15 unit cells stacked on top of one another, corresponding to a total of 300 lattice sites (see section 5.1, eqn (5.1)). Although this was a relatively small lattice size compared to a $(5, 0)$ tube produced in experiments, which have lengths approximately one thousand times greater than their circumference, it enabled a detailed investigation of the stationary states of the system.

4.2 Finding the Minimum Energy

4.2.1 Absorption of Kinetic Energy

In order to find and then investigate the static configuration through simulation it was necessary to absorb energy from the equations. One method of achieving this involved the addition of the following damping terms to the respective right-hand sides of the equations of motion (3.69) and (3.70):

$$-\nu \frac{du_{i,j,\rho}}{dt} \quad \text{and} \quad -\nu \frac{dv_{i,j,\rho}}{dt}, \tag{4.3}$$

where ν determines the strength of the damping. These terms have the effect of gradually absorbing the kinetic energy of the sites vibrating about their equilibrium positions. Figure 4.1 shows the descent of the system energy for three different values of the damping parameter ν. The parameters used for simulation were $K = 1, J = 1, G_2 = 0$ and $\chi_1 = 5.0$. The initial conditions involved field configurations corresponding to a state localised mainly around a single lattice site, which indeed proved to be the ground state for these and many other values of the couplings. In this particular case it was found that $\nu \approx 1.0$ produced the quickest descent to the minimum energy, however varying the couplings had a slight effect upon the optimum damping coefficient. Similar effects were observed for other values of G_2 and χ_1.

4.2.2 Absorbtion of Energy from the Electron Field

The method described in section 4.2.1 was effective in reducing the system energy. However, it was found that the speed of the process could be greatly increased by introducing a direct absorption of energy from the electron field. The equation of motion for ϕ (3.68) contains only a first order derivative with respect to time, and so the introduction of a damping term similar to that in (4.3) would destroy the system dynamics. An approximate method was therefore introduced so that the damping term could be included.
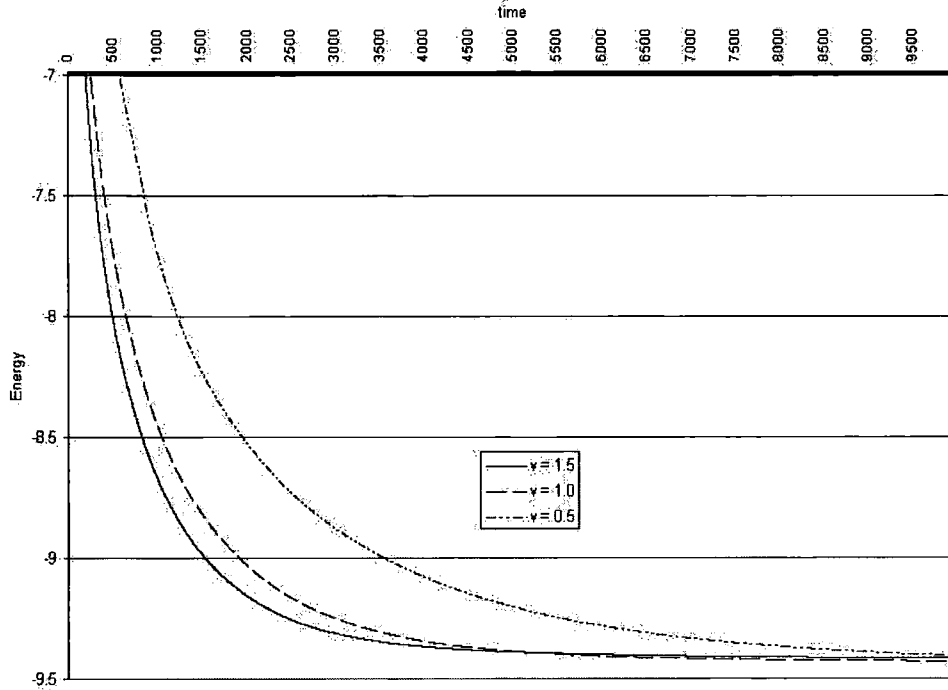
Figure 4.1: *Variation of the system energy due to the addition to the equations of motion of the damping terms in (4.3). The results for three different damping parameters $\nu = 0.5, 1.0$ and 1.5 are shown.*

For a stationary quantum state, the time dependence of the wave function is that of a monochromatic wave. The eigenfunctions $\phi(x)$ are the stationary states of the system:

$$\phi_{i,j,\rho}(t) = \psi_{i,j,\rho} \exp\left(\frac{-iEt}{\hbar}\right) \tag{4.4}$$

The variation of ϕ over an infinitessimal time step t is then:

$$i\hbar\frac{\partial \phi_{i,j,\rho}}{\partial t} = E\exp\left(\frac{-iEt}{\hbar}\right)\psi_{i,j,\rho} + i\hbar\exp\left(\frac{-iEt}{\hbar}\right)\frac{\partial \psi_{i,j,\rho}}{\partial t} \tag{4.5}$$

In the presence of damping, the stationary states $\psi_{i,j,\rho}$ have some small time dependence. The value of the electron energy E was calculated at all stages in the simulation, and the LHS of (4.5) is specified by the equation of motion (3.68). Using (4.4) to re-write ϕ in terms of ψ, and cancelling the exponential functions, yields the equation:

$$i\hbar\frac{\partial \psi_{i,j,\rho}}{\partial t} = -E\psi_{i,j,\rho} + F(\psi_{i,j,\rho}),\qquad(4.6)$$

where $F(\psi_{i,j})$ is the RHS of equation (11) with ψ replacing ϕ. The right hand side of this equation was calculated within the simulation. A damping term could then be introduced without destroying the system dynamics, since the time variation in (4.4) had been accounted for:

$$(a + i\hbar)\frac{\partial \psi_{i,j,\rho}}{\partial t} = -E\psi_{i,j,\rho} + F(\psi_{i,j,\rho})\qquad(4.7)$$

where the magnitude of a specifies the strength of the absorption.

The implementation of this method resulted in an enormous reduction in the time taken to reach the stationary configuration. It was found that a combination of the two methods for extracting the energy (4.3) and (4.7) produced the quickest descent to the minimum energy. Figure 4.2 shows the variation of the energy in two seperate cases. The first case utilises only the damping given by (3.4), the second curve uses a combination of the two. The differences are quite astounding.

It was found that the electron field absorption became less effective when the energy approached that of the stationary configuration. Under these circumstances the damping of the kinetic energy became more useful, particularly for smaller values of ν. Throughout the remainder of the investigation, a value of $\nu = 0.4$ was used in damping the system kinetic energy, in order to supplement the absorption from the electron field.

The disadvantage in using the electron field absorption was manifest in a violation of the normalisation condition (3.71). The magnitude of this violation was dependent upon the strength of the damping coefficient a. We were therefore careful to choose a damping magnitude that was small enough to have insignificant impact upon the simulation results.
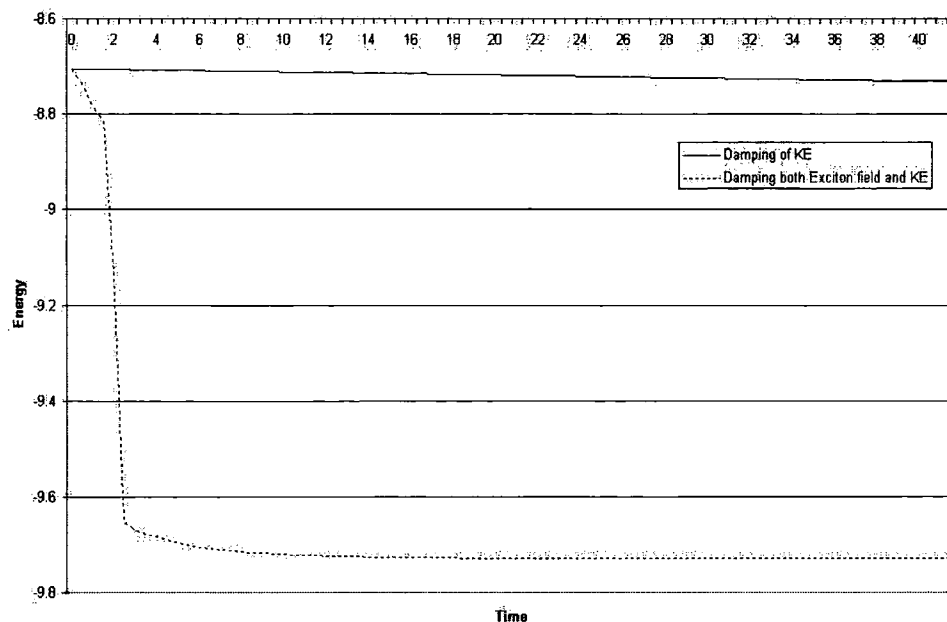
Figure 4.2: *Variation of the system energy due to damping. The first case involves a simple damping of the lattice kinetic energy with $\nu = 1.0$. The second case involves a mixture of damping from the electron field, and damping of the kinetic energy with $\nu = 0.4$. The magnitude of the electron field damping was set proportional to the rate of change of energy.*

4.3 Ground-state configuration as a function of χ and G

4.3.1 Varying χ for fixed G

The aim was to determine the minimum energy configurations for various values of the couplings χ and G. The couplings J and K were set equal to 1, as discussed in section 3.1. Initially the value of G was fixed at 0.6, in order to mimic the parameter values predicted by the literature. Since an estimate of χ was unknown, this parameter was varied from 0 to 5 in increments of 0.2. For each set of values of the electron-phonon coupling parameters the stationary configuration was found by absorbing energy by use of the methods described in the previous section. Once the rate of change of the energy with time fell below some pre-determined magnitude

it was determined that the state was sufficiently close to the ground state. The values of the lattice and electron field configurations were recorded and the value of χ incremently increased. Upon reaching a value of 5, χ was then gradually reduced down to 0 in order to analyze any hysteresis effects.
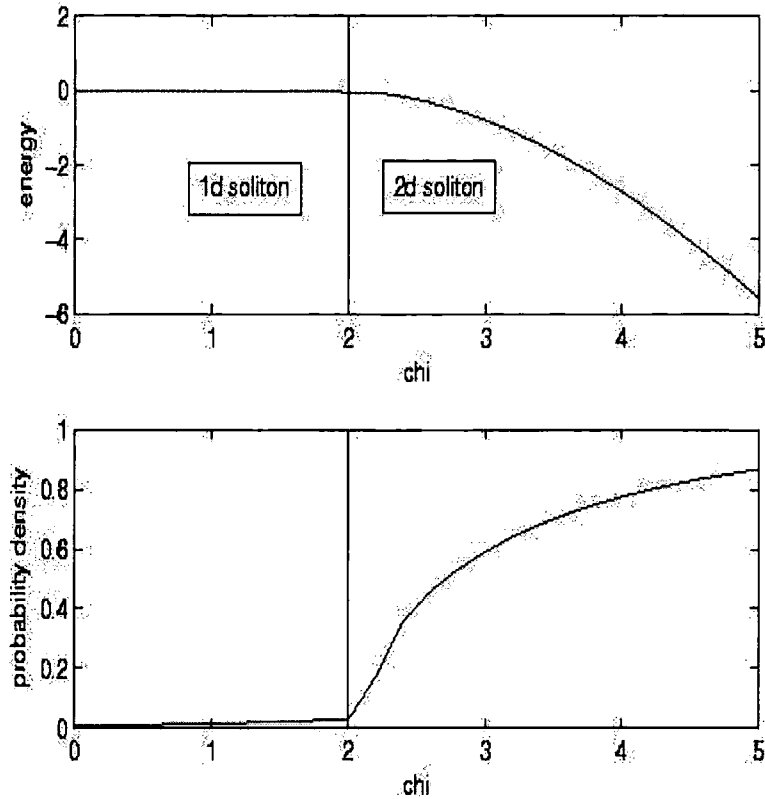
Figure 4.3: *Energy and maximum value of the probability density* $|\phi_{i,j,\rho}|^2_{max}$ *as a function of* χ *and for a fixed value of* $G = 0.6$

Figure 4.3 shows the variation in the groundstate energy and maximum in the electron probability density with respect to χ. The energy is calculated with respect to the bottom of the conduction band. The figure is segregated into two separate regimes. For $0 < \chi < 2$ the groundstate is localized in one lattice dimension, so that the probability density is a function only of the y-coordinate. The region $\chi > 2$ corresponds to a completely localized ground state probability density. The energies of the delocalized and 1d soliton states are very similar for small values of χ. In certain simulations the ground state was observed to be delocalized, however this was due

to the finite size effects of the lattice. For higher electron-phonon coupling, where the ground state is localized in two dimensions, the energy is a rapidly decreasing function of χ.

An illustration of the 1d soliton is given in figure 4.4 for coupling values $G = 0.6$ and $\chi = 1.6$, where we follow the method of presentation in [76]. Figure 4.4 depicts the actual physical displacements. The electron probability density is described by the shaded circles, with a darker shade indicating higher probability density.
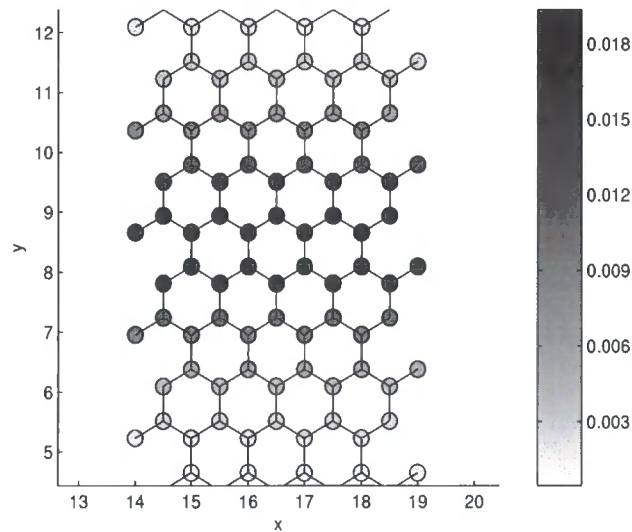
Figure 4.4: *Ground-state configuration for $\chi = 1.6, G = 0.6$*

The figure illustrates the extremely small site displacements in the vicinity of the 1d soliton. In fact, there exists a drawing in of the sites towards the centre of the soliton, and this distortion is uniform in the x-direction, i.e. parallel to the circumference. The magnitude of the displacement is larger for sites closer to the soliton. The width of the soliton was also found to depend upon χ, with the localization being more pronounced for higher values of χ.

Two typical two dimensional solitons are shown in figures 4.5 ($G = 0.6, \chi = 2.2$) and 4.6 ($G = 0.6, \chi = 3.4$). These pictures illuminate the dependence of the degree of localization on the electron-phonon coupling parameter χ. In fig 4.5, the majority of the electron probability density is spread symmetrically over thirteen sites, with the maximum of around 0.17 lying at the centre. The dragging in of the lattice sites

towards the centre of the polaron is much more evident than in the case of the 1d soliton. In the case of fig 4.6, the polaron has become localized mainly around 4 sites, again in a symmetrical pattern. The lattice distortions around such a localized state are much more significant, due to the larger value of the electron-phonon coupling constant. In this regime the assumption of small displacements become invalid and one must consider higher-order contributions to the lattice potential in order to successfully describe a real crystal.
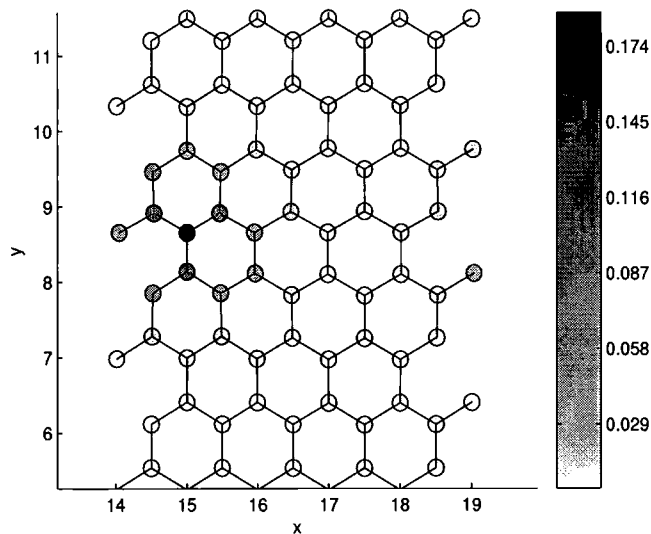
Figure 4.5: *Ground-state configuration for* $\chi = 2.2, G = 0.6$

4.3.2   Hysteresis due to varying χ, $G = 0.6$

During the the simulations for $G = 0.6$, the value of χ was both increased and decreased in order to observe any hysteresis effects in the observed stationary states. Figure 4.7 shows the energy and the maximum in the probability density of the observed stationary states. The solid line represents the observed stationary states for increasing χ, the dotted line for decreasing χ. The figure shows that there is a small region $2.2 < \chi < 3.0$ where the 1d soliton becomes a metastable excited state with a slightly higher energy than the groundstate (which is the 2d soliton). In order to analyse the stability of the one-dimensional soliton in this region, perturbations were performed by increasing the electron field slightly in the centre of the soliton,
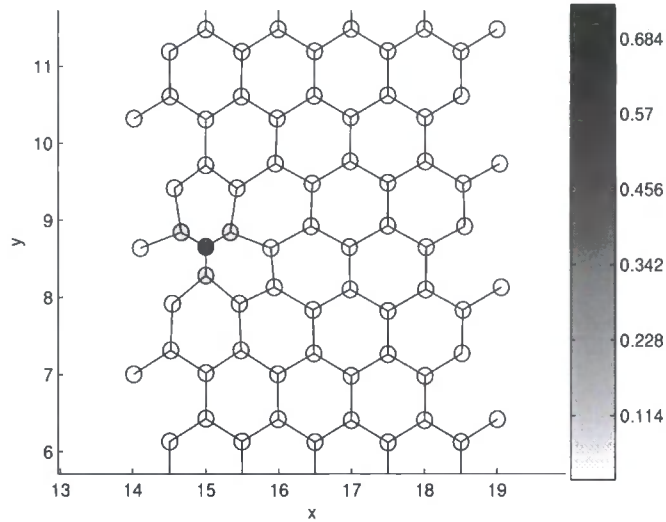
Figure 4.6: *Ground-state configuration for* $\chi = 3.4, G = 0.6$

and then renormalising. This practice was carried out in an attempt to move the system closer to the more localised ground state. However the attempts to produce a transition were unsuccessful, and so it seemed that the one-dimensional soliton may be stable in an even larger part of the χ coupling space than predicted by fig 4.3.

Although invisible on the figure, there is also a region close to $\chi = 0$ where the ground state of the system is the delocalized state, and the 1d soliton is again some metastable state. In the case of the delocalized state, this energy corresponds to the bottom of the conduction band. The energy of the 1d soliton in this region of coupling space is extremely close to this value.

4.3.3   Ground state dependence upon both χ and G

So far we have analysed the possible localized and delocalized states obtained in the tight-binding zeroth order adiabatic approximation for values of the system parameters consistent with current research lterature. It was interesting, however, to observe the ground state in the complete phase space of G and χ. Figure 4.8 shows the energy of the ground state over this space. The value of the energy for each value of the couplings is given by the degree of shading, with a lighter colour
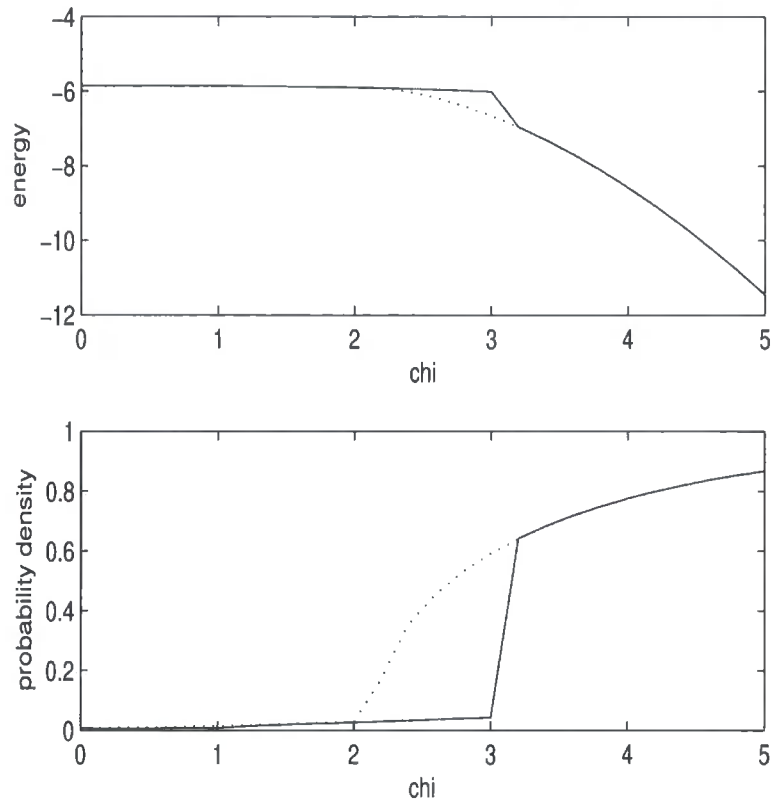
Figure 4.7: *Hysteresis of observed stationary states for $G = 0.6$ and varying χ.*

indicating higher energy. Complete white specifies an energy equal to zero in our units, and this energy corresponds to the bottom of the conduction band in the pure undistorted crystal. The values of $|\phi_{i,j,\rho}|^2_{max}$ corresponding to the energies in fig 4.8 are depicted in figure 4.9.

The coupling phase space involving χ and G contains three separate regions, corresponding to the one-dimensional soliton state, and two different types of solitons localized in two dimensions. The darkest region in fig 4.9 represents the symmetrically distributed localized state as in figures 4.5 and 4.6. The lightest region represents the less localized states, with the bottom left corner occupied by the completely delocalized state, and the rest of the region occupied by the 1d soliton states. The case $G = 0$ was considered in [51], where similar results were found. The intermediately shaded region occupying the right-hand side of figure 4.10 represents a different type of soliton localized in two-dimensions. The form of this solution is
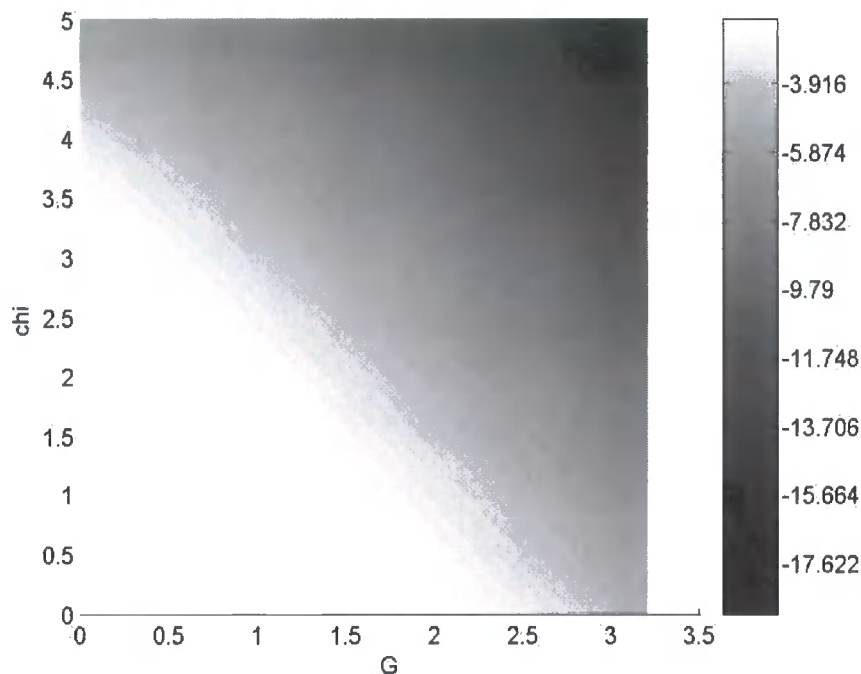
Figure 4.8: *Energy of the ground state configuration as a function of G and χ.*

shown in fig 4.10.

The probability density is shared mostly over 6 sites. In contrast to the 2d soliton already discussed (fig 4.5,4.6) where the maximum in the probability density is situated at a single central site, the soliton depicted in fig 4.10 has its maximum at two central sites. Their four nearest neighbours hold the majority of the remaining electron probability density. In order to determine the variation in this state with G, we fixed the value $\chi = 1$ and scanned a range of values of G. The findings are presented in figure 4.11.

For this particular value of χ, the transition between the 1d and 2d soliton occurred at $G \approx 1.3$. As G was increased past this critical value, the maximum in the probability density was found to tend towards a value of $|\phi_{i,j,\rho}|^2_{max} = 0.5$. For high enough values of G, the probability density was almost exclusively concentrated around the two central sites.
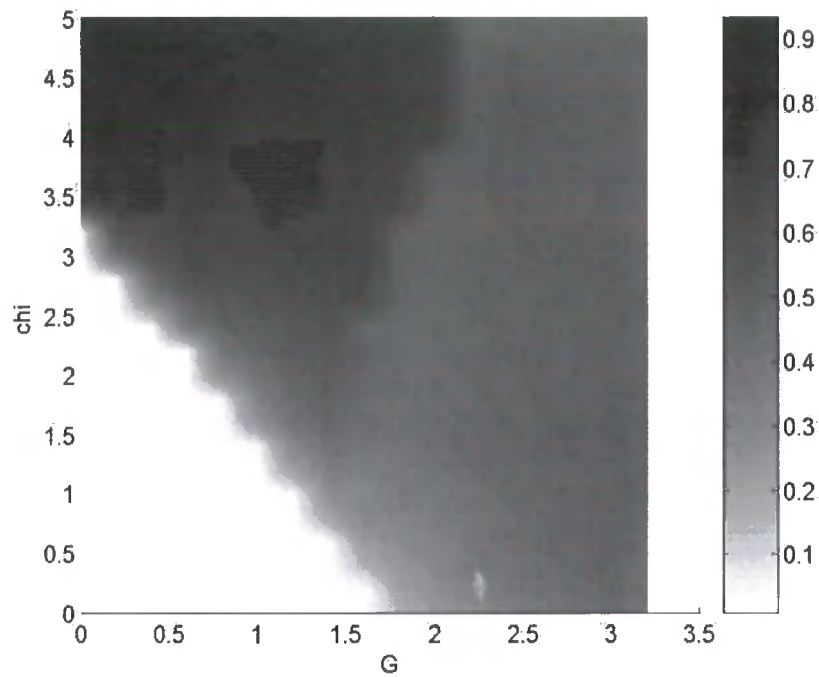
Figure 4.9: *Maximum in the probability density of the ground state as a function of G and χ.*
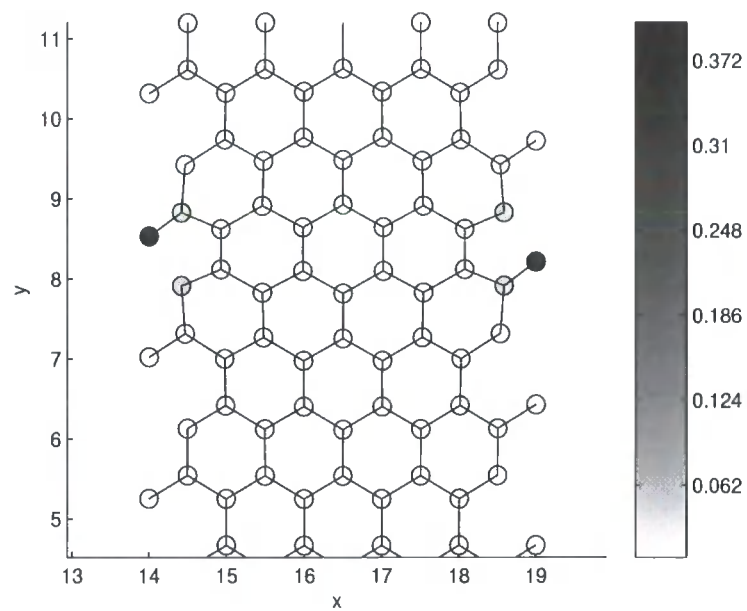
Figure 4.10: *Ground state configuration for $G = 2.4$ and $\chi = 1$.*
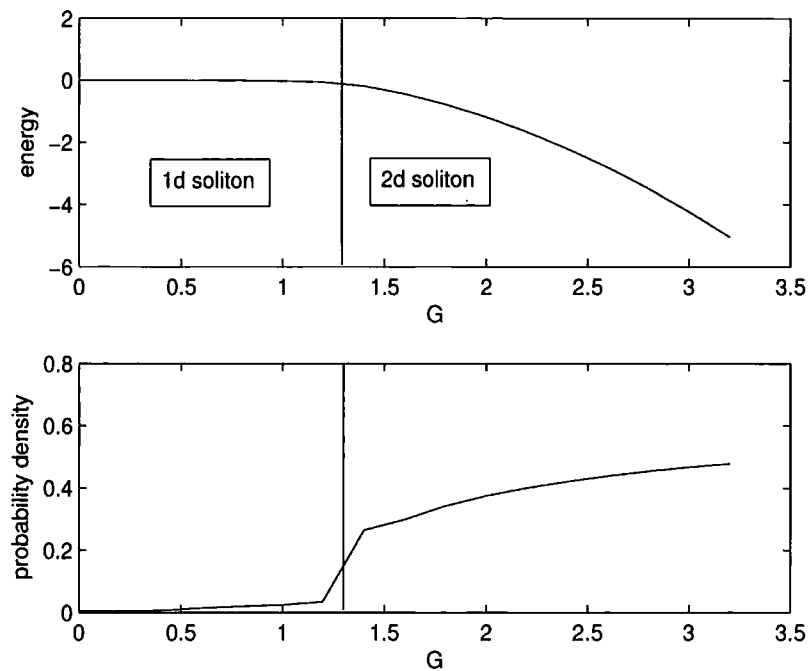
Figure 4.11: *Energy and maximum in the probability density for $\chi = 1$.*

4.4 Section summary

This section has concentrated upon the numerical solutions to the semi-classical equations that refer to the tight-binding hamiltonian of electron-phonon interactions formulated upon the two dimensional hexagonal lattice. The equations, that are analagous to the case of the zeroth-order adiabatic approximation, yielded a rich variety of localised states. It was found that the states could be classified into four distinct catergories: (a) The completely delocalized state; (b) A soliton type solution localised in one lattice dimension; (c) A solution localized in two dimensions with one site containing the central maximum in the probability density; (d) A second solution localized in both lattice dimensions with two central sites sharing the maximum in the probability density. Regimes (b), (c) and (d) were found to be the groundstate in different regions of the electron-phonon coupling phase space. For the values of parameters predicted by the literature [22], [73], [74], [24], only the states (b) and (c) were observed. Naively assuming a value of χ approximately the same as the predicted value of G, the ground state lies on the boundary between the delocalized

state and the 1d soliton state. Thus localized electron states might well be found to exist in graphite and nanotubes.

The lattice distortions accompanying the electron state were also observed. In the case of the state (a) there should be no definite displacament, only the thermal vibrational energy of each atom in the crystal will contribute to displacements. In the case (b) there is a slight distorting of the lattice which results in an average displacement of sites towards the maximum in the probability density distribution. The magnitude of the distortion gets larger as one approaches the soliton, however in the centre, as expected, the displacement is zero. The states (c) and (d) both produced a more significant lattice distortion, and for values of $\chi, G > 3$ the distortion is approaching magnitudes where higher order terms in the lattice potential become important. The results for the case $G = 0$ were found to closely agree with the results considered in [51].

These results were extremely interesting in providing an insight into the kinds of polaronic states that may exist in carbon nanotubes. However, it was next necessary to remove some of the limitations of the model that involve the geometry. The remaining chapters focus upon this task by considering the precise three-dimensional geometry and displacements of a carbon nanotube.

Chapter 5

Polarons in carbon nanotubes

In this chapter we formulate the tight-binding hamiltonian on a general nanotube. Both the on-site and exchange energies are corrected up to first order in the phonon fields. Lattice displacements are allowed in the plane of the nanotube surface and perpendicular to this surface. This model was first considered in collaboration on a zig-zag nanotube [76], [77]. We apply the model to nanotubes of any chirality and derive the semi-classical equations of motion that correspond to the zeroth order adiabatic approximation. These equations depend appropriately upon the nanotube parameters (n, m). We then look at one type of approximate solution that takes on the form of a nonlinear Schrödinger equation.

5.1 Geometry of Carbon Nanotubes

5.1.1 Nanotube parameters

In order to formulate the tight-binding hamiltonian describing electron-phonon interactions on a three-dimensional nanotube it is necessary first to consider the lattice geometry [22], [33]. Nanotubes are most easily thought of in terms of taking a 2d hexagonal lattice, the geometry of which was considered in section 3.2, and rolling it into a cylinder. There are an infinite class of tubes that can be made in this way, by rolling the tube at different angles and with different sized circumferences. Each individual tube is specified by the chiral vector $\mathbf{C}_h$, which is directed parallel to a

cross section of the nanotube, and has a magnitude equal to the tube circumference (see vector **OA** fig 5.1):
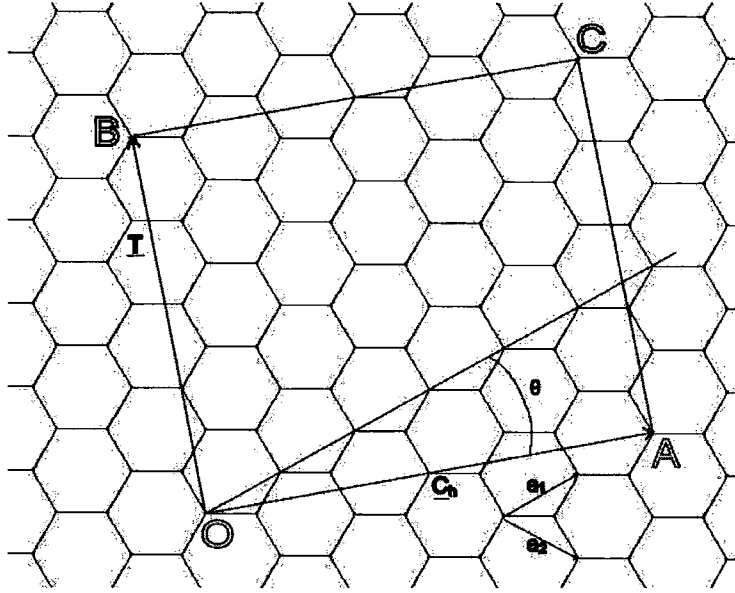
Figure 5.1: *The nanotube parameters*

The chiral vector is defined in the 2d hexagonal lattice and is specified by the integers (n, m):

$$\mathbf{C}_h = n\mathbf{a}_1 + m\mathbf{a}_2; \qquad |\mathbf{C}_h| = a\sqrt{n^2 + m^2 + nm}. \tag{5.1}$$

All nanotubes belong to one of two groups: achiral or chiral tubes. The achiral tubes form a small subset of all nanotubes. There are only two members of this group corresponding to the cases $m = 0$ (zig-zag) and $m = n$ (armchair). The lattice studied in chapters 3 and 4 of this work corresponds to the zig-zag case with nanotube parameters $(n, m) = (5, 0)$. All other nanotubes belong to the chiral class. The study of achiral tubes provides an important step in understanding the properties of carbon nanotubes. However since the majority of tubes produced in experiments are chiral [86] [87], it is important to consider the effects of chirality upon the nanotube properties, including the excited electron states.

The nanotube unit cell is specified by $\mathbf{C}_h$ and another vector, known as the translation vector **T**. This is the shortest vector that is perpendicular to the chiral vector (i.e. parallel to the nanotube axis) and adjoins two equivalent sites in the

2d graphite sheet (see vector **OB** fig 5.1). The nanotube structure is then invariant under translations by the vector **T**. The translation vector is specified by two integers (t_1, t_2), where [22]:

$$\mathbf{T} = t_1 \mathbf{a_1} + t_2 \mathbf{a_2}; \tag{5.2}$$

$$t_1 = \frac{2m+n}{d_R}; \qquad t_2 = -\frac{2n+m}{d_R}, \tag{5.3}$$

and d_R is the greatest common divisor of the numerators in (5.3). The nanotube unit cell is therefore given in figure 5.1 by the rectangle $OACB$. A nanotube of extended length is constructed by the stacking of such nanotube unit cells.

5.1.2 Three-dimensional coordinates

In order to write down the 3d cartesian coordinates of the nanotube lattice sites, we take the x and y directions perpendicular to the nanotube axis and z parallel to this axis. It is convenient to specify the x and y coordinates of the lattice sites in terms of three angles ξ, γ and θ. Rotating the nanotube about its own axis by an angle of γ is related to translating a point by the vector $\mathbf{a_1}$ in the two-dimensional hexagonal lattice (i.e. by increasing the index i by unity). The angles θ and ξ are related in the same way to the respective translations $\mathbf{q} = \mathbf{a_1} - \mathbf{a_2}$ and $\mathbf{p} = \frac{1}{3}(2\mathbf{a_1} - \mathbf{a_2})$ (increasing j and ρ respectively by unity). The z-coordinate is calculated from a projection of $r_{i,j,\rho}$ on to the translation vector **T**. The 3d cartesian coordinates are then:

$$x_{i,j,\rho} = R\sin(i\gamma + j\theta + \rho\xi); \tag{5.4}$$

$$y_{i,j,\rho} = R\cos(i\gamma + j\theta + \rho\xi); \tag{5.5}$$

$$z_{i,j,\rho} = \frac{d_R \mathbf{r}_{i,j,\rho}.\mathbf{T}}{\sqrt{3}L}. \tag{5.6}$$

The three angles γ, θ and ξ can be written down in terms of the parameters n and m. Taking first the 3d rotation angle γ corresponding to the translation $\mathbf{a_1}$ in the 2d lattice, we make f integral combinations of this vector from the origin. After a finite number of additions, the projection of the resulting vector on to $\mathbf{C_h}$ will be equal to an integral multiple g of $|\mathbf{C_h}| = L$:

$$f\frac{\mathbf{a_1}.\mathbf{C_h}}{L} = gL \qquad (f, g \text{ integral}). \tag{5.7}$$

There is always a solution for some f and g since eqn (5.7) involves only rational quantities. We also have:

$$f\gamma = 2\pi g, \tag{5.8}$$

since a translation of C_h in the 2d lattice represents a rotation of 2π about the nanotube axis in three dimensions. Eliminating f and g gives (in the non-trivial case):

$$\gamma = \frac{\pi(2n + m)}{n^2 + m^2 + nm}, \tag{5.9}$$

where we have used $L = |C_h| = a\sqrt{n^2 + m^2 + nm}$. Following a similar procedure for the angles θ and ξ we find:

$$\theta = \frac{\pi(n - m)}{n^2 + m^2 + nm}; \tag{5.10}$$

$$\xi = \frac{\pi n}{n^2 + m^2 + nm}. \tag{5.11}$$

Thus the three angles that we use to describe site coordinates are now specified in terms of the parameters of the chiral vector C_h. In the case of a zig-zag nanotube $m = 0$, hence $\xi = \theta$ and $\gamma = 2\theta = 2\xi$ as expected. Note that there is a relation between the three angles:

$$\theta + \gamma = 3\xi, \tag{5.12}$$

since only two angles are required to label any site within the lattice. In order to allow the elimination of the radius R from the equations we again consider the projections of the vectors $\mathbf{p}$, $\mathbf{a_1}$ and $\mathbf{q}$ onto the chiral vector (figure 5.2), and arrive at the relations:

$$
\begin{aligned}
a = \sqrt{3}d &= \frac{4RL'}{n}\sin\left(\frac{\xi}{2}\right) \\
&= \frac{4RL'}{n + m}\sin\left(\frac{\gamma - \xi}{2}\right) \\
&= \frac{4RL'}{m}\sin\left(\frac{\xi - \theta}{2}\right);
\end{aligned} \tag{5.13}
$$

$$L' = \frac{L}{a} = \sqrt{n^2 + m^2 + mn}. \tag{5.14}$$

February 28, 2006
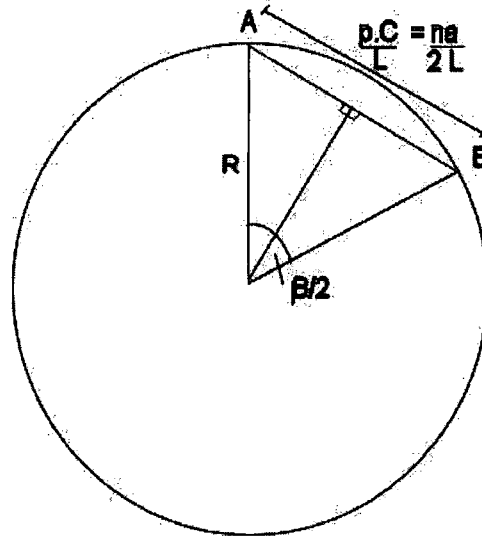
Figure 5.2: *Nanotube cross section. The vector* **p** *is projected onto the chiral vector to give the side AB. This allows the expression of the angle ξ in terms of the parameters n and m. A similar method gives a relation between* $\mathbf{a_1}$ *and* γ *and* $\mathbf{q}$ *and* θ

In the absence of any site displacements, the positions of the atoms are:

$$\mathbf{R}^0_{i,j,\rho} = R\sin(i\gamma + j\theta + \rho\xi)\hat{e}_x + R\cos(i\gamma + j\theta + \rho\xi)\hat{e}_y + \Theta(i,j,\rho)\hat{e}_z, \qquad (5.15)$$

where, from equation (5.6):

$$\Theta(i,j,\rho) = \frac{3d}{2L'}\left[[im + j(m+n)] + \frac{(n+2m)\rho}{3}\right]. \qquad (5.16)$$

Defining the lattice site displacement fields as $u_{i,j,\rho}$ tangent to the cylinder and perpendicular to the nanotube axis, $s_{i,j,\rho}$ perpendicular to the cylinder and the nanotube axis, and $v_{i,j,\rho}$ parallel to the nanotube axis gives:

$$\mathbf{u}_{i,j,\rho} = |u_{i,j,\rho}|[\cos(i\gamma + j\theta + \rho\xi)\hat{e}_x - \sin(i\gamma + j\theta + \rho\xi)\hat{e}_y]; \qquad (5.17)$$

$$\mathbf{s}_{i,j,\rho} = |s_{i,j,\rho}|[\sin(i\gamma + j\theta + \rho\xi)\hat{e}_x + \cos(i\gamma + j\theta + \rho\xi)\hat{e}_y]; \qquad (5.18)$$

$$\mathbf{v}_{i,j,\rho} = |v_{i,j,\rho}|\hat{e}_z. \qquad (5.19)$$

Next we define the local displacement vector as:

$$\mathbf{P}_{i,j,\rho} = \mathbf{u}_{i,j,\rho} + \mathbf{v}_{i,j,\rho} + \mathbf{s}_{i,j,\rho}, \qquad (5.20)$$

so that the displaced positions of the lattice sites are described by the vectors:

$$\mathbf{R}_{i,j,\rho} = \mathbf{R}^0_{i,j,\rho} + \mathbf{P}_{i,j,\rho}. \tag{5.21}$$

It is again extremely convenient to use the indices functions (3.3) to simplify the equations. In this notation the index δ may refer to each of the three nearest neighbours of any site r, l, d. The lattice vectors adjoing nearest neighbours in the fixed lattice are:

$$\mathbf{D}\delta^0_{i,j,\rho} = \mathbf{R}^0_{\delta(i,j,\rho)} - \mathbf{R}^0_{i,j,\rho}, \tag{5.22}$$

The actual nearest neighbour separation in the dynamic lattice is:

$$\mathbf{D}\delta_{i,j,\rho} = \mathbf{R}_{\delta(i,j,\rho)} - \mathbf{R}_{i,j,\rho}. \tag{5.23}$$

The local displacement vectors are:

$$\mathbf{d}\delta_{i,j,\rho} = \mathbf{P}_{\delta(i,j,\rho)} - \mathbf{P}_{i,j,\rho} \tag{5.24}$$

so that $\mathbf{D}\delta_{i,j,\rho} = \mathbf{D}\delta^0_{i,j,\rho} + \mathbf{d}\delta_{i,j,\rho}$. Using the above definitions, the fixed lattice vectors are:

$$\mathbf{Dr}^0_{i,j,0} = \frac{\sqrt{3}dn}{2L'}\cos\left(i\gamma + j\theta + \frac{\xi}{2}\right)\hat{e}_x - \frac{\sqrt{3}dn}{2L'}\sin\left(i\gamma + j\theta + \frac{\xi}{2}\right)\hat{e}_y + \frac{d}{2L'}(n+2m)\hat{e}_z;$$

$$\mathbf{Dl}^0_{i,j,0} = -\frac{\sqrt{3}d}{2L'}(n+m)\cos\left((i-1/2)\gamma + j\theta + \frac{\xi}{2}\right)\hat{e}_x$$

$$+ \frac{\sqrt{3}d}{2L'}(n+m)\sin\left((i-1/2)\gamma + j\theta + \frac{\xi}{2}\right)\hat{e}_y + \frac{d}{2L'}(n-m)\hat{e}_z;$$

$$\mathbf{Dd}^0_{i,j,0} = \frac{\sqrt{3}d}{2L'}m\cos\left(i\gamma + (j-1/2)\theta + \frac{\xi}{2}\right)\hat{e}_x$$

$$- \frac{\sqrt{3}d}{2L'}m\sin\left(i\gamma + (j-1/2)\theta + \frac{\xi}{2}\right)\hat{e}_y - \frac{d}{2L'}(2n+m)\hat{e}_z;$$

$$\mathbf{Dr}^0_{i,j,1} = -\mathbf{Dr}^0_{i,j,0};$$

$$\mathbf{Dl}^0_{i,j,1} = -\mathbf{Dl}^0_{i+1,j,0};$$

$$\mathbf{Dd}^0_{i,j,1} = -\mathbf{Dd}^0_{i,j+1,0}, \tag{5.25}$$

where as expected the magnitude of each of these vectors is equal to the nearest neighbour separation in the 2d hexagonal lattice.:

$$|\mathbf{Dr}^0_{i,j,\rho}| = |\mathbf{Dl}^0_{i,j,\rho}| = |\mathbf{Dd}^0_{i,j,\rho}| = \frac{a}{\sqrt{3}} = d. \tag{5.26}$$

The local displacement vectors are:

$$\mathbf{dr}_{i,j,0} = \left[u_{i,j,1} \cos\left(i\gamma + j\theta + \xi \right) + s_{i,j,1} \sin\left(i\gamma + j\theta + \xi \right) \right.$$
$$\left. - u_{i,j,0} \cos\left(i\gamma + j\theta \right) - s_{i,j,0} \sin\left(i\gamma + j\theta \right) \right] \hat{e}_x$$
$$+ \left[-u_{i,j,1} \sin\left(i\gamma + j\theta + \xi \right) + s_{i,j,1} \cos\left(i\gamma + j\theta + \xi \right) \right.$$
$$\left. + u_{i,j,0} \sin\left(i\gamma + j\theta \right) - s_{i,j,0} \cos\left(i\gamma + j\theta \right) \right] \hat{e}_y$$
$$+ (v_{i,j,1} - v_{i,j,0}) \hat{e}_z$$

$$\mathbf{dl}_{i,j,0} = \left[u_{i-1,j,1} \cos\left((i-1)\gamma + j\theta + \xi \right) + s_{i-1,j,1} \sin\left((i-1)\gamma + j\theta + \xi \right) \right.$$
$$\left. - u_{i,j,0} \cos\left(i\gamma + j\theta \right) - s_{i,j,0} \sin\left(i\gamma + j\theta \right) \right] \hat{e}_x$$
$$+ \left[-u_{i-1,j,1} \sin\left((i-1)\gamma + j\theta + \xi \right) + s_{i-1,j,1} \cos\left((i-1)\gamma + j\theta + \xi \right) \right.$$
$$\left. + u_{i,j,0} \sin\left(i\gamma + j\theta \right) - s_{i,j,0} \cos\left(i\gamma + j\theta \right) \right] \hat{e}_y$$
$$+ (v_{i-1,j,1} - v_{i,j,0}) \hat{e}_z$$

$$\mathbf{dd}_{i,j,0} = \left[u_{i,j-1,1} \cos\left(i\gamma + (j-1)\theta + \xi \right) + s_{i,j-1,1} \sin\left(i\gamma + (j-1)\theta + \xi \right) \right.$$
$$\left. - u_{i,j,0} \cos\left(i\gamma + j\theta \right) - s_{i,j,0} \sin\left(i\gamma + j\theta \right) \right] \hat{e}_x$$
$$+ \left[-u_{i,j-1,1} \sin\left(i\gamma + (j-1)\theta + \xi \right) + s_{i,j-1,1} \cos\left(i\gamma + (j-1)\theta + \xi \right) \right.$$
$$\left. + u_{i,j,0} \sin\left(i\gamma + j\theta \right) - s_{i,j,0} \cos\left(i\gamma + j\theta \right) \right] \hat{e}_y$$
$$+ (v_{i+1,j-1,1} - v_{i,j,0}) \hat{e}_z$$

$$\mathbf{dr}_{i,j,1} = -\mathbf{dr}_{i,j,0}$$
$$\mathbf{dl}_{i,j,1} = -\mathbf{dl}_{i+1,j,0}$$
$$\mathbf{dd}_{i,j,1} = -\mathbf{dd}_{i,j+1,0} \tag{5.27}$$

5.1.3   Nearest neighbour separations

The quantities that are required in the construction of the tight-binding hamiltonian are the lowest order corrections to the magnitudes of the lattice vectors due to site displacements. Again we employ the simplifying assumption that the atoms in the crystal only undergo small displacements from their equilibrium positions

$|\mathbf{d}\delta_{i,j,\rho}| \ll d$. Calculating the magnitude of the vectors $|\mathbf{D}\delta_{i,j,\rho}|$:

$$|\mathbf{D}\delta_{i,j,\rho}| = |\mathbf{D}^0\delta_{i,j,\rho} + \mathbf{d}\delta_{i,j,\rho}|, \tag{5.28}$$

and expanding these quantities up to first order in the displacements u, v and s gives:

$$|\mathbf{D}\delta_{i,j,\rho}| = d + \frac{\mathbf{D}\delta_{i,j,\rho} \cdot \mathbf{d}\delta_{i,j,\rho}}{d} = d + W\delta_{i,j,\rho}, \tag{5.29}$$

where:

$Wr_{i,j,\rho}$

$$
\begin{aligned}
= & \frac{\sqrt{3}n}{2L'}\left[(-1)^\rho \cos\left(\frac{\xi}{2}\right)(u_{r(i,j,\rho)} - u_{i,j,\rho}) + \sin\left(\frac{\xi}{2}\right)(s_{r(i,j,\rho)} + s_{i,j,\rho})\right] \\
& + \frac{(-1)^\rho(n + 2m)}{2L'}(v_{r(i,j,\rho)} - v_{i,j,\rho});
\end{aligned}
$$

$Wl_{i,j,\rho}$

$$
\begin{aligned}
= & \frac{\sqrt{3}(n + m)}{2L'}\left[(-1)^\rho \cos\left(\frac{\gamma - \xi}{2}\right)(u_{i,j,\rho} - u_{l(i,j,\rho)}) + \sin\left(\frac{\gamma - \xi}{2}\right)(s_{l(i,j,\rho)} + s_{i,j,\rho})\right] \\
& + \frac{(-1)^\rho(n - m)}{2L'}(v_{l(i,j,\rho)} - v_{i,j,\rho});
\end{aligned}
$$

$Wd_{i,j,\rho}$

$$
\begin{aligned}
= & \frac{\sqrt{3}m}{2L'}\left[(-1)^\rho \cos\left(\frac{\xi - \theta}{2}\right)(u_{d(i,j,\rho)} - u_{i,j,\rho}) + \sin\left(\frac{\xi - \theta}{2}\right)(s_{d(i,j,\rho)} + s_{i,j,\rho})\right] \\
& - \frac{(-1)^\rho(2n + m)}{2L'}(v_{d(i,j,\rho)} - v_{i,j,\rho}). \tag{5.30}
\end{aligned}
$$

The angles $\frac{\xi}{2}, \frac{\gamma - \xi}{2}$ and $\frac{\xi - \theta}{2}$ represent the angular separations about the nanotube axis of the three nearest neighbours r, l, d. For example, $\frac{\xi}{2}$ represents the angular separation about the nanotube axis of the sites $R_{i,j,0}$ and $R_{i,j,1}$. For W_l and W_d the relevant angles are $\frac{\gamma - \xi}{2}$ and $\frac{\xi - \theta}{2}$ respectively. The quantities $W\delta$ will be used in the construction of the electron-phonon interaction and lattice potential terms of the tight-binding hamiltonian in a similar manner to in chapter 3.

A detailed analysis of tight-binding polaronic states in zig-zag tubes is presented in [76]. Note that all of the formulations that appear in this chapter describing chiral nanotubes reduce to the expressions considered in this reference when we take the case $m = 0$. Further correspondances can be made with the work discussed

February 28, 2006

in chapter 3 if one again takes the case $m = 0$ and then takes the limit of large tube radius. In this limit the angles γ, ξ and θ are set equal to zero. The equations describing the fields $W\delta$ then correctly reduce to those considered in chapter 3. One may expect to observe that the quasi-particle ground states of tubes with large radii would resemble some of those observed in the numerical analysis of chapter 4. We can therefore expect to observe similar solutions to those explored in chapter 4.

5.1.4 Nanotube bending

In order to correctly describe the twisting motion of atoms in a single graphite sheet, where the displacements are out of the plane of the lattice, it is necessary to consider at least up to fourth nearest neighbour interactions [22]. If we were to consider such interactions in our description of the lattice potential of a carbon nanotube, the model complexity would be enormous. It was therefore necessary to consider some other method to correctly describe the bending modes of our nanotubes. Certain recent work has suggested that this bending could be accounted for by expanding the cosines of the angles between adjacent lattice vectors up to first order in the lattice displacements [73]. However, the term that we chose to add depended upon the solid angle formed by a centre point with its three nearest neighbours. This is a generalisation of the method used to represent the effects of curvature in the nano-circle [27]. Either of these two choices involves a model that deals only with nearest neighbour interactions, and so each provides a tractible model. As we shall see, the solid angle representation leads to an elegant approximate solution to the stationary equations.

The solid angle span by the three lattice vectors surrounding the site (i, j, ρ) is:

$$
\begin{aligned}
S_{i,j,\rho} &= \frac{(\mathbf{D}r_{i,j,\rho} \times \mathbf{D}l_{i,j,\rho}).\mathbf{D}d_{i,j,\rho}}{|\mathbf{D}r^0_{i,j,\rho}||\mathbf{D}l^0_{i,j,\rho}||\mathbf{D}d^0_{i,j,\rho}|} \\
&\approx S^0_{i,j,\rho}\left(1 - \frac{Wr_{i,j,\rho} + Wl_{i,j,\rho} + Wd_{i,j,\rho}}{d}\right) \\
&+ \frac{(\mathbf{D}r^0_{i,j,\rho} \times \mathbf{D}l^0_{i,j,\rho}).\mathbf{d}d^0_{i,j,\rho} + (\mathbf{D}r^0_{i,j,\rho} \times \mathbf{d}l^0_{i,j,\rho}).\mathbf{D}d^0_{i,j,\rho} + (\mathbf{d}r^0_{i,j,\rho} \times \mathbf{D}l^0_{i,j,\rho}).\mathbf{D}d^0_{i,j,\rho}}{|\mathbf{D}r^0_{i,j,\rho}||\mathbf{D}l^0_{i,j,\rho}||\mathbf{D}d^0_{i,j,\rho}|},
\end{aligned}
\tag{5.31}
$$

where expansions up to first order in the lattice displacements have been performed.

The quantity $S^0_{i,j,\rho}$, which represents the solid angle in the undisplaced lattice, is given by:

$$S^0_{i,j,\rho} = \frac{(\mathbf{D}r^0_{i,j,\rho} \times \mathbf{D}l^0_{i,j,\rho}).\mathbf{D}d^0_{i,j,\rho}}{|\mathbf{D}r^0_{i,j,\rho}||\mathbf{D}l^0_{i,j,\rho}||\mathbf{D}d^0_{i,j,\rho}|}$$

$$= \frac{3}{8L'^3}\left\{(n+m)\left[m(2m+n)\sin\left(\frac{\gamma-\theta}{2}\right) + n(2n+m)\sin\left(\frac{\gamma}{2}\right)\right]\right.$$

$$\left. +nm(m-n)\sin\left(\frac{\theta}{2}\right)\right\}. \tag{5.32}$$

Performing the calculation in (5.31) yields the following expression for the solid angle:

$$S_{i,j,\rho} = S^0_{i,j,\rho} + \frac{\sqrt{3}}{2d}C_{i,j,\rho}. \tag{5.33}$$

The function $C_{i,j,\rho}$ of the local site displacements is the first-order correction to $S^0_{i,j,\rho}$:

$$C_{i,j,\rho} = (-1)^\rho[\Delta^u u_{i,j,\rho} + \Delta^{ur} u_{r(i,j,\rho)} + \Delta^{ul} u_{l(i,j,\rho)} + \Delta^{ud} u_{d(i,j,\rho)}] +$$

$$+[\Delta^s s_{i,j,\rho} + \Delta^{sr} s_{r(i,j,\rho)} + \Delta^{sl} s_{l(i,j,\rho)} + \Delta^{sd} s_{d(i,j,\rho)}] +$$

$$+(-1)^\rho[\Delta^v v_{i,j,\rho} + \Delta^{vr} v_{r(i,j,\rho)} + \Delta^{vl} v_{l(i,j,\rho)} + \Delta^{vd} v_{d(i,j,\rho)}]. \tag{5.34}$$

The coefficients Δ depend upon the nanotube parameters n and m and the angles γ, θ and ξ and they take on a complicated form. Therefore the expressions describing these coefficients have been situated in Appendix A1.

We now have almost all of the necessary tools to write down the tight-binding hamiltonian containing first order electron-phonon interactions for a chiral nanotube. However, one must also consider terms that are necessary in removing the zero modes of the phonon hamiltonian. We address these in the next section, where we formulate the hamiltonian.

5.2 Tight-binding Hamiltonian in Carbon Nanotubes

Once again the hamiltonian is split into three parts as follows:

$$\hat{H} = \hat{H}_e + \hat{H}_{ph} + \hat{H}_{int}. \tag{5.35}$$

In this section each of the three parts is examined individually, beginning with the electron hamiltonian.

5.2.1 Electron Hamiltonian

The tight-binding electron hamiltonian is identical to that considered in section 3.3 for the 2d hexagonal case. This is due to the our only considering nearest neighbour interactions. The first nearest neighbour equilibrium separations are identical in the two lattices, however those of the second nearest neighbours are not. The electron hamiltonian is thus written as:

$$\hat{H}_e = \sum_{i,j,\rho}\left[E_0 a^\dagger_{i,j,\rho}a_{i,j,\rho} - J\sum_\delta a^\dagger_{i,j,\rho}a_{\delta(i,j,\rho)}\right], \tag{5.36}$$

where as before the electron on-site and exchange energies in the undisplaced lattice are respectively E_0 and J. The diagonalisation procedure would therefore be the same as that in chapter 3.

5.2.2 Phonon Hamiltonian

The obvious choice for the classical phonon hamiltonian is to take a combination of the squares of the terms $W\delta$ and C:

$$
\begin{aligned}
H_{ph} &= \frac{1}{2}\sum_{i,j,\rho}\left(\frac{p^2_{i,j,\rho}}{M} + \frac{q^2_{i,j,\rho}}{M} + \frac{r^2_{i,j,\rho}}{M}\right.\\
&\left. +k[Wr^2_{i,j,\rho} + Wl^2_{i,j,\rho} + Wd^2_{i,j,\rho}] + k_c C^2_{i,j,\rho}\right),
\end{aligned}
\tag{5.37}
$$

where K and K_c are the two individual elasticity coefficients. The momenta conjugate to u, v and s are respectively p, q and r. There is however a problem in taking the phonon hamiltonian in this form, since in the continuum limit it contains a zero mode. To see this we use the approximate Taylor expansions where the nearest neighbour separation $d \to 0$:

$$
\begin{aligned}
u_{i,j,1} - u_{i,j,0} &= \cos\left(\frac{\pi}{6} + \psi\right)u_x + \sin\left(\frac{\pi}{6} + \psi\right)u_y;\\
u_{i-1,j,1} - u_{i,j,0} &= \cos\left(\frac{\pi}{6} - \psi\right)u_x + \sin\left(\frac{\pi}{6} - \psi\right)u_y;\\
u_{i,j-1,1} - u_{i,j,0} &= \sin(\psi)u_x - \cos(\psi)u_y;\\
v_{i,j,1} - v_{i,j,0} &= \cos\left(\frac{\pi}{6} + \psi\right)v_x + \sin\left(\frac{\pi}{6} + \psi\right)v_y;\\
v_{i-1,j,1} - v_{i,j,0} &= \cos\left(\frac{\pi}{6} - \psi\right)v_x + \sin\left(\frac{\pi}{6} - \psi\right)v_y;\\
v_{i,j-1,1} - v_{i,j,0} &= \sin(\psi)u_x - \cos(\psi)v_y.
\end{aligned}
\tag{5.38}
$$

Here ψ is the chiral angle, defined as the angle between the chiral vector $\mathbf{C_h}$ and the lattice vector $\mathbf{a_1}$ (i.e. the angle between the chiral vector and the zig-zag direction). The cosine and sine of the chiral angle are given by the scalar products:

$$
\begin{aligned}
\cos(\psi) &= \frac{\mathbf{a_1}.\mathbf{C_h}}{|\mathbf{a_1}||\mathbf{C_h}|} = \frac{2n+m}{2L'}; \\
\sin(\psi) &= \frac{|\mathbf{a_1} \times \mathbf{C_h}|}{|\mathbf{a_1}||\mathbf{C_h}|} = \frac{\sqrt{3}m}{2L'},
\end{aligned}
\tag{5.39}
$$

and thus:

$$
\begin{aligned}
u_{i,j,1} - u_{i,j,0} &= \frac{\sqrt{3}n}{2L'}u_x + \frac{n+2m}{2L'}u_y; \\
u_{i-1,j,1} - u_{i,j,0} &= -\frac{\sqrt{3}(n+m)}{2L'}u_x + \frac{n-m}{2L'}u_y; \\
u_{i,j-1,1} - u_{i,j,0} &= \frac{\sqrt{3}m}{2L'}u_x - \frac{2n+m}{2L'}u_y; \\
v_{i,j,1} - v_{i,j,0} &= \frac{\sqrt{3}n}{2L'}v_x + \frac{n+2m}{2L'}v_y; \\
v_{i-1,j,1} - v_{i,j,0} &= -\frac{\sqrt{3}(n+m)}{2L'}v_x + \frac{n-m}{2L'}v_y; \\
v_{i,j-1,1} - v_{i,j,0} &= \frac{\sqrt{3}m}{2L'}v_x - \frac{2n+m}{2L'}v_y.
\end{aligned}
\tag{5.40}
$$

The candidate phonon hamiltonian (5.37), written in the continuum limit is:

$$
\begin{aligned}
H_{ph(cont} &= \frac{1}{2}\int [3v_y^2 + 3u_x^2 + u_y^2 + v_x^2 + 2u_xv_y + 2u_yv_x] \\
&= \frac{1}{2}\int [2(u_x^2 + v_y^2) + (u_x + v_y)^2 + (v_x + u_y)^2] + \\
&\quad + \frac{1}{2}\int \frac{1}{8}(s_{xx} + s_{yy})^2
\end{aligned}
\tag{5.41}
$$

Notice that u_x and v_y appear in the two combinations $(u_x^2 + v_y^2)$ and $(u_y - v_x)^2$, however the quantities v_x and u_y occur only in the term $(v_x + u_y)^2$, indicating that there is a zero mode. The problem was eliminated in a similar fashion to that in chapter 3, where extra fields were introduced in order to kill the zero modes. The

required prescription was to add terms that are quadratic in the following fields:

$$
\begin{aligned}
\Omega r_{i,j,\rho} &= \frac{(n+2m)}{2L'}\left[(-1)^\rho \cos\left(\frac{\xi}{2}\right)(u_r - u) + \sin\left(\frac{\xi}{2}\right)(s_r + s)\right] \\
&\quad - \frac{(-1)^\rho\sqrt{3}n}{2L'}(v_r - v); \\
\Omega l_{i,j,\rho} &= \frac{(n-m)}{2L'}\left[(-1)^\rho \cos\left(\frac{\gamma - \xi}{2}\right)(u - u_l) + \sin\left(\frac{\gamma - \xi}{2}\right)(s_l + s)\right] \\
&\quad - \frac{(-1)^\rho\sqrt{3}(n+m)}{2L'}(v_l - v); \\
\Omega d_{i,j,\rho} &= -\frac{(2n+m)}{2L'}\left[(-1)^\rho \cos\left(\frac{\xi - \theta}{2}\right)(u_d - u) + \sin\left(\frac{\xi - \theta}{2}\right)(s_d + s)\right] \\
&\quad - \frac{(-1)^\rho\sqrt{3}m}{2L'}(v_d - v).
\end{aligned}
\tag{5.42}
$$

These terms are added into the phonon hamiltonian in the following way:

$$
\begin{aligned}
H_{ph} &= \frac{1}{2}\sum_{i,j,\rho}\left(\frac{p_{i,j,\rho}^2}{M} + \frac{q_{i,j,\rho}^2}{M} + \frac{r_{i,j,\rho}^2}{M}\right. \\
&\quad + k[W r_{i,j,\rho}^2 + W l_{i,j,\rho}^2 + W d_{i,j,\rho}^2 + \Omega r_{i,j,\rho}^2 + \Omega l_{i,j,\rho}^2 + \Omega d_{i,j,\rho}^2] \\
&\quad \left. + k_c C_{i,j,\rho}^2 \right).
\end{aligned}
\tag{5.43}
$$

In the continuum limit the terms that depend upon Ω give a contribution:

$$
\begin{aligned}
H_\Omega &= \frac{1}{2}\int [3v_x^2 + 3u_y^2 + u_x^2 + v_y^2 - 2u_x v_y - 2u_y v_x] \\
&= \frac{1}{2}\int [2(u_y^2 + v_x^2) + (u_y - v_x)^2 + (u_x - v_y)^2].
\end{aligned}
\tag{5.44}
$$

This completes the formulation of the phonon hamiltonian. All that is remaining is to consider electron-phonon interactions, and it is this subject to which we now turn our attention.

5.2.3 Electron-phonon interaction

The geometrical quantities $W\delta$ and C formulated in the previous section are used to couple the electron field ϕ to the lattice site displacements. The fields $W\delta$ are coupled in a similar vein to the method imposed upon the hexagonal lattice in chapter 3. Since $C_{i,j,\rho}$ is a quantity that is symmetrical about the site (i,j,ρ), it is

sensible to include the following coupling in the interaction hamiltonian:

$$\hat{H}_{int(C)} = \chi_2 \sum_{i,j,\rho} a_{i,j,\rho}^{\dagger} a_{i,j,\rho} \hat{C}_{i,j,\rho} \tag{5.45}$$

This is the natural way to couple such a quantity, which is centred upon the site (i, j, ρ). In order to simplify matters, we chose to ignore the coupling of the exchange interaction to the solid angle terms. There are already enough parameters to investigate in order to significantly advance our knowledge of polaron states in carbon nanotubes by investigating the off-cylinder displacements. The total interaction hamiltonian is:

$$
\begin{aligned}
\hat{H}_{int} =\ & \chi_1 a_{i,j,\rho}^{\dagger} a_{i,j,\rho} (\hat{W} r_{i,j,\rho} + \hat{W} l_{i,j,\rho} + \hat{W} d_{i,j,\rho}) + \chi_2 a_{i,j,\rho}^{\dagger} a_{i,j,\rho} \hat{C}_{i,j,\rho} \\
&+ G[(a_{i,j,\rho}^{\dagger} a_{r(i,j,\rho)} + a_{r(i,j,\rho)}^{\dagger} a_{i,j,\rho}) \hat{W} r_{i,j,\rho} + (a_{i,j,\rho}^{\dagger} a_{l(i,j,\rho)} + a_{l(i,j,\rho)}^{\dagger} a_{i,j,\rho}) \hat{W} l_{i,j,\rho} \\
&+ (a_{i,j,\rho}^{\dagger} a_{d(i,j,\rho)} + a_{d(i,j,\rho)}^{\dagger} a_{i,j,\rho}) \hat{W} d_{i,j,\rho}].
\end{aligned}
\tag{5.46}
$$

There are now three electron-phonon couplings χ_1, χ_2 and G to consider. The addition of yet another coupling G_2 that could couple the exchange interation to the nanotube bending would make things even more complicated. In a moment we concentrate upon writing down the semi-classical hamiltonian. We assume that the semi-classical case corresponds to the zeroth-order adaibatic approximation as in chapter 3. Note that much of the discussion into the zeroth-order adiabatic approximation in chapter 3 is valid here if we assume the zone-folding approximation, where we assume that we can represent the effects of the small circumference by restricting the allowed electron wavevectors to a subset of those in 2d graphite. Of course, due to the modified potential and interaction terms there would be a morecomplicated diagonalization of the phonon hamiltonian, and also a more complicated interaction term $\Phi(\mathbf{k}, \mathbf{q})$ in the Frölich hamiltonian. Note that in reality the situation is much more complicated than this due to the effects of the curvature on the hybridisation of the electron orbitals [90].

5.3 Semi-classical treatment

This method involves treating the lattice displacements classically and working with the average value of the hamiltonian $\langle \Psi | \hat{H} | \Psi \rangle$. The state $|\Psi\rangle$ is a product of the

electronic and phonon wavefunctions:

$$|\Psi\rangle = |\psi_e\rangle|\Phi\rangle \tag{5.47}$$

The displacement operators u, v and s act upon the coherent phonon state, giving the classical lattice displacements:

$$\hat{u}_{i,j,\rho}|\Phi\rangle = u_{i,j,\rho}|\Phi\rangle$$

$$\hat{v}_{i,j,\rho}|\Phi\rangle = v_{i,j,\rho}|\Phi\rangle$$

$$\hat{s}_{i,j,\rho}|\Phi\rangle = s_{i,j,\rho}|\Phi\rangle. \tag{5.48}$$

The electron wavefunction is:

$$|\psi_e\rangle = \sum_{i,j,\rho} \phi_{i,j,\rho} a^\dagger_{i,j,\rho}|0\rangle, \tag{5.49}$$

where $|0\rangle$ is the quasiparticle vacuum state. The average value of the hamiltonian for a system with state vector of this form is:

$$\begin{aligned}
\tilde{H} &= \langle\Psi|\hat{H}|\Psi\rangle \\
&= \sum_{i,j,\rho} \Bigg((W+\epsilon)|\phi_{i,j,\rho}|^2 - j(\phi^*_{i,j,\rho}\phi_{r(i,j,\rho)} + \phi^*_{r(i,j,\rho)}\phi_{i,j,\rho} \\
&\quad + \phi^*_{i,j,\rho}\phi_{l(i,j,\rho)} + \phi^*_{l(i,j,\rho)}\phi_{i,j,\rho} + \phi^*_{i,j,\rho}\phi_{d(i,j,\rho)} + \phi^*_{d(i,j,\rho)}\phi_{i,j,\rho}) \\
&\quad + \chi_1|\phi_{i,j,\rho}|^2(Wr_{i,j,\rho} + Wl_{i,j,\rho} + Wd_{i,j,\rho}) + \chi_2|\phi_{i,j,\rho}|^2 C_{i,j,\rho} \\
&\quad + G_2[(\phi^*_{i,j,\rho}\phi_{r(i,j,\rho)} + \phi^*_{r(i,j,\rho)}\phi_{i,j,\rho})Wr_{i,j,\rho} + (\phi^*_{i,j,\rho}\phi_{l(i,j,\rho)} + \phi^*_{l(i,j,\rho)}\phi_{i,j,\rho})Wl_{i,j,\rho} \\
&\quad + (\phi^*_{i,j,\rho}\phi_{d(i,j,\rho)} + \phi^*_{d(i,j,\rho)}\phi_{i,j,\rho})Wd_{i,j,\rho}]\Bigg). \tag{5.50}
\end{aligned}$$

The normalisation of the state $|\psi_e\rangle$ requires that the coefficients $\phi_{i,j,\rho}$ obey the normalisation condition:

$$\sum_{i,j,\rho} |\phi_{i,j,\rho}|^2 = 1. \tag{5.51}$$

In modelling the semi-classical equations this condition must be taken into account at all times. The equations of motion corresponding to this transformed hamiltonian are the Schrödinger equation for the field ϕ and hamilton's equations for the three displacement fields. The three equations describing the displacement fields are long,

however we present them here due to their central importance. The four equations are:

$$i\frac{\partial \phi_{i,j,\rho}}{\partial t} = (W + \epsilon)\phi - 2j(\phi_r + \phi_l + \phi_d) + \chi_1\phi(W_r + W_l + W_d)$$

$$+\chi_2\phi C + 2G_2[\phi_r W_r + \phi_l W_l + \phi_d W_d] \tag{5.52}$$

$$\frac{\partial^2 u_{i,j,\rho}}{\partial t^2} = -\left\{ \frac{k(-1)^\rho}{L'} \left[\sqrt{3}(n+m)\cos\left(\frac{\gamma-\xi}{2}\right)W_l - \sqrt{3}n\cos\left(\frac{\xi}{2}\right)W_r \right.\right.$$

$$-\sqrt{3}m\cos\left(\frac{\xi-\theta}{2}\right)W_d + (n-m)\cos\left(\frac{\gamma-\xi}{2}\right)\Omega_l$$

$$-(n+2m)\cos\left(\frac{\xi}{2}\right)\Omega_r + (2n+m)\cos\left(\frac{\xi-\theta}{2}\right)\Omega_d\bigg]$$

$$+k_c(-1)^\rho[\Delta^u C - \Delta^{ur}C_r - \Delta^{ul}C_l - \Delta^{ud}C_d]$$

$$+\frac{\sqrt{3}(-1)^\rho\chi_1}{2L'}\left\{ |\phi|^2\left[(n+m)\cos\left(\frac{\gamma-\xi}{2}\right) - n\cos\left(\frac{\xi}{2}\right) \right.\right.$$

$$-m\cos\left(\frac{\xi-\theta}{2}\right)\bigg] - n\cos\left(\frac{\xi}{2}\right)|\phi_r|^2$$

$$+(n+m)\cos\left(\frac{\gamma-\xi}{2}\right)|\phi_l|^2 - m\cos\left(\frac{\xi-\theta}{2}\right)|\phi_d|^2\bigg\}$$

$$+\chi_2(-1)^\rho[\Delta^u|\phi|^2 - \Delta^{ur}|\phi_r|^2 - \Delta^{ul}|\phi_l|^2 - \Delta^{ud}|\phi_d|^2]$$

$$+\frac{\sqrt{3}(-1)^\rho G_2}{L'}\left[(\phi^*\phi_l + \phi_l^*\phi)(n+m)\cos\left(\frac{\gamma-\xi}{2}\right) \right.$$

$$\left.\left.-(\phi^*\phi_r + \phi_r^*\phi)n\cos\left(\frac{\xi}{2}\right) - (\phi^*\phi_d + \phi_d^*\phi)m\cos\left(\frac{\xi-\theta}{2}\right)\right]\right\} \tag{5.53}$$

$$\frac{\partial^2 s_{i,j,\rho}}{\partial t^2} = -\left\{\frac{k}{L'}\left[\sqrt{3}n\sin\left(\frac{\xi}{2}\right)W_r + \sqrt{3}(n+m)\sin\left(\frac{\gamma-\xi}{2}\right)W_l\right.\right.$$

$$+\sqrt{3}m\sin\left(\frac{\xi-\theta}{2}\right)W_d + (n+2m)\sin\left(\frac{\xi}{2}\right)\Omega_r$$

$$+(n-m)\sin\left(\frac{\gamma-\xi}{2}\right)\Omega_l - (2n+m)\sin\left(\frac{\xi-\theta}{2}\right)\Omega_d$$

$$+k_c[\Delta^s C + \Delta^{sr}C_r + \Delta^{sl}C_l + \Delta^{sd}C_d]$$

$$+\frac{\sqrt{3}\chi_1}{2L'}\left\{|\phi|^2\left[(n+m)\sin\left(\frac{\gamma-\xi}{2}\right) + n\sin\left(\frac{\xi}{2}\right)\right.\right.$$

$$+m\sin\left(\frac{\xi-\theta}{2}\right)\Big] + n\sin\left(\frac{\xi}{2}\right)|\phi_r|^2$$

$$+(n+m)\sin\left(\frac{\gamma-\xi}{2}\right)|\phi_l|^2 + m\sin\left(\frac{\xi-\theta}{2}\right)|\phi_d|^2\bigg\}$$

$$+\chi_2[\Delta^s|\phi|^2 + \Delta^{sr}|\phi_r|^2 + \Delta^{sl}|\phi_l|^2 + \Delta^{sd}|\phi_d|^2]$$

$$+\frac{\sqrt{3}G_2}{L'}\left[(\phi^*\phi_l + \phi_l^*\phi)(n+m)\sin\left(\frac{\gamma-\xi}{2}\right)\right.$$

$$\left.\left.+(\phi^*\phi_r + \phi_r^*\phi)n\sin\left(\frac{\xi}{2}\right) + (\phi^*\phi_d + \phi_d^*\phi)m\sin\left(\frac{\xi-\theta}{2}\right)\right]\right\} \quad (5.54)$$

$$\frac{\partial^2 v_{i,j,\rho}}{\partial t^2} = -\left\{\frac{k(-1)^\rho}{L'}\left[(2n+m)W_d - (n-m)W_l - (n+2m)W_r + \sqrt{3}n\Omega_r\right.\right.$$

$$+\sqrt{3}(n+m)\Omega_l + \sqrt{3}m\Omega_d\Big]$$

$$+k_c(-1)^\rho[\Delta^v C - \Delta^{vr}C_r - \Delta^{vl}C_l - \Delta^{vd}C_d]$$

$$+\frac{(-1)^\rho\chi_1}{2L'}\left[(2n+m)|\phi_d|^2 - (n-m)|\phi_l|^2 - (n+2m)|\phi_r|^2\right]$$

$$+\chi_2(-1)^\rho[\Delta^v|\phi|^2 - \Delta^{vr}|\phi_r|^2 - \Delta^{vl}|\phi_l|^2 - \Delta^{vd}|\phi_d|^2]$$

$$+\frac{(-1)^\rho G_2}{L'}\left[(\phi^*\phi_d + \phi_d^*\phi)(2n+m)\right.$$

$$\left.\left.-(\phi^*\phi_l + \phi_l^*\phi)(n-m) - (\phi^*\phi_r + \phi_r^*\phi)(n+2m)\right]\right\} \quad (5.55)$$

In each case the subscript $\delta = r, l, d$ refers to the index $\delta(i, j, \rho)$. We also use the notation $\phi \equiv \phi_{i,j,\rho}$, $u \equiv u_{i,j,\rho}$ etc. Let us now look at the equations that describe tubes of large radii.

5.3.1 Approximate solution c.f.

We now investigate the equations (5.52-5.55) in the approximation describing tubes of large radii . This is a straightforward generalisation to a chiral nanotube of the method presented in [51], [72]. In this limit it is assumed that the angles γ, θ and ξ are equal to zero. This greatly simplifies the hamiltonian and equations of motion. We then make the further simplification that $G = 0$, i.e. only the electron on-site energy is coupled to the lattice. With these considerations taken into account, the equations of motion become:

$$i\frac{\partial \phi}{\partial t} = (W + \epsilon)\phi + \chi_1 \phi Z + \chi_2 \phi C \qquad (5.56)$$

$$\frac{\partial^2 u}{\partial t^2} = 2K(u_r + u_l + u_d - 3u) + \\ + \frac{(-1)^\rho \sqrt{3}\chi_1}{2L'}\left(n|\phi_r|^2 - (n+m)|\phi_l|^2 + m|\phi_d|^2\right)\Big] \qquad (5.57)$$

$$\frac{\partial^2 s}{\partial t^2} = -K_c(C_r + C_l + C_d - 3C) + \chi_2(3|\phi|^2 - |\phi_r|^2 - |\phi_l|^2 - |\phi_d|^2) \qquad (5.58)$$

$$\frac{\partial^2 v}{\partial t^2} = 2K(v_r + v_l + v_d - 3v) + \\ + \frac{(-1)^\rho \chi_1}{2L'}\left((2m+n)|\phi_r|^2 + (n-m)|\phi_l|^2 - (2n+m)|\phi_d|^2\right)\Big] \qquad (5.59)$$

where:

$$Z = \frac{(-1)^\rho}{2L'}\Big[\sqrt{3}(nu_r - (n+m)u_l + mu_d) + \\ + (2m+n)v_r + (n-m)v_l - (2n+m)v_d\Big] \qquad (5.60)$$

These equations are extremely interesting, since for example the quantity $(u_l + u_d + u_r - 3u)$ is the finite difference approximation to the laplacian $\Delta_4 u$ centred upon the site (i, j, ρ). Imposing the constraint that the equations are stationary, one arrives at the following system of equations:

$$0 = \lambda\phi - 2(\phi_r + \phi_l + \phi_d) + \chi_1\phi Z + \chi_2\phi C \qquad (5.61)$$

$$\Delta_4 u = \frac{\sqrt{3}\tilde{g}_1}{4L'}\left((n+m)|\phi_l|^2 - n|\phi_r|^2 - m|\phi_d|^2\right) \qquad (5.62)$$

$$\Delta_4 C = \tilde{g}_2\Delta_3|\phi|^2 \qquad (5.63)$$

$$\Delta_4 v = \frac{\tilde{g}_1}{4L'}\left((2n+m)|\phi_d|^2 - (n-m)|\phi_l|^2 - (2m+n)|\phi_r|^2\right) \qquad (5.64)$$

where $\tilde{g}_1 = \chi_1/K$ and $\tilde{g}_2 = \chi_2/K_c$. The stationary equations describing the displacement fields are now used to eliminate Z and C from the expression (5.61). Equations (5.62) and (5.64) describe the four-point laplacians of the respective u and v fields around a central site (i, j, ρ). These relations are used to calculate the four-point laplacian of the quantity Z:

$$\begin{aligned} \Delta_4 Z &= \frac{\tilde{g}_1}{4}(6|\phi_{i,j,0}|^2 - |\phi_{i+1,j-1,0}|^2 - |\phi_{i-1,j,0}|^2 - \\ &\quad -|\phi_{i,j+1,0}|^2 - |\phi_{i+1,j,0}|^2 - |\phi_{i-1,j+1,0}|^2 - |\phi_{i,j-1,0}|^2) \\ &= -\frac{\tilde{g}_1}{4}\Delta_7|\phi_{i,j,0}|^2 \end{aligned} \tag{5.65}$$

The above form is that of a seven-point laplacian that includes one central site and its six next to nearest neighbours. Precisely the same form of expression holds for the case $\rho = 1$ with its six next to nearest neighbours. Therefore we have the expression:

$$\Delta_4 Z = -\frac{\tilde{g}_1}{4}\Delta_7|\phi|^2 \tag{5.66}$$

There exists a simple solution to this equation (as observed in [51]). In fact, the four-point laplacian of the following quantity provides the remedy:

$$Z = -\frac{\tilde{g}_1}{4}(|\phi_r|^2 + |\phi_l|^2 + |\phi_d|^2 + 3|\phi|^2) \tag{5.67}$$

The stationary equation for the s field (5.63) provides us with the relation:

$$\Delta_4 C = -\tilde{g}_2\Delta_4|\phi|^2 \tag{5.68}$$

which is trivially solved by $C = -\tilde{g}_2|\phi|^2$. Inserting this result, along with (5.67) into the stationary equation for ϕ (5.61) gives:

$$\lambda\phi_{i,j,0} - 2\Delta_4\phi_{i,j,0} - \frac{\tilde{g}_1}{4}\phi(\Delta_4|\phi_{i,j,0}|^2 + 6|\phi_{i,j,0}|^2) - \chi_2\tilde{g}_2\phi_{i,j,\rho}|\phi_{i,j,\rho}|^2 \tag{5.69}$$

This is a two-dimensional modified discrete nonlinear schrodinger equation with an extra term (MDNLS). The discrete nonlinear schrodinger equation has been well studied in two dimensions [69]. Many results are available for the square lattice (see [70], [68] for references), and the equation has also been studied on triangular and hexagonal lattices [71]. In this final reference localized solutions were found

February 28, 2006

which exhibited some of the properties that were discussed in chapter 4. The authors showed that there existed states localized in both lattice dimensions when the non-linearity parameter lay above some critical value. At lower values of the nonlinearity parameter the system was found to move into a state which is delocalized.

5.4 Chapter Summary

The focus of this chapter has been to formulate the models discussed in the previous chapters onto a general three-dimensional chiral nanotube. We started by considering the nanotube geometry, each individual tube being specified by a pair of integers (n, m), which define the tube chiral vector. These parameters enter the expressions that were formulated to describe the displacement of the lattice sites. The consideration of the nanotube geometry led on to the formulation of the tight-binding hamiltonian with nearest neighbour interactions. The lattice potential was modified to contain extra terms which describe the bending modes of the lattice. These terms were also naturally coupled to the electron on-site energy. The final hamiltonian contained three electron-phonon coupling parameters. Two described the coupling of the electron on-site energy to the stretching and bending modes of the nanotube, the other coupled the exchange energy to the stretching modes. Any impact of the nanotube bending upon the exchange interaction was neglected for simplicity.

Treating the lattice displacements classically and the electron field quantum mechanically led to a system of semi-classical equations. As an approximation the coupling of the exchange interaction to the lattice was neglected. In such a case it was shown that the stationary equations could be combined into a single equation describing the electron field. Furthermore the form of this equation was that of a two-dimensional modified discrete nonlinear Schrödinger equation. This equation has been studied intensively [69] and has been found to admit localised solutions.

In the following chapter we look for localized numerical solutions to the full system of semi-classical equations (5.50-5.55) in two types of nanotube - one chiral and one achiral, and analyse the stability of certain excited states.

February 28, 2006

Chapter 6

Numerical simulations of localized quasiparticles in carbon nanotubes

In this chapter we present some numerical results obtained through simulation of the semi-classical equations of motion derived in chapter 5 for a chiral carbon nanotube. Various ground states are shown to exist for different values of the system couplings. We briefly mention some attempts to describe excited polaron states.

6.1   Introduction

The previous chapter dealt with the formulation of the tools required to study polaron states in chiral carbon nanotubes. A number of simplifications were involved in the model construction. The model was based on a tight-binding approximation and the lattice site displacements were assumed to be small. It was observed that in the case of the 2d hexagonal lattice, this second assumption was valid providied that the electron-phonon coupling was not too large. The third assumption is that it is valid to work in the zeroth-order adiabatic approximation when considering these systems. It has been shown that in the one-dimensional chain this is indeed the case provided that the electron-phonon coupling is not too small [18]. Thus there exists a range of applicability of the model that may lead to predictions verifiable by experiment. The determination of the exact range of applicability is not our concern here. We simply note that there will be some range of real physical applicability

which will lie in the regime where the electron-phonon coupling is significant and the maximum lattice distortion can still be considered small.

It is the aim of this chapter to investigate numerically some of the self-trapped electron states in carbon nanotubes, based on the semi-classical approximation. The chapter focusses around results for two types of tube: an $(8,0)$ zig-zag tube and an $(8,4)$ chiral tube. The main aim of this section is to present the types of states that are seen in the semi-classical equations. Many of these states are found to closely resemble those examined in chapter 4, however they have a more complex and interesting structure due to the presence of the off-cylindrical displacements.

6.2   Parameters

Here we discuss the approximate values of the parameters that one may expect to describe carbon nanotubes. From the broad spectrum of nanotube research we have the following predictions [22], [73], [74], [24] (chapter 4):

$$
\begin{aligned}
d &= 1.42A; & J &= 2.4 - 3.1eV; & G &\approx 4.8 - 6\frac{eV}{A}; \\
K &= 36.5 \times 10^4 \frac{dyn}{cm}; & K_c &= 9.8 \times 10^4 \frac{dyn}{cm}.
\end{aligned}
\tag{6.1}
$$

As in the case of the two-dimensional hexagonal lattice, we represent the energies in units of J:

$$
\begin{aligned}
u &= lU; & v &= lV; & s &= lS; & K &= \frac{\kappa}{l^2}J \\
K_c &= \frac{\kappa_c}{l^2}J; & \chi_1 &= \frac{X_1}{l^2}J; & \chi_2 &= \frac{X_2}{l^2}J; & G_1 &= \frac{G}{l^2}J \\
\epsilon_0 &= \tilde{\epsilon}_0 J.
\end{aligned}
\tag{6.2}
$$

Again the length scale is chosen so that $\kappa = 1$, which gives a length scale of one quarter the size of the nearest-neighbour distance d. We then have approximately $G \approx 0.7$ and $\kappa_c \approx 0.25$. The values of χ_1 and χ_2 were unknown. It has been estimated that reasonable values for the on-site coupling parameters are $X_1 \approx 0.8$ and $X_2 \approx 0.2$ [76]. We have determined the ground state for these estimates of the parameters. We also present the ground states for other values of the couplings, in order to observe the variation in states that the model produces.

February 28, 2006

6.3   State Observation

6.3.1   Energy absorption

In order to model the stationary equations, absorbative terms were again introduced into the equations of motion, as discussed in chapter 4. Due to the long execution times of the simulations into 3d nanotubes, it was important to discover the optimum damping coefficient, particularly in the case of the kinetic damping. Figure 6.1 displays curves that describe the evolution of the system kinetic energy for three different values of the damping parameter ν. It was decided that the optimum damping corresponded to a value of $\nu = 1$, since this produced a comparatively rapid relaxation to within proximity of the ground state energy. This value was identical to that chosen when modelling the flat hexagonal system in chapter 4.
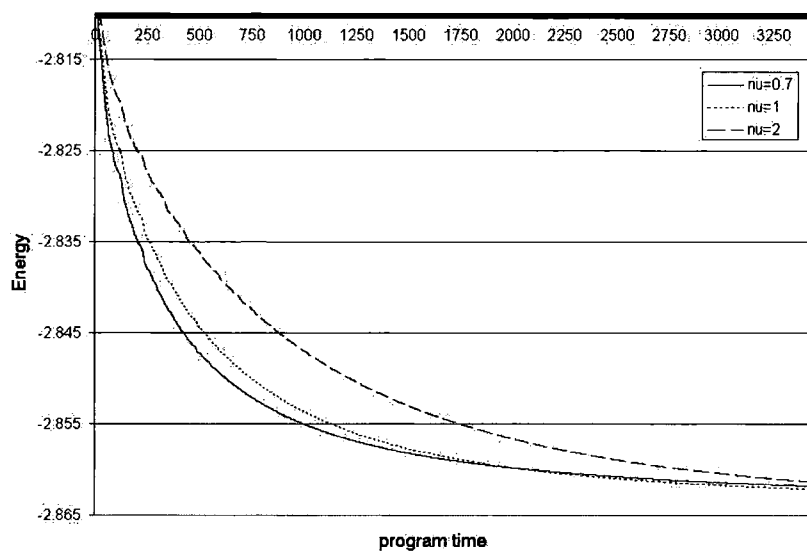
Figure 6.1: *Kinetic energy damping curves for $G = 0.7, X_1 = 0.8$ and $X_2 = 0.2$. The three curves correspond to three differing values of the damping parameter ν.*

The process of absorbing energy from the electron field proved to be more destructive than in the graphite model. This destructiveness was manifest in the magnitude in the violation of the normalization condition (5.51). It was therefore necessary to remain careful at all times to ensure that the electron field damping was kept at a sufficiently low level. Note that the presence of the damping again

resulted in a vast decrease in the amount of time required to reach the stationary configuration.

6.3.2 Quasiparticle states in carbon nanotubes

Simulations once again involved the use of a fourth-order Runge-Kutta method to integrate the equations of motion. Simulations were carried out on a zig-zag nanotube with parameters (8,0) and a chiral tube with parameters (8,4). The length of the zig-zag tube was set to 30 nanotube cells. This corresponded to a total of 960 lattice sites. The length of the chiral tube was 10 cells, producing a total of 1120 lattice sites (see section 5.1). The size of the nanotube unit cell is much larger for the (8,4) chiral tube than for the zig-zag tube due to the larger magnitude of the nanotube translation vector $\mathbf{T}$. The boundary conditions in the circumferential direction were obviously periodic. It was decided in this case that the boundary conditions in the direction of the tube axis should be free, instead of periodic. This allowed for a stretching or compression of the nanotube along its axis due to the presence of localized solutions. In order to stop a global translation of the tube a single lattice site was fixed by a quadratic potential, as was the method used in [76]. In this paper the equations for zig-zag nanotubes were constructed analogously to those derived in chapter 5. The chiral equations utilized here form a generalization of the zig-zag equations. In the paper the quasiparticle ground state was investigated as a function of the couplings X_1, X_2 and G_1. Here we simply quote some the main results of the investigations and further verify the results by showing some of the states that were observed here also.

In order to completely represent the state of the quasiparticle in a single diagram, we use the method of presentation introduced in [76]. The circumferential direction corresponds to the x-axis. The tube is unrolled and plotted on a two-dimensional plane. One should then envisage the right and left hand sides of each figure to be connected, although in many of the figures only a small section of the full nanotube is plotted. The deformation fields u and v are given explicitly by showing the displaced positions of the lattice sites. The probability density is represented by a shaded circle at the centre of each nanotube site. Darker colours indicate higher

<div align="right">**February 28, 2006**</div>

probability densities, however the scale varies between diagrams and is given on the right hand side of each picture. The off-cylinder displacements s are described by an arrow eminating from the centre of each site. The length of the arrow determines the size of the distortion. If the arrow points downwards the displacement is towards the nanotube axis. Upward pointing arrows represent displacements away from the axis.

We begin the analysis of the observed states by examining the ground state in an $(8,0)$ and an $(8,4)$ nanotube for the values of the couplings predicted in section 6.2.

Predicted ground state in (8,0) nanotube

The predicted ground state is shown in fig 6.2. This state has been named type I [76].
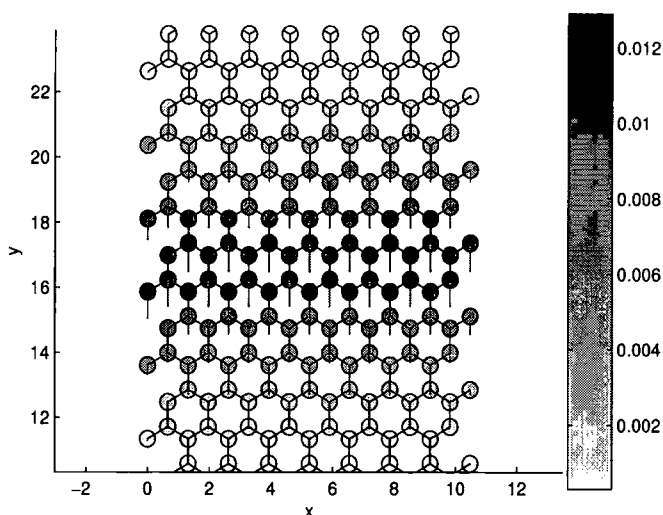
Figure 6.2: *Type I solution in an* $(8,0)$ *nanotube for* $G = 0.7$, $X_1 = 0.8$ *and* $X_2 = 0.2$

The solution is in many ways identical to the 1d soliton seen in the 2d hexagonal lattice and discussed in chapter 4. There is a uniform drawing in of the nanotube sites towards the soliton centre. This distortion is greatest at points in the lattice which are close to the soliton. The magnitude of the displacement is again quite small, and is invisible in the figure. The solution is uniform in the circumferential

direction (i.e. along the x-axis). The most interesting development upon the 2d hexagonal model involves the predictions for the out of plane displacements s. The type I solution distorts the tube in such a way that the sites in its immediate vicinity are dragged in towards the centre of the nanotube. This distortion is greatest along the central ridge of the soliton. The magnitude of the s displacement was in fact quite small, and the arrows were therefore magnified by a factor of twenty. They are scaled to fit with the y-axis, so that an arrow of length equal to unity represents an off cylinder displacement of $d/20$.

Predicted ground state in (8,4) nanotube

We next examine the ground state for the same parameters in the $(8, 4)$ nanotube, which is plotted in figure 6.3.
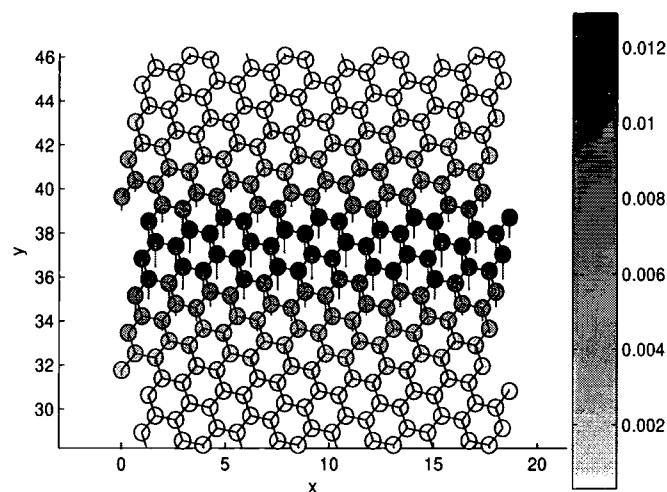
Figure 6.3: *Type I solution in an* $(8, 4)$ *nanotube for* $G = 0.7$, $X_1 = 1.6$ *and* $X_2 = 0.2$

It is straightforward to see that the states in the two differing nanotubes share the same characteristics. The same magnifications have been performed upon the displacement fields. The sites close to the soliton have again been drawn in toward the tube axis. The magnitudes of the displacements in the $(8, 0)$ and $(8, 4)$ nanotubes are evidently very similar for this type of solution. It seems that in this case the chirality has no significant effect upon the ground state of the system. We now turn

February 28, 2006

our attention to an examination of some of the other observed states.

Type II solitons (Localized mainly around one site) (fig 6.4)

The probability density is situated mostly on a single central site ($|\phi|^2_{max} \approx 0.7$). The remaining density is distributed mostly over the three nearest neighbour sites (cf fig 4.6). As in the case of the 2d hexagonal lattice, the surrounding sites are drawn in towards the centre of the soliton. In figure 6.4 the displacements are magnified by a factor of 2 in order to make them more visible. The magnitudes of the displacements around the type II soliton increase with increasing X_1. The s displacements in this case are again very interesting. Most of the sites around the soliton centre, including the central site, are dragged in towards the tube axis. The magnitude of displacement is greatest at the central site and the other three surrounding sites. The displacement does not simply reduce in magnitude as one moves from the soliton centre - there are also sites which are pushed away from the tube axis, most notably the one directly below the central site in the figure. Such complex displacement patterns are a very interesting feature of the localized quasiparticle states in the three-dimensional model which for obvious reasons do not arise in the corresponding 2d model.
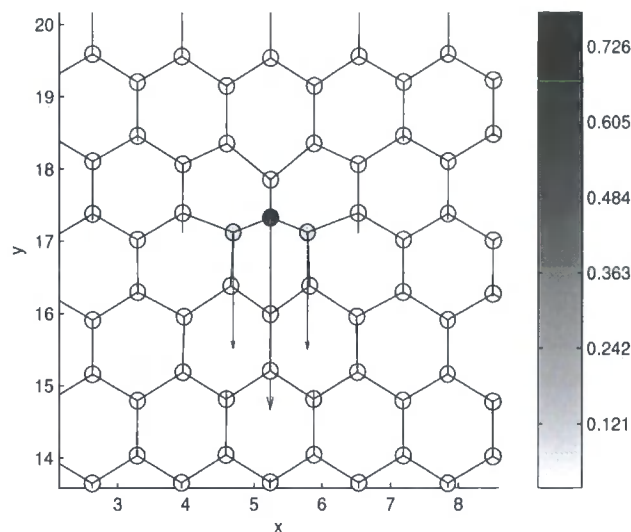

Figure 6.4: *Type II solution in an $(8, 0)$ nanotube for $G = 0.7$, $X_1 = 2.4$ and $X_2 = 0.2$*

Figure 4.5 shows the same state observed in the chiral $(8, 4)$ nanotube. It is evident once again that the structures of the two states show the same characteristics. However, the s-displacement field shows an even more complex structure, with certain sites drawn out of the tube and others pushed inwards. In this and the previous case the s displacements have been magnified by a factor of 4 compared to the real displacements.

Figure 6.5: *Type II solution in an* $(8, 4)$ *nanotube for* $G = 0.7$, $X_1 = 2.4$ *and* $X_2 = 0.2$

Type III solitons (Localized mainly around two sites) (fig 6.6)

This state is analogous to the state in fig (4.10) and represents a solution trapped predominantly around two lattice sites in the chiral tube. The u and v displacements have again been magnified by a factor of 2. As is evident from the figure, the two central sites have been drawn considerably closer towards one another. As have the other four nearest neighbours. All of the six central sites have been drawn in considerably towards the centre of the nanotube. The sites that surround these six have mostly then been pushed outwards, once again creating a rippling in the nanotube surface.
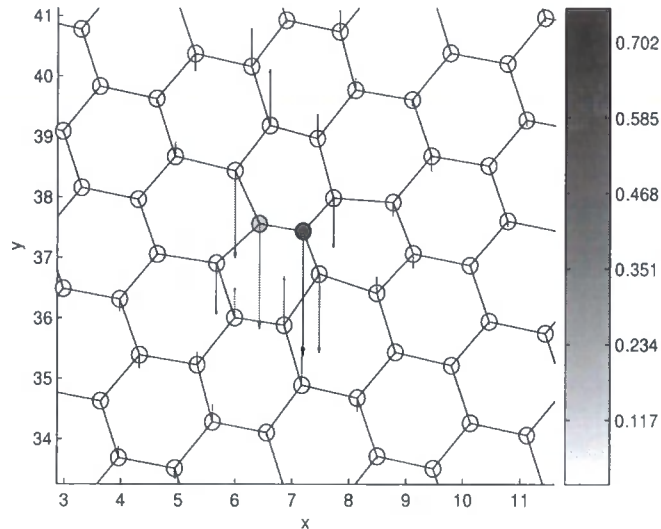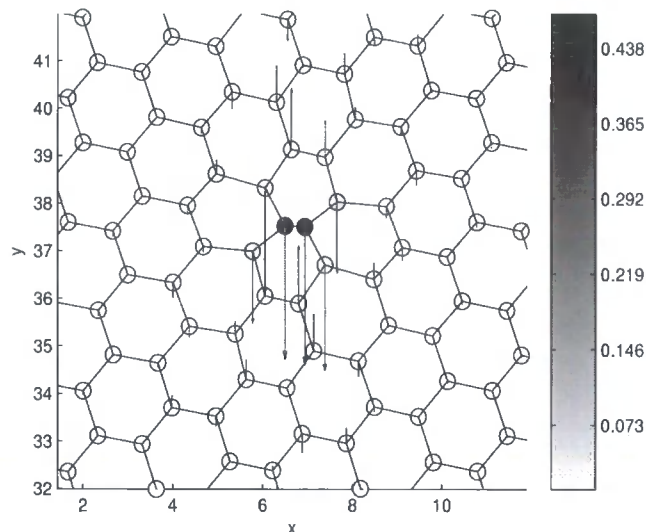
Figure 6.6: *Type III solution in an (8,0) nanotube for* $G = 2.5, X_1 = 1.6$ *and* $X_2 = 0.2$

Type IV solitons (Localized mainly around three sites) (fig 6.7)

The type IV solution is localized mainly on three lattice sites. The central site contains around 50 percent of the probability density, with most of the rest residing on the two closest neighbours. These neighbours have been drawn in considerably closeer to the central site than its other nearest neighbour. The value of s field on the three central sites is large and negative (i.e. the sites are drawn in towards the nanotube axis). The site directly beneath the central site in the figure however shows distortion away from the centre of the cylinder. Note that for the values of the couplings used to produce figure 6.7, the results obtained did not correspond to the ground state, which was known from [76] to be type III. Interestingly the type IV solution that was observed showed little willingness to decay into the lower energy state, indicating a fairly high degree of stability. Such a topic would be interesting for future investiagtion.

In order to determine if the initial conditions would alter the pattern of deformation around the soliton, a number of simulations were carried out starting from different inital conditions. These conditions corresponded to some of the states already discussed in this chapter. Two sets of parameters were chosen, which were
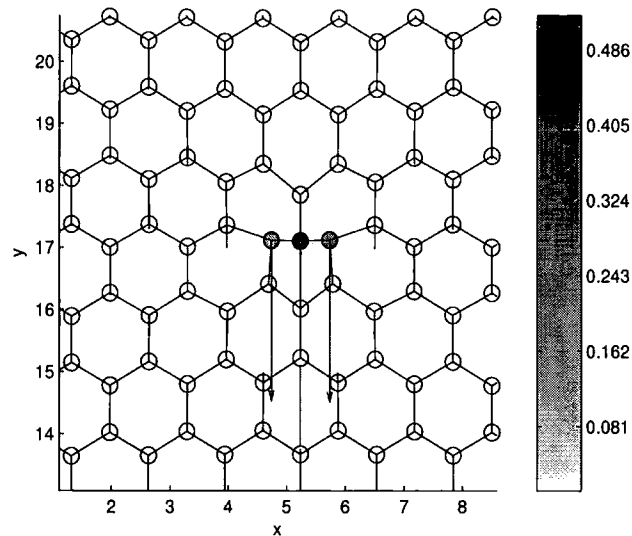
Figure 6.7: *Type IV solution in an* $(8,0)$ *nanotube for* $G = 3.5, X_1 = 1.6$ *and* $X_2 = 0.2$

known to have respective ground states corresponding to a type II and type III solution respectively. Two simulations were carried out for each set of couplings, one corresponding to delocalized initial conditions, the other to some form of 2d localized initial conditions. In each case the stationary configuration was observed to be independent of the initial conditions.

Scanning of parameters

Because of the nature of the program used to model the states presented in this chapter, simulation times were extremely large. This was due to use of the Runge-Kutta method of integration. It was therefore difficult to scan the coupling phase space in order to observe the ground state regions, as was done for the hexagonal lattice in chapter 4. The Runge-Kutta method however proved to be useful in the modelling of excited nanotube states, for which the absorption of energy from the electron field was destructive (see section 6.4). The electron-phonon coupling parameters have however been fully scanned for a zig-zag nanotube in a separate procedure using a relaxation method, the results of which are presented in our collaboration paper [76]. We settle here for a small summary of the results presented

in this paper:

First consider the case where X_1 and X_2 are fairly small (in the paper they were set to 0.6 and 0.2 respectively). At $G = 0$ the ground state is a type I solution. Upon increasing G the ground state does not change until $G \approx 1.2$. The ground state is then type III (localized mainly around two central sites). This remains the ground state until very high values of G (exceeding 5), where the type IV solution appears. Note that the degree of localization around the central two sites increases with the electron-phonon coupling.

Now keeping G and X_2 small and increasing X_1, the ground state is again the type I solution (Davydov soliton) for $X_1 < 1.2$. The ground state for higher values of X_1 is then type II. The degree of localization is again found to increase, with the electron probability density approaching 1 at the central site for very large values of X_1.

Finally, for increasing X_2 while keeping G and X_1 small the system tends to want to move towards the type I state. In all three regimes described above, once localization in both lattice dimensions occurs, the energy decreases fairly rapidly with the electron-phonon coupling, in a similar fashion to figure 4.8. The results are in good agreement with those in the two-dimensional hexagonal system. However the off-cylinder displacements provide for a richer variability in the main catergories of states, and for more detail one is urged to refer to [76].

6.4 Excited Nanotube states

As has already been mentioned, one of the most remarkable properties of carbon nanotubes is that their geometry determines whether they are semiconducting or metallic in nature. The reason for this is that due to the circumferential boundary conditions imposed upon the electronic wavefunction, the two dimensional energy dispersion in graphite is split into one-dimensional cross sections that determine the nanotube band structure. The procedure of 'chopping' the 2d graphite dispersion is known as the zone-folding approximation, which we now use to predict the energy band structure of an $(8,0)$ nanotube. This is a standard procedure that is available

in a wide range of literature (see for e.g. [22]).

In a nanotube of circumference L, the electron wavelengths λ_x perpendicular to the tube axis are restricted by the following periodic condition:

$$q\lambda_x = L, \tag{6.3}$$

where q is an integer. This restricts the allowed values of k_x:

$$k_x = \frac{2\pi q}{L} \tag{6.4}$$

The number of values of k_x is restricted due to the equivalence of states related by a reciprocal lattice vector. The energy dispersion of two dimensional graphite was found in section 3.32 to be:

$$E_\xi(\mathbf{k}) = \epsilon_0 \pm J\sqrt{3 + 2\cos(\mathbf{k}.\mathbf{a_1}) + 2\cos(\mathbf{k}.\mathbf{a_2}) + 2\cos(\mathbf{k}.(\mathbf{a_1} - \mathbf{a_2}))}. \tag{6.5}$$

which for a zig-zag nanotube becomes:

$$E_\xi(\mathbf{k}) = \epsilon_0 \pm J\sqrt{1 + 4\cos\left(\frac{\sqrt{3}a}{2}k_x\right)\cos\left(\frac{a}{2}k_y\right) + 4\cos^2\left(\frac{a}{2}k_y\right)}. \tag{6.6}$$

For an $(8, 0)$ nanotube with circumference given by (5.1) the conditions imposed on the electron wavevectors result in the band structure depicted in figure 6.8. The lowest band corresponds to the case $k_x = 0$ (i.e. $\lambda \to \infty$). We consider now the type I solutions (Davydov solitons) that were observed in the numerical procedures. Upon closer inspection of the quasiparticle amplitude, it was obvious that there was no phase in the azimuthal component of the wavefunction. This state was therefore, as expected, composed of electron states near the lowest band minimum. In order to try and simulate excited states, the wavefunction was modulated by a phase around the nanotube circumference. The phase was chosen so that a state was created that corresponded to superpositions of electron states in the second lowest band $(q = 1)$. These initial conditions were supplemented by the deformation field from the state with $k_x = 0$. Energy was absorbed only from the lattice kinetic terms, to ensure that there was no violation of the electron field normalisation that could affect the excited state. The resulting quaiparticle state was stable for quite a large amount of time, however eventually was found to decay into the state $q = 0$.
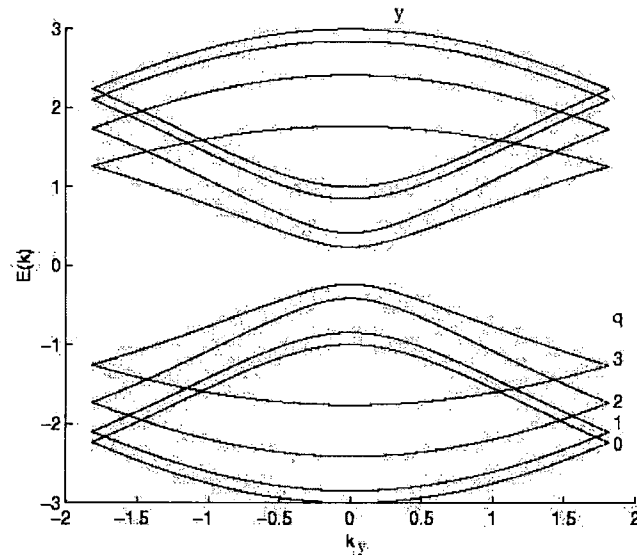
February 28, 2006

Figure 6.8: *Energy dispersion of an* $(8,0)$ *carbon nanotube predicted by zone-folding*

6.4.1 States from the upper bands

In order to investigate states from the lowest upper band, certain inital conditions have been predicted [77]. These conditions amount to modulating the ground state solution by a phase corresponding to $q = 3$ and inserting negative signs in front of amplitudes defined on selected sites. Solutions were sought that corresponded to these initial conditions. Unfortunately the state specified by the initial conditions decayed immediately. Note that in each case it was assumed that the lattice displacements were the same as the ground state, which may be the case, since the probability density for the electron is unaltered. For the time being the stability is unobserved.

6.5 Summary

In this chapter we have examined some of the numerical solutions to the equations of motion derived in the semi-classical case on the nanotube. Some very interesting states have been observed both in a chiral and a zig-zag nanotube. Firstly, there are obvious parallels between the states observed in the 2d hexagonal system and those observed here. The ground state variation in the coupling phase space [76]

follows a very similar pattern to that presented in chapter 4. Secondly, the states that have been observed in the three dimensional model provide captivating new insight due to the presence of the out-of plane displacement field s. Numerical simulations showed that accompanying the localized solutions were complex patterns of s displacements that quite often produced 'ripples' in the nanotube surface. In a small scale investigation the dependence of the stationary configuration upon the initial conditions was examined, motivated by a rich structure in the s-field in the vicinity of the 2d localised solutions. As one would expect, no effect of the initial conditions upon the stationary states was observed.

We have searched for excited states from the lower and upper energy bands. The first excited state in the lower bands ($q = 1$) was found to decay after a short time into the ground state ($q = 0$). The first excited state from the upper band disintegrated immediately, and therefore it may be possible that the predicted initial conditions [77] were incorrect. This is another topic for future investigation.

Chapter 7

Conclusions

The focus of the work presented in this thesis has been the analysis of self-trapped electron (polaron) states in structures relating to carbon nanotubes. The aim was to derive a system of equations that could be solved numerically in order to observe the dependence of the electronic localization upon the electron-phonon coupling parameters.

We started from a tight-binding description of electrons and phonons and generalised the ideas that have been considered in one dimensional atomic chains and two dimensional square lattices to the case of a hexagonal lattice. Certain complications arose due to the two-atom basis, however it was shown that the system equations lead to a Frölich type Hamiltonian, which has been long been used to model electron-phonon interactions. Under certain circumstances in the adiabatic approximation the equations were shown to reduce to the semi-classical case, just as with 1d and simpler 2d models. The semi-classical description involves a classical treatment of the lattice displacement fields by calculating Hamilton's equations.

The numerical modelling of the system of semi-classical equations led to the observation of a rich variety of states with different degrees of localization. The system ground state was explored as a function of the electron-phonon coupling terms on a hexagonal lattice with the dimension in the zig-zag direction considerably smaller than in the armchair direction. The observed solutions were found to exhibit differing degrees of localization. For zero, or extremely small coupling of the electron field to the lattice, the ground state was found to be the 1d type (or Davydov) soliton,

localized in the axial lattice direction i.e. the armchair direction. In this case the state looked like a 1d Davydov soliton in the armchair direction, but remained delocalized in the short zig-zag direction. For larger coupling strengths the ground state was found to be localized in both lattice dimensions. There were two main types of this kind of solution. The first has a probability density localized principally upon a single central site, the second is localized mainly upon two central sites. In both cases the lattice contained a characteristic deformation which pulled the surrounding sites towards the soliton centre. Furthermore, the magnitude of this deformation was found to increase with the electron-phonon coupling. The ground state corresponding to the region of parameters predicted by the current literature was the solution localised in one of the lattice dimensions.

The aim of the numerical studies was to provide a first insight into the kinds of self-trapped states that would be observed in carbon nanotubes. However, the restrictions of the model were evident in the non-zero curvature of the hexagonal lattice and the fixing of the lattice sites to lie in the plane. Due to the significant distortions that accompany the localized solutions, one would expect that out-of-plane site displacements are important in determining the self-trapped ground states in carbon nanotubes, particularly since it has been shown that carbon nanotubes can undergo quite violent bending without permanent deformation [46]. The formulation of the model on a three-dimensional cylinder therefore provided a great advancement in our knowledge of the states that could occur in a real nanotube. The hamiltonian was adapted to describe interactions in this structure and the focus lay in establishing the semi-classical equations, which could be solved numerically. The complications arising due to the three-dimensional treatment resided largely in the choice of the terms in the lattice potential that would describe the bending of the nanotube surface, since usually one-must consider up to fourth-nearest neighbour interactions. A bending potential was chosen that depended upon the solid angle formed by each site with its three nearest neighbours. The equations of motion corresponding to this system led to a nice approximate analytical solution.

The numerical solution of the semi-classical equations on the 3d nanotube led to a number of observed states with a rich structure occuring due to the presence of the

off-cylindrical displacements. These states were found to agree closely with the those discovered in the 2d hexagonal lattice. However the fine structure of these states was found to be much more intruiging due movements of the sites out of the plane of the nanotube. The states that were localised in both lattice directions caused the central sites to move inwards towards the centre of the tube, while in certain circumstances the surrounding sites were pushed outwards. For the values of the system couplings corresponding to physically realistic magnitudes, the ground state was once again observed to be the solution localised in the tube axial direction, but periodic around the tube circumference. This state produced a drawing in of the surrounding sites that was uniform around the circumference, however these displacements were small. There was also a small pinching of the tube in the vicinity of the soliton, whereby the sites are pulled slightly towards the tube axis. All of these displacements were small in magnitude compared to those surrounding the solutions that were localised in two dimensions. The observed states were seen not only in a zig-zag tube, but also in the chiral case. In fact, the states were found to be very similar, particularly in the case of the 1d soliton, where all of the main characteristics of the zig-zag solution were found in the corresponding chiral solution. In the two-dimensionally localised solutions the lattice deformation characteristics showed differences, which was somewhat expected due to the differences in the nanotube geometries.

These solutions give a stimulating insight into the kinds of polaronic states that could play a part in determining the properties of carbon nanotubes. However, it is important to discuss in more detail the limitations of the models considered here. The equations are based on a host of approximations that are necessary in providing a solvable model. The first of these approximations is the tight-binding method which has been a powerful method in condensed matter theory since its introduction, and continues to be of considerable use today. It has been used to accurately predict the electronic band structure of certain carbon nanotubes [22]. We therefore assume that this approximation is a valid one. The introduction of next-to-nearest neighbour interactions into the hamiltonian would be possible, however the complexity of the model would be extreme, with the tight-binding case considered here already being particularly numerically intensive.

Next we consider the validity of the adiabatic approximation. As has been stated in the text, this approximation is valid in the case of sufficiently high electron-phonon coupling. This assumption has been discussed in detail for the one-dimensional case [18] and also under certain approximations for the two dimensional case [19], where the non-adiabatic corrections have been calculated using perturbation theory and a number of substances in which the adiabatic approximation is valid were stated. The application of the ideas in these research papers to carbon nanotubes would be extremely useful future work.

Another major approximation is that of low temperature. This assumption was necessary due so that the electron-electron interactions could be neglected. The stability of Davydov solitons at higher temperatures has been investigated in great detail, paticularly in relation to the life-times of localized solutions in the alpha-helix. There has been some confusion as to the degree of stability [78], [79], [80]. However, more recent calculations predict a life-time sufficient for energy transport to occur through the Davydov Mechanism [82], [83]. If Davydov solitons have significant lifetimes in nanotube related structures then the applicability of these studies depend upon the extent to which electron-electron interactions may be neglected at higher temperatures. This will obviously depend upon the band gap of the particular nanotube under consideration.

Other approximations relate to the treatment of the properties of the carbon nanotube. Those of the achiral tubes, namely the armchair and zig-zag tubes are well established. However it is now clear through STM [84], electron diffraction [86] and Raman scattering experiments [87] that nanotube synthesis processes produce a homogeneous distribution of chiralities. This means that the vast majority of nanotubes are chiral. Furthermore, because of the unique caharacteristics of each type of nanotube, it is very difficult to make generalisations about their properties. For instance, the zone-folding technique is accurate in predicting the band structure of some nanotubes, while for others it is not [89]. The effects of curvature on the electronic band structure are not fully understood. The hybridisation pattern seen in graphite is changed due to the nanotube curvature [90], and this effect is also chirality dependent [90]. Another example lies in the phonon modes. For example, in

an $(8, 4)$ nanotube (studied in chapter 6), the eigenvectors of the very high frequency mode point in the circumferential direction, while in a $(9, 3)$ nanotube they point along one of the bond directions [91]. The direction of the eigenvectors can even in some cases show an angular dependence. Studies of zig-zag and armchair tubes have been relatively speaking straightforward due to the separation of the problem into axial and circumferential modes. This can not be taken for granted when dealing with chiral tubes. Many new properties of chiral nanotubes are therefore coming to light which may lead to modifications of the model considered here.

The existence of polarons has been predicted in carbon nanotubes [93]. Photo luminescence experiments have also shown the existence of stable exitonic states [94]. An exciton can be thought of as an excited electron-hole pair and may also undergo self-trapping [95]. Other experiments involving laser excitations have backed up this research [97], concluding that exciton states showed extremely stable characteristics. Furthermore, ab inito calulations, examining excitonic states in a $(4, 2)$ nanotube have shown localised patterns for the wavefunction that resemble extremely well the Davydov (or type I) solitons found in our investigations [96]. These results are encouraging in terms of validating the studies that have been performed here.

Research into the solutions of the semi-classical equations in chiral nanotubes is on-going. A future aim is to run simulations of chiral tubes that are more suited to scanning a wide range of electron-phonon couplings. The coupling phase space could then be compared for differing chiralities. The investigation into excited states is also on-going. It should be noted that there are also more complex structures relating to carbon nanotubes that could be used to further our investigation. For example, it is straightforward to join various nanotubes of different size together using only a single pentagon and heptagon [22]. There are only therefore minor modifications to be made to the lattice. One would then have to consider how to alter the potential at these points. Such structures have sparked much interest recently due to them representing a simple candidate for forming a metal-semiconductor junction [92]. An analysis of the polaron ground states in these systems would be interesting. Likewise, it is possible to construct helical or toroidal patterns of tubing, which have been observed experimentally [22], [98]. In each case a specified small number

of pentagon-heptagon pairs is required to form the geometry. An analysis of the one dimensional soliton in these structures would be extremely interesting. It would be particularly interesting to observe the patterns of lattice distortion in these different geometries. There are thus a wide range of more complicated geometries relating to nanotubes to which our model could be adapted.

The lattice models of electron-phonon intreactions that we have considered are nice because they allow a direct visualization of the predicted small-scale physical effects. The Davydov method is nice because it starts with the interactions between the actual neighbouring lattice sites. Such models are elegant in their simplicity due to the very differing degrees of localization predicted by a system that considers only short-ranged interactions. The solutions also predict the fine structure of the states such as a prediction for the average displacement of single atoms. The discussions undertaken in this work are a stepping stone in a long line of research, stretching back to the discovery of Davydov solitons in proteins, and reaching forward to the understanding of polaron and other electronic effects in the important field of nanophysics. The level of research performed on carbon nanotubes is immense, and the field will doubtlessly make rapid advances, part of which will hopefully build upon the work in this thesis.

Bibliography

[1] N.W. Ashcroft and N.D. Mermin, *Solid State Physics*, (Harcourt College, 1976).

[2] J. R. Hook and H. E. Hall, *Solid State Physics* (2nd ed), (John Wiley & Sons Ltd., 1991).

[3] C. Kittel, *Introduction to Solid State Physics*, (Wiley, 2005).

[4] N. N. Bogolubov and N. N. Bogolubov Jr., *Polaron Theory: Model Problems*, (OPA, 2000).

[5] A. S. Davydov, *Solitons in Molecular Systems*, (Riedel, Dordrecht, 1985).

[6] P. L. Taylor and O. Heinonen, *A Quantum Approach to Condensed Matter Physics*, (Cambridge, 2002).

[7] S. L. Altman, *Band Theory of Solids: An Introduction from the point of view of Symmetry*, (Oxford University Press, 1991).

[8] R. G. Chambers, *Electrons in Metals and Semiconductors*, (Cahpman and Hall, 1990).

[9] G. D. Mahan, *Many Particle Physics*, (Plenum, 1990).

[10] R.A.Cowley, Rep. Prog. Phys. **31**, pp123-166 (1968)

[11] A. V. Zolotaryuk, A. Mistriotis, E. N. Economoru Phys. Rev. B **48**, 13518 (1994).

[12] A. S. Davydov, Phys. Stat. Sol. **36**, 211 (1969).

[13] M. Peyrard, *Nonlinear excitations in biomolecules*, (Springer, Berlin, 1996).

[14] A. S. Davydov and N. I. Kislukha, Phys. Stat. Sol. (B) **59**, 465 (1973).

[15] A. Scott, Phys. Rep 217, pp1-67 (1992).

[16] L. Brizhik, A. Eremko, B. Piette and W. Zakrzewski, Phys. Rev. E **70**, 031914 (2004).

[17] L. Brizhik and A. Eremko, physica D **81**, 295 (1995).

[18] L. Brizhik and A. Eremko, Synth. Met. **109**, 117 (2000).

[19] L. Brizhik, A. Eremko, B. Piette and W. Zakrzewski, Phys. Rev. B **68**, 104301 (2003).

[20] P. L. Christiansen and A. Scott (*eds.*), *Davydov's soliton revisited*, (Plenum, 1990).

[21] H. Dai, Surf. Sci. **500**, 208 (2002).

[22] R. Saito, G. Dresselhaus, M. S. Dresselhaus, *Physical Properties of Carbon Nanotubes*, (Imperial College Press, 1998).

[23] S. Reich, C. Thomsen and J. Maultzsch, *Carbon nanotubes: Basic concepts and physical properties*, (Wiley, 2004).

[24] K.-P. Bohnen, R. Heid, H. J. Liu and C. T. Chan cond-mat/0411515 (2004).

[25] L. Brizhik, A. Eremko, B. Piette and W. Zakrzewski, Physica D **159**, pp71-90 (2001).

[26] L. Brizhik, A. Eremko, B. Piette and W. Zakrzewski, Physica D **146**, pp275-288 (2001).

[27] L. Brizhik, A. Eremko, B. Piette and W. Zakrzewski, cond-mat/0503366.

[28] L. Brizhik, A. Eremko, and A. La Magna, Phys Lett A **200**, 213 (1995).

[29] L. Brizhik, A. Eremko, Z. Phys. B **104**, 771 (1997).

[30] N. K. Efremidis, J. Hudock, D. N. Christodoulides, J. W. Fletcher, O. Cohen and M. Segev Phys. Rev. E **91**, 213906 (2003).

[31] P. J. F. Harris, *Carbon Nanotubes and Related Structures*, (Cambridge University Press, 1999).

[32] E. T. Thostenson, Z. Ren and T. Chou, Comp. Sci. Tech. **61**, 1899 (2001) .

[33] G. Dresselhaus, M. S. Dresselhaus and P. C. Eklund *Science of fullerenes and related structures*, (San Diego Academic Press, 1996).

[34] C. Dekker, Physics Today May 1999, pp22-28.

[35] http://www.sriconsulting.com/SRIC/Public/NewsEventsArt/CarbonFibersHajduk.pdf

[36] L. Duclaux, Carbon **40**, 1751 (2002).

[37] S.Iijima, Nature **354**, 56 (1991).

[38] Thess, A. et al, Science **273**, 483-487 (1996).

[39] J Kong, H. T. Soh, A. M. Cassell, C. F. Quate and H. Dai, Nature **395**, 878 - 881 (1998).

[40] M. J. Bronikowski, P. A. Willis, D. T. Colbert, K. A. Smith, and R. E. Smalley Journal of Vacuum Science and Technology **19** 1800 (2001)

[41] S. J. Tans, M. H. Devoret, H. Dai, A. Thess, R. E. Smalley, L. J. Georliga and C. Dekker, Nature **386**, 474 (1997).

[42] S. Frank, P. Poncharal, Z. L. Wang and W. A. de Heer, Science **280**, 1744 (1998).

[43] A. Batchtold, C. Strunk, J. P. Salvetat, J. M. Bonard, L. Forro, T. Nussbaumer, and C. Schönenberger Nature **397**, 673 (1999).

[44] R. Saito, M. Fujita, G. Dresselhaus, M. S. Dresselhaus, Phys. Rev. B **46** 1804 (1992).

[45] D. Sanchez-Portal, E. Artacho, J. M. Soler, A. Rubio and P.Ordejon, Phys. Rev. B **59** 12678 (1999).

[46] M. Endo, K. Takeuchi, S. Igarashi, K. Kobori, M. Shiraishi and H. W. Kroto, J. Phys. Chem. Solids **54**, 1841 (1993).

[47] H. Dai and N. Franklin and J. Han, App. Phys. Lett. **73** 1508 (1998)

[48] A. Rothschild, S. R. Cohen and R. Tenne, App. Phys. Lett. **75** 4025 (1999)

[49] *http://science.nasa.gov/headlines/y2000/ast07sep_1.htm*

[50] B. I. Jacobson, C. J. Brabec and J. Bernholc, Phys. Rev. Lett. **76**, 2511 (1996).

[51] B. Hartmann and W. Zakrzewski, Phys. Rev. B **68**, 184302 (2003).

[52] L. D. Landau, Phys. Zs. Sowjet., Vol. 3 (1993)

[53] E.I.Rashba, in *Excitons*, (North Holland, Amsterdam, 1982.).

[54] Y. Toyozawa, Prog. Theor. Phys. **26**, 29 (1959)

[55] J. Singh, *Excitation Energy Transfer Processes in Condensed Matter: Theory and Applications*, (Plenum, New York, 1994.)

[56] M. Zoli, J. Phys: Condensed Matter **13**, 10845 (2001)

[57] F.Mauri and R. Car, Phys. Rev. Lett. **75**, 3166 (1995)

[58] D. Ceresali, J. Phys: Condensed Matter **17**, 4621 (2001)

[59] E. A. Bartnik, J. A. Tuszynski and D. Sept, cond-mat/9503131 (1995).

[60] Z. Ivic and D. W. Brown, Phys. Rev. B **63**, 426 (1989).

[61] A.V. Zolotaryuk, K. H. Spatschek and O. Kluth, Phys. Rev. B **47**, 7827 (1993).

[62] H. Frölich, Proc. Roy. Soc. London A **215**, 291 (1952).

[63] R. Loudon *The Quantum Theory of Light (3rd ed.)*, (Oxford University Press, 2000).

[64] X. Wang, D. W. Brown, K. Lindenberg and B. J. West, Phys. Rev. A **37**, 3557 (1988).

[65] W. C. Kerr and P. S. Lomdahl, Phys. Rev. B **35**(7), 3629 (1987).

[66] A. Eremko, Y. Gaididei, A. Vakhnenko, Phys. Stat. Sol. B **127**, 703 (1985).

[67] A. M. Clogston, H. K. McDowell, P. Tsai and J. Hanssen, Phys. Rev. E **58**(5), 6407 (1998).

[68] J. C. Eilbeck and M. Johansson, PS/0211049 (2002).

[69] M. J. Ablowitz, B. Prinari, A. D. Trubatch, *Discrete and Continuous Nonlinear Schrödinger Systems*, (Cambridge University Press, 2004).

[70] P. G. Kevrekidis, K. Rasmussen and A. R. Bishop Int. J. Mod. Phys. B **15** 2833 (2001).

[71] P. G. Kevrekidis, B. A. Malomed and Yu. B. Gaididei Phys. Rev. E **66** 016609 (2002).

[72] W. J. Zakrzewski, hep-th/0412117 (2004).

[73] G. D. Mahan, Phys. Rev. B **68** 125409 (2003).

[74] L. M. Woods and G. D. Mahan, Phys. Rev. B **61**(16) 10651 (2000).

[75] G. D. Mahan, Phys. Rev. B **65** 235402 (2002).

[76] L. Bratek, L. Brizhik, A. Eremko, B. Piette, M. Watson and W. Zakrzewski, cond-mat/0510338.

[77] L. Bratek, L. Brizhik, A. Eremko, B. Piette, M. Watson and W. Zakrzewski, cond-mat/0510775.

[78] L. Cruziero, J. Halding, P. L. Christiansen, O. Skovgaard and A. Scott, Phys. Rev. A **37**(3) 880 (1988).

[79] J. P. Cottingham and J. W. Schweitzer, Phys. Rev. Lett. **62** 1792 (1989).

[80] L. Cruziero-Hansson, Phys. Rev. Lett. **73** 2927 (1994).

[81] L. Cruziero-Hansson and S. Takeno, Phys. Rev. E **56** 894 (1997).

[82] P. Xiao-feng, Phys. Rev. E **62** 6989 (2000).

[83] P. Xiao-feng, Eur. Phys. J. B **19** 2977 (2001).

[84] T. W. Odom, J. L. Huang, P. Kim and C. M. Lieber Nature **391** 62 (1998).

[85] T. Pichler, M. Knupfer, M. S. Golden, J. Fink, A. Rinzler and R.E. Smalley Phys. Rev. Lett. **80** 4729 (1998).

[86] L. Henrard, A. Loiseau, C. Journet and P. Bernier, Eur. Phys. J. B **13** 661 (2000).

[87] A. Jorio, R. Saito, J. H. Hafner, C. M. Lieber, M. Hunter, T. McClure, G. Dresselhaus, M. S. Dresselhaus, Phys. Rev. Lett. **86** 1118 (1994).

[88] A. Jorio, R. Saito, J. H. Hafner, C. M. Lieber, M. Hunter, T. McClure, G. Dresselhaus, M. S. Dresselhaus, Phys. Rev. Lett. **86** 1118 (1994).

[89] X. Blase, L. X. Benedict, E. L. Shirley , Phys. Rev. Lett. **72** 1878 (1994).

[90] A. Kleiner and S. Eggert, Phys. Rev. B **64**, 113402 (2001).

[91] S. Reich, C. Thomsen and P. Ordejon, Phys. Rev. B **64**, 195416 (2001).

[92] Madhu Menon and Deepak Srivastava Phys. Rev. Lett. **79**, 4453 (1997).

[93] M. Verissimo-Alves, R. B. Capaz, B. Koiller, E. Artacho and H. Chacham Phys. Rev. Lett. **86** 3372 (2001).

[94] J. Maultzsch, R. Pomraenke, S. Reich, E. Chang, D. Prezzi, A. Ruini, E. Molinari, M. S. Strano, C. Thomsen and C. Lienau cond-mat/0505150 (2005).

[95] D. L. Dexter and R. S. Knox, *Excitons*, (New York, 1965).

[96] E. Chang, G. Bussi, A. Ruini and E. Molinari Phys. Rev. Lett. **92**(19) 196401 (2004).

February 28, 2006

[97] G. N. Ostojic, S. Zaric, J. Kono, V. C. Moore, R. H. Hauge and R. E. Smalley cond-mat/0408667 (2004).

[98] S. Iijima Mater. Sci. Eng. B **19** 172 (1993).

Appendix A

Basic and Auxiliary Results

A.1   Coefficients of the solid angle

The solid angle between formed by the central lattice sites with its three nearest neighbours in a nanotube is:

$$S_{i,j,\rho} = S^0_{i,j,\rho} + \frac{\sqrt{3}}{2d} C_{i,j,\rho} \tag{A.1.1}$$

The function $C_{i,j,\rho}$ of the local site displacements gives the first-order correction to $S^0_{i,j,\rho}$:

$$
\begin{aligned}
C_{i,j,\rho} = {} & (-1)^\rho [\Delta^u u_{i,j,\rho} + \Delta^{ur} u_{r(i,j,\rho)} + \Delta^{ul} u_{l(i,j,\rho)} + \Delta^{ud} u_{d(i,j,\rho)}] + \\
& + [\Delta^s s_{i,j,\rho} + \Delta^{sr} s_{r(i,j,\rho)} + \Delta^{sl} s_{l(i,j,\rho)} + \Delta^{sd} s_{d(i,j,\rho)}] + \\
& + (-1)^\rho [\Delta^v v_{i,j,\rho} + \Delta^{vr} v_{r(i,j,\rho)} + \Delta^{vl} v_{l(i,j,\rho)} + \Delta^{vd} v_{d(i,j,\rho)}] \tag{A.1.2}
\end{aligned}
$$

The coefficients Δ are:

$$\Delta^u = \frac{3}{16L'^4}\left\{(m+n)^2\left[m(2m+n)\sin\left(\frac{3\gamma}{2}-2\xi\right)-3nm\sin(\gamma-\xi)\right.\right.$$

$$+3(2m^2+3mn+2n^2)\sin\left(\frac{\gamma-\xi}{2}\right)+n(m+2n)\sin\left(\gamma-\frac{\xi}{2}\right)]$$

$$-m^2(m+n)\left[(2m+n)\sin\left(\frac{3\gamma-5\xi}{2}\right)+3n\sin(\gamma-2\xi)\right]$$

$$-n^2(m+n)\left[3m\sin(\xi)+(2n+m)\sin\left(\frac{\gamma+\xi}{2}\right)\right]$$

$$+m^2(m-n)\left[n\sin\left(\gamma-\frac{5\xi}{2}\right)-3(2m+n)\sin\left(\frac{\gamma}{2}-\xi\right)\right]$$

$$+n^2(m-n)\left[m\sin\left(\frac{\gamma}{2}-2\xi\right)-3(2n+m)\sin\left(\frac{\xi}{2}\right)\right]\right\} \qquad (A.1.3)$$

$$\Delta^{ur} = \frac{1}{16L'^4}\left\{(5n^2+8mn+8m^2)\left[m(m-n)\sin\left(\frac{\gamma}{2}-2\xi\right)\right.\right.$$

$$-(m+2n)(m+n)\sin\left(\frac{\gamma+\xi}{2}\right)]+3n^2(m+2n)(m+n)\sin\left(\frac{\gamma-\xi}{2}\right)$$

$$+mn(m+n)(2m+n)\left(\sin(\gamma-\xi)+\sin(\gamma-2\xi)\right)+3mn^2(n-m)\sin\left(\frac{\gamma}{2}-\xi\right)\right\} \quad (A.1.4)$$

$$\Delta^{ul} = \frac{1}{16L'^4}\left\{(11n^2+14mn+11m^2)\left[m(2m+n)\sin\left(\frac{3\gamma}{2}-2\xi\right)\right.\right.$$

$$+n(2n+m)\sin\left(\gamma-\frac{\xi}{2}\right)]+3nm(n-m)(n+m)\left[\sin(\gamma-2\xi)\right.$$

$$-\sin(\xi)]+3(m+n)^2\left[m(2m+n)\sin\left(\frac{\gamma}{2}-\xi\right)\right.$$

$$+n(2n+m)\sin\left(\frac{\xi}{2}\right)]\right\} \qquad (A.1.5)$$

$$\Delta^{ud} = \frac{1}{16L'^4}\left\{(8n^2+8mn+5m^2)\left[n(m-n)\sin\left(\gamma-\frac{5\xi}{2}\right)\right.\right.$$

$$-(m+n)(2m+n)\sin\left(\frac{3\gamma-5\xi}{2}\right)]+3nm^2(m-n)\sin\left(\frac{\xi}{2}\right)$$

$$+3m(m+n)\left[n(2n+m)\left(\sin(\gamma-\xi)+\sin(\xi)\right)\right.$$

$$+m(2m+n)\sin\left(\frac{\gamma-\xi}{2}\right)]\right\} \qquad (A.1.6)$$

$$\Delta^s = \frac{3}{16L'^4}\left\{-(m+n)^2\left[3(2m^2+3mn+2n^2)\cos\left(\frac{\gamma-\xi}{2}\right)+m(2m+n)\cos\left(\frac{3\gamma}{2}-2\xi\right)\right.\right.$$
$$\left.+3mn\cos\left(\gamma-\xi\right)+n(m+2n)\cos\left(\gamma-\frac{\xi}{2}\right)\right]$$
$$-(m+n)\left[m^2(2m+n)\cos\left(\frac{3\gamma-5\xi}{2}\right)-3nm^2\cos\left(\gamma-2\xi\right)\right.$$
$$\left.+n^2(m+2n)\cos\left(\frac{\gamma+\xi}{2}\right)-3n^2m\cos(\xi)\right]+nm(n-m)\left[n\cos\left(\frac{\gamma}{2}-2\xi\right)\right.$$
$$\left.-m\cos\left(\gamma-\frac{5\xi}{2}\right)\right]-3\left[m^2(2m^2+mn+n^2)\cos\left(\frac{\gamma}{2}-\xi\right)\right.$$
$$\left.\left.+n^2(m^2+mn+2n^2)\cos\left(\frac{\xi}{2}\right)\right]\right\} \tag{A.1.7}$$

$$\Delta^{sr} = \frac{1}{16L'^4}\left\{(5n^2+8mn+8m^2)\left[m(m-n)\cos\left(\frac{\gamma}{2}-2\xi\right)\right.\right.$$
$$\left.+(m+n)(m+2n)\cos\left(\frac{\gamma+\xi}{2}\right)\right]+3(m+n)\left[mn(2m+n)\left(\cos(\gamma-2\xi)\right.\right.$$
$$\left.\left.-\cos(\gamma-\xi)\right)+n^2(m+2n)\cos\left(\frac{\gamma-\xi}{2}\right)\right]$$
$$+3mn^2(m-n)\cos\left(\frac{\gamma}{2}-\xi\right)\right\} \tag{A.1.8}$$

$$\Delta^{sl} = \frac{1}{16L'^4}\left\{(5n^2+2mn+5m^2)\left[m(2m+n)\cos\left(\frac{3\gamma}{2}-2\xi\right)\right.\right.$$
$$\left.+n(2n+m)\cos\left(\gamma-\frac{\xi}{2}\right)\right]+3nm(n+m)(n-m)\left[\cos(\xi)-\cos(\gamma-2\xi)\right]$$
$$+3(m+n)^2\left[m(2m+n)\cos\left(\frac{\gamma}{2}-\xi\right)+n(2n+m)\cos\left(\frac{\xi}{2}\right)\right]\right\} \tag{A.1.9}$$

$$\Delta^{sd} = \frac{1}{16L'^4}\left\{(8n^2+8mn+5m^2)\left[(n+2m)(n+m)\cos\left(\frac{3\gamma-5\xi}{2}\right)\right.\right.$$
$$\left.+n(n-m)\cos\left(\gamma-\frac{5\xi}{2}\right)\right]-3mn(m+2n)(m+n)\left[\cos(\gamma-\xi)-\cos(\xi)\right]$$
$$+3nm^2(n-m)\cos\left(\frac{\xi}{2}\right)+3m^2(m+n)(2m+n)\cos\left(\frac{\gamma-\xi}{2}\right)\right\} \tag{A.1.10}$$

$$\Delta^v = \frac{\sqrt{3}}{2L'^2}\left\{ m(n+m)\sin\left(\frac{\gamma-3\xi}{2}\right) \right.$$
$$\left. +mn\sin\left(\gamma-\frac{3\xi}{2}\right) - n(n+m)\sin\left(\frac{\gamma}{2}\right) \right\} \qquad (A.1.11)$$

$$\Delta^{vr} = \frac{\sqrt{3}}{8L'^2}\left\{ n(n+2m)\left[m(n-m)\sin\left(\frac{\gamma-3\xi}{2}\right) + (2n+m)(m+n)\sin\left(\frac{\gamma}{2}\right) \right] \right.$$
$$\left. -3n^2 m(m+n)\sin\left(\gamma-\frac{3\xi}{2}\right) \right\} \qquad (A.1.12)$$

$$\Delta^{vl} = \frac{\sqrt{3}}{8L'^2}\left\{ (n-m)(m+n)\left[m(2m+n)\sin\left(\gamma-\frac{3\xi}{2}\right) \right.\right.$$
$$\left.\left. +n(2n+m)\sin\left(\frac{\gamma}{2}\right) \right] - 3mn(m+n)^2\sin\left(\frac{\gamma-3\xi}{2}\right) \right\} \qquad (A.1.13)$$

$$\Delta^{vd} = \frac{\sqrt{3}}{8L'^2}\left\{ m(2m+n)\left[-(2n+m)(n+m)\sin\left(\gamma-\frac{3\xi}{2}\right) \right.\right.$$
$$\left. +n(m-n)\sin\left(\frac{\gamma-3\xi}{2}\right) \right]$$
$$\left. +3m^2 n(m+n)\sin\left(\frac{\gamma}{2}\right) \right\} \qquad (A.1.14)$$